UNIVERSITY OF BIRMINGHAM

Mathematical Modelling Of Chemical Reactions: The Vitamin C Clock Reaction.

Aliya Ali Alsaleh

Supervisors:

Sara Jabbari, & David Smith

Thesis submitted to The University of Birmingham

for the degree of Doctor of Philosophy

October 29, 2024

Contents

List of Figures

List of Tables

Abstract

The thesis presents a mathematical model and accompanying analysis to gain insights into the chemical clock reaction associated with vitamin C, hydrogen peroxide and iodine. Chemical clock reactions are identified by a reproducible induction period that is followed by in a rapid change in a solution triggered by a rise in a specific chemical concentration. In the vitamin C clock reaction, vitamin C converts iodine to iodide (the fast reaction) and simultaneously hydrogen peroxide converts iodide to iodine (the slow reaction). The fast reaction dominates until the vitamin C is depleted, at which point the iodine concentration rises, resulting in a rapid colour change in the system. Three new models are presented. Firstly, both the fast and slow reactions are considered under the assumption that hydrogen peroxide levels are moderate. Secondly, the slow reaction is considered in isolation and in more detail, revealing the effect of hydrogen peroxide concentration on the reaction kinetics and resolving differences in the existing literature. Thirdly, the fast reaction is reincorporated with the more detailed slow reaction to create a unified model that can capture the clock reaction dynamics under both moderate and high hydrogen peroxide regimes. All models are studied through numerical and asymptotic analysis. Using asymptotic analysis, formulae are derived that can predict the length of the induction period. Finally, experiments are carried out to

generate data to parameterise the models and test the associated formulae, which are shown to be accurate for both hydrogen peroxide regimes.

Acknowledgements

I am truly honoured to have received generous support from both the Ministry of Education of Saudi Arabia and the University of Birmingham. Their support has shaped my academic and professional skills. I want to thank my supervisors, Dr Sara Jabbari and Prof. David Smith (Department of Mathematics), whose expertise, understanding, and patience greatly improved my graduate experience. I appreciate all the valuable guidance and encouragement. Their unique way of explaining made the learning process enjoyable and effective. Their insights helped me grow as a researcher and person, teaching me how to manage my time wisely and juggle multiple responsibilities.

This path was anything but easy, especially as a mother. Balancing the demands of motherhood with the rigorous challenges of academic life required immense perseverance, patience, and, above all, effective time management. PhD journey has shown me that with proper time management and a supportive network, even the toughest challenges can be overcome.

Throughout my academic journey, I owe much of my success to my family, whose unwavering support allowed me to continue pursuing my dream. I am pleased to express my deepest gratefulness to my parents (Ali Ahmed Alsaleh and Laila Alhonfoush) for their endless love, support and encouragement. Their belief

in my abilities has been the basis of my success. I am also profoundly grateful to my brother (Hussain Alsaleh) for attentive listening, faithful support, understanding and patience from the beginning has been essential in my achievements. His thoughtful advice and belief in me have given me the strength and motivation to chase my dreams fearlessly. I also appreciate my other siblings (Duaa, Lamya and Mohammed Alsaleh) for inspiring and motivating me to keep going and never give up. In addition, I extend my sincere appreciation to my husband (Mohammed Altoma) for being by my side with loyal support and love. His patience and understanding have been valuable during this challenging journey, ultimately helping me to stay focused on achieving my goal. I am lucky to have my two daughters (Norah and Nada Altoma), thanks for being my source of joy and inspiration. Their smiles and love have been a positive energy for me and have given me the strength to continue.

This thesis would not have been possible without the collective support of all of them, and I commit this achievement to all of them.

Dedication

To my husband, Mohammed,

for patience, love, friendship, and support.

And to my smart, beautiful daughters, Norah and Nada,

for letting me experience the worth of inspiration.

Chapter 1

Introduction to Clock Reactions

This chapter introduces the motivation and outline of the thesis, as well as a review of basic clock chemical reactions and methodologies relevant to the thesis, including a review of related mathematical models.

1.1 Motivation

Mathematical models in chemistry play an important role in science. It is of interest to study chemical reactions and understand how the natural world works using mathematical models. In particular, models can take phenomena in science from a specific application area, and convert them into mathematical formulations that provide insightful analysis and valuable direction for that application. Analysis of the model allows us to understand its behavior, estimate the model parameters, and make reliable predictions for future behavior. Chemical reactions drive many important processes. For instance, some examples from daily life that are the result of chemical reactions include: turning food into fuel for the body,

the changes in food when it is cooked, washing detergent removing stains, and making fireworks explode. In the laboratory, for example, chemical reactions are used to detect proteins, bacteria, viruses, and identify DNA and RNA sequences [17, 47]. One timely instance of this relates to the COVID-19 pandemic which has threatened the lives of families and their children around the world. We highlight a study issued by [2] where certain chemical reactions were used on samples collected from patients in order to develop diagnostic COVID-19 tests. It is clear chemical reactions are ubiquitous.

Overall, a chemical reaction can be formulated using a mathematical model, where variables represent the reactants. An aim may be to predict the evolution of the concentration of certain chemical species in a time interval of interest or to identify which of the chemical species dominate in the reaction [3]. In [51], the authors use the analogy between chemical reactions and the spread of COVID-19 to motivate a framework for modelling both types of events in an education setting.

The main aim of this thesis is to use mathematical modeling to understand a specific chemical reaction: the vitamin C clock reaction. The remainder of this chapter will review some of the basic chemical reaction preliminaries needed in the thesis. Previous mathematical models of the clock reaction and its applications are also discussed.

1.2 Chemical Kinetics

The process of the transformation of reactants into products that occurs over time based on specific mechanisms is referred as chemical kinetics. The study of chemical kinetics has been carried out for over 100 years. The first chemical kinetics

study was by the German physicist L. F. Wilhemy in 1850 [18, 42, 53]. Chemical kinetics do not only concern the reaction rate and concentration of reactants, but also the mechanisms governing these reactions. Chemical kinetics have a significant impact in some areas, such as biochemistry, radiation chemistry, electrochemistry, photochemistry [14, 18]. There have been numerous studies to investigate chemical kinetics reactions with applications, for example [1, 8, 13, 25]; some of these will be discussed below.

1.2.1 Law of Mass Action

One of the fundamental chemical kinetics laws is the law of mass action, formulated by two Swedish scientists: the mathematician C. M. Guldberg and the chemist P. Waage, in 1864 [14, 18, 42, 53]. The law of mass action states that the rate of a chemical reaction is proportional to the product of the concentrations of the reactants (the active masses of the reactants as the molar per unit volume). Consider that substance A reacts with substance B to produce the substance C. This can be represented by the chemical reaction equation

$$aA + bB \rightarrow C, \tag{1.1}$$

where a, b are the stoichimetric coefficients of the reactants, which indicate how many molecules of the reactants are involved in the reaction. According to the law of mass action, the rate of the reaction (R) is indicated as:

$$R \propto [A]^a[B]^b, \tag{1.2}$$

the concentrations of the reactants are expressed with square brackets; $[A]$ and $[B]$. Thus, the law of mass action tells us that the rate of the reaction is given by

$$R = k[A]^a[B]^b, \tag{1.3}$$

where k is the reaction rate constant; we will continue to use this notation going forward.

In the next section, we will define the clock reaction and explore its applications.

1.3 The Clock Reaction and Applications

The "clock reaction" has been studied for more than a century. It was noted for the first time by Landolt in the 1880s with the sulfite/iodate reaction [23, 25, 27, 28, 38]. A clock reaction is defined as a chemical reaction where, after mixing the reactants, a sudden increase in the concentration of one product occurs, followed by a visible change, with a well-defined and reproducible time lag. The time lag is sometimes named a Landolt time, a clock time, or an induction period (we will typically refer to this as the induction period in this thesis). The visible change is marked at the end of the induction period and could be by a color change or a flash of light, for example, depending on the specific reaction. The species that appears after the induction period is called the clock species, and the chemical species involved in the chemical clock reaction are termed the clock chemicals. A more comprehensive description of the clock reaction can be found in [29].

There are considerable applications of chemical clock reactions across a variety of fields. The clock reactions have long been used in chemistry education [15],

have industrial applications [6, 7] and alongside experiments have been studied through mathematical and computation models [1, 8, 9, 13, 16, 27]. For further details, see the reviews [25, 32]. Clock reactions are of current interest through recent applications as diverse as a chemical clock car activity used in an educational setting [40], the evaluation of 3D printed mixing devices [22] and the determination of microconcentrations of the potentially toxic dye indigo carmine [39].

1.4 Categories of Clock Reactions

There are two core clock reaction mechanisms that have been studied: *induction* and *inhibition* [8, 9, 27]. Based on these mechanistic differences, clock reactions have been classified into two types by [25]: *auto-catalysis* driven clock reactions (induction) and *substrate-depletive* clock reactions (inhibition). More details are given in the following sections; along with a description of some pseudo clock behavior.

1.4.1 *Auto-catalysis* Driven Clock Reaction

Although there is some discussion over whether *auto-catalysis* should be considered as a clock reaction because of the lack of stoichiometric constraints (the stoichiometric constraints are related to the mass balance of reactants in the chemical equation) [29], we include *auto-catalysis* as a clock reaction due to the abrupt concentration change of a substance in a well-defined time [25, 38].

The mechanistic background of this phenomenon is *induction* (*auto-catalysis*).

The simplest scheme of this mechanism is the following:

$$P + 2B \rightarrow 3B \quad \text{at rate} \quad k[P][B]^2, \tag{1.4}$$

where P is a precursor chemical and B is the clock chemical (*auto-catalyst*). Since one of the reaction products is also a catalyst for the chemical reaction, this is called an *auto-catalytic* reaction. Examples belonging to this *auto-catalysis* mechanism are the iodate-arsenous acid reaction and the iodine-bisulphate clock reaction [8, 9, 24].

While a catalyst is an element that increases the rate of a chemical reaction, in contrast, an inhibitor is an element that decreases the rate or stops a chemical reaction; this will be addressed in the next section.

1.4.2 *Substrate-Depletive* Clock Reaction

The mechanistic background of this phenomenon is *inhibition*, and the simplest scheme of this mechanism is the following:

$$P \rightarrow B \quad \text{at rate} \quad k_0[P], \tag{1.5a}$$

$$B + C \rightarrow D \quad \text{at rate} \quad k_1[B][C], \tag{1.5b}$$

where B is the clock chemical and C is the inhibitor. The clock chemical reacts with an inhibitor to form the product D, limiting the concentration of the clock chemical. The concentration of the clock chemical rises once the inhibitor is completely consumed. Examples belonging to this *inhibition* mechanism are the photopolymerization of vinyl acetate inhibited by benzoquinone, and the photo-

synthesis of hydrogen chloride inhibited by ammonia [8, 9, 12]. The reaction (1.5) has the following properties:

i) If $P(0) > C(0)$, the clock species B appears when the reactant C is totally used up.

ii) If $P(0) < C(0)$, the clock species never appears, and the clock reaction is not observed,

where $P(0)$ and $C(0)$ are the initial concentrations of the reactants $[P]$ and $[C]$, respectively. In this thesis, we will study in detail the vitamin C clock reaction, which is substrate-depletive. Full details will be given in Chapter 2.

In short, the *substrate-depletive* clock reactions are described by the appearance of the clock species B only after the depletion of the substrate C after a well-defined delay time (induction period).

1.4.3 Reactions that Exhibit Two Mechanisms

Some chemical reactions could employ both induction and inhibition mechanisms depending on the initial concentrations of the reactants [8, 9]. For example, it has been found that the iodate-arsenous acid model demonstrates a clock reaction with a combination of *inhibition* and *indirect autocatalysis*. The reactants in the model are iodine ($B \equiv I_2$), arsenite ion ($C \equiv AsO_3^{3-}$), iodate ($P \equiv IO_3^-$), and iodide ($A \equiv I^-$), and the reaction scheme is given by,

$$P + 5A \rightarrow 3B, \tag{1.6a}$$

$$B + C \rightarrow 2A. \tag{1.6b}$$

The model (1.6) has *indirect autocatalysis* in one of the reactants, A, while C acts as the inhibitor, the clock chemical is B, and P is the precursor. Hence, the model (1.6) is *autocatalytic* overall because the reactant A is a catalyst in the first reaction (1.6a), and also a product in the second reaction (1.6b).

1.4.4 Pseudo Clock Behavior

A chemical reaction which has poor reproducibility of the induction period or irregular appearance of a clock species is categorized as pseudo clock behavior. Thus, these reactions cannot be classified as clock reactions [25, 26, 49]. Examples include the chlorite/thiosulfate [25, 35] and iodide/chlorite [25, 36] reactions in unbuffered media, in which the pH changes significantly. These reactions indicate fluctuations in concentrations for individual experiments.

The following section is a literature review of clock reaction models and their contributions to our thesis.

1.5 Previous Mathematical Models of Clock Reactions

In science, mathematical modeling is being increasingly realized as a powerful tool for the understanding of kinetic systems. The framework uses variables, parameters, and their interrelationships through mathematical language to describe phenomena or predict future events [21, 43]. Several mathematical modeling studies have tried to capture clock reactions. Chien [13] modelled two-step reactions via nonlinear differential equations. Integration of the kinetic equations for cer-

tain types, such as uni-unimolecular, uni-bimolecular and bi-bimolecular reactions, was considered. The obtained solutions were expressed in terms of dimensionless variables and parameters. The work used experimental data to evaluate the rate constants of each step in order to assess the possible reaction mechanism. A crucial analytical technique was presented, solving a Riccati type equation (a useful step that we also employ in our asymptotic analysis sections) resulting from quadratic reaction kinetics. Moreover, Anderson [1] exhibited the iodine clock reaction with modelling and simulation using numerical simulations of the system dynamics. Further development of mathematical modelling using sample laboratory processes for the kinetics of the iodine-clock reaction can be found in [16, 31, 44]. In addition, the chemical and equipment required for these experiments were feasible for institutions and students, i.e. the work should be relatively straightforward to reproduce.

An early study of mathematical modelling of clock reactions by Billingham and Needham [8] examined the two mechanisms: *induction* and *inhibition*, that can lead to clock reactions via three model schemes. The first model scheme was the cubic auto-catalysis model which exhibits a clock reaction with an *induction* mechanism and the solution can be collapsed onto two asymptotic regions. The simple model with an inhibitor was addressed in the second model scheme. In addition, the iodate-arsenous acid system was considered as the third model scheme which exhibits a clock reaction with a combination of *inhibition* and *indirect autocatalysis* mechanisms (as discussed in Section 1.4). The solutions can be reduced into four asymptotic regions for the second and third model schemes. The analysis indicated that *induction* dominates during the induction and inhibition period when the two mechanisms co-exist in the model. Simple expressions were obtained for

the induction and inhibition periods in terms of parameters of the model. Asymptotic analysis (which will be introduced in Section 2.4.3) was the main approach used for examining these models of clock reactions. Burgess & Davidson [11] have also examined the kinetics of the iodine reaction with ascorbic acid (vitamin C) and associated persulfate (peroxydisulfate ion; $S_2O_8^{2-}$).

Copper and Koubek [16] presented an experiment on the modified iodine chemical clock reaction that was suitable for students to reproduce. The experimental data included observations of the reaction rate, which indicated that the rate of iodine production should be linear in iodide (I^-). The hydrogen peroxide concentrations used were similar to the other substrates. More recently, the study by Kerr et al., [27] showed a detailed mathematical model of the related vitamin C *substrate-depletive* multi-step clock reaction via a system of nonlinear ordinary differential equations – here iodine is again the clock species. Iodine, hydrogen peroxide, and vitamin C are mixed. Vitamin C is the inhibitor, converting iodine to iodide. When vitamin C is depleted, the hydrogen peroxide converts iodide to iodine. The model was analysed through matched asymptotic expansions, and it was found that asymptotic analysis and numerical analysis closely agree in distinct time regions. The authors also conducted experiments to parameterise the model, and in contrast to [16], found that assuming that the rate of iodine production was quadratic in iodide enabled the model to match the data. Here, much higher concentrations of hydrogen peroxide were used than the other chemicals (and hydrogen peroxide was not considered explicitly in the model). Finally, the authors obtained a formula at leading order for the switchover time that was dependent on initial concentrations of vitamin C and iodine, and one of the reaction rates. The indicated formula compared well against data where two series in the initial

concentrations of both iodine and vitamin C were generated.

A further study of the vitamin C clock reaction is by Parra Cordova and Peña [40] which aims to integrate learning by combining chemistry kinetics and electronics via a hands-on activity for students. A chemical-driven car is designed whereby how long it takes for the color to change to dark blue (i.e. the induction period) determines the distance traveled by the car. A simple clock reaction model was studied alongside experiments and an approximate formula for the length of the induction period was obtained through a quasi-steady argument.

Some key goals of this thesis are to extend the work of [16] and [27] to understand the difference in their model structures (linear vs. quadratic), to examine the role that hydrogen peroxide plays in these differences, and to compare these findings with the more recent study by Parra Cordova and Peña [40].

1.6 Thesis Outline

The thesis is organized as follows:

- **Chapter 2**: A new model of the simple clock reaction (which will be named HPL – hydrogen peroxide linear) is designed to extend the work of Kerr et al. [27] to include hydrogen peroxide explicitly in the model. The assumptions are also modified to consider the case where hydrogen peroxide is present in moderate concentrations, akin to Copper and Koubek [16]. Therefore, the rate of the slow reaction is linear in both iodine and hydrogen peroxide concentrations. Our asymptomatic analysis shows agreement between approximate solutions and numerical solutions in the appropriate time regions. This enables us to obtain a formula for the switchover time to identify the

significant occurrence of when the clock reaction occurs and the solution appears dark blue. We find that our formula for switchover time is closely correlated with the results by Parra Cordova and Peña [40].

- **Chapter 3**: A new model of the slow reaction (iodine production) in isolation (which will be named ISR – isolated slow reaction) is formulated to understand how hydrogen peroxide concentration affects the kinetics of the chemical clock reaction. We include the hypoiodous acid reactant and reverse reaction. The analysis demonstrates that the clock reaction can exhibit either linear or quadratic kinetics depending on the ratio of hydrogen peroxide to iodide.

- **Chapter 4**: A full model of the clock reaction (which will be named Model FCR – full clock reaction) is performed by combining Model ISR (from Chapter 3) and the fast reaction (vitamin C consumption). We show that one unified model can capture both moderate and high hydrogen peroxide concentration regimes, identifying and validating the appropriate mathematical model for the vitamin C clock reaction. Asymptotic analysis enables us to obtain an approximate formula for the dependence of the switchover time dependent on the initial concentration of the reactants in each hydrogen peroxide regime. This empowers the comparison of the full clock reaction model, Model FCR, to results for the Model HPL (the simple model with moderate hydrogen peroxide in Chapter 2), and to the model with high hydrogen peroxide by Kerr et al., [27].

- **Chapter 5**: Experiments with varying amounts of hydrogen peroxide, iodine, and vitamin C demonstrate the high accuracy of the switchover time

formulations for both the moderate and high hydrogen peroxide regimes (from Chapter 4). Parameter estimates are obtained through least-squares relative error fitting with uncertainties estimated through log-likelihood ratio and bootstrapping. Through several permutations of fitting and testing data we observe excellent data fits and consistent parameter estimates for ϕ and k_3.

- **Chapter 6**: The main mathematical contributions of the thesis, including some areas for future work, are summarized.

We summarise the models and the chemical reactions that they describe in Table 1.1.

Model	Hydrogen Peroxide Regimes	Reactions
Kerr et al. [27]	high	$2D \to I$, $I + C \to 2D$.
Copper and Koubek [16]	moderate	$2D + P \to I$, $I + C \to 2D$.
HPL	moderate	$2D + P \to I$, $I + C \to 2D$.
ISR	moderate and high	$D + P \to Q$, $D + Q \to I$, $Q + P \to D$.
FCR	moderate and high	$D + P \to Q$, $D + Q \to I$, $Q + P \to D$, $I + C \to 2D$.

Table 1.1: The models developed in this thesis (HPL: hydrogen peroxide linear; ISR: isolated slow reaction; FCR: full clock reaction) alongside their associated chemical reactions. The reactants are iodide (D), hydrogen peroxide (P), iodine (I), vitamin C (C) and hypoiodous acid (Q). For ease of comparison, the models developed in Kerr et al. [27] and Copper and Koubek [16] (where thiosulfate is used in place of vitamin C) are also included.

Chapter 2

Model HPL: A Simple Model Of Chemical Clock Reaction With Moderate Hydrogen Peroxide

2.1 Motivation

As reported in Chapter 1, Kerr et al. [27] carried out clock reaction experiments using concentrations of hydrogen peroxide (H_2O_2) that were markedly higher than those of the other reactants. In these experiments, iodine (I_2) is generated as the clock chemical from the reaction between iodide (I^-) and hydrogen peroxide (H_2O_2). Through mathematical analysis, the researchers in [27] found that assuming the kinetics were quadratic in hydrogen peroxide was consistent with the experimental data. However, Copper and Koubek [16] observed a linear rate of reaction when operating with moderate hydrogen peroxide concentrations.

This chapter builds upon Kerr et al.'s findings [27] by focusing on modeling the

moderate-peroxide regime and including hydrogen peroxide explicitly in the model which we will develop and analyze accordingly. We will provide an introduction to the study of the vitamin C clock reaction by first discussing the background and context, followed by the model formulation, and numerical and asymptotic analyses of the model.

2.2 Introduction

In this study, we consider the chemical reaction described by Wright [27, 55, 56] as follows:

$$2H^+(aq) + 2I^-(aq) + H_2O_2(aq) \rightarrow I_2(aq) + 2H_2O(l), \tag{2.1}$$

and

$$I_2(aq) + C_6H_8O_6(aq) \rightarrow 2H^+(aq) + 2I^-(aq) + C_6H_6O_6(aq), \tag{2.2}$$

where the (aq) and (l) signs indicate the substance is dissolved in water and the substance is a liquid, respectively. Isolated hydrogen ions are symbolized by H^+, and H_2O is commonly known as water. The dehydroascorbic acid ($C_6H_6O_6$) is made from the oxidation of ascorbic acid ($C_6H_8O_6$; vitamin C). Briefly, there are two reactions (2.1) and (2.2). The first reaction (2.1) is a slow reaction: iodide (I^-) is converted to iodine (I_2) in the presence of hydrogen peroxide (H_2O_2). It is worth mentioning that H_2O_2 is used up too, and the fact the supply is limited will be a focus of this chapter. The second reaction (2.2) is a fast reaction: iodine (I_2) is converted to iodide (I^-) in the presence of vitamin C ($C_6H_8O_6$, ascorbic acid), and uses up vitamin C in the process. The solution changes colour when

vitamin C is depleted, yielding more iodine from (2.1). We will focus on specific reactants that are crucial in the clock chemical reactions, rather than all involved substances. The model does not explicitly account for production or consumption of dehydroascorbic acid ($C_6H_6O_6$), isolated hydrogen ions (H^+) or water (H_2O) for the following reasons. Dehydroascorbic acid ($C_6H_6O_6$) is only a product and therefore does not affect the concentrations of other species in the system, and therefore we omit it from the modelling. We assume that the produced isolated hydrogen ions (H^+) and water (H_2O) do not significantly change the pH. More details will be discussed in the next section.

An illustration diagram of the vitamin C clock reaction is depicted in Figure 2.1, adapted from [10]. A complete discussion of the chemistry process for the vitamin C clock reaction is described by [55].

We note that the vitamin C clock reaction has lately been discussed by two authors in the literature. Burgess & Davidson [11] have investigated a similar reaction with associated persulfate (peroxydisulfate ion; $S_2O_8^{2-}$) in place of hydrogen peroxide (H_2O_2). As mentioned in Chapter 1, Kerr et al., [27] have modelled and analysed the vitamin C reaction without involving hydrogen peroxide (H_2O_2) in the model. In this chapter, we build on [27] by incorporating hydrogen peroxide explicitly and considering the moderate-peroxide regime where the reaction is assumed to be linear. The modified model will be developed and analysed in the following sections.

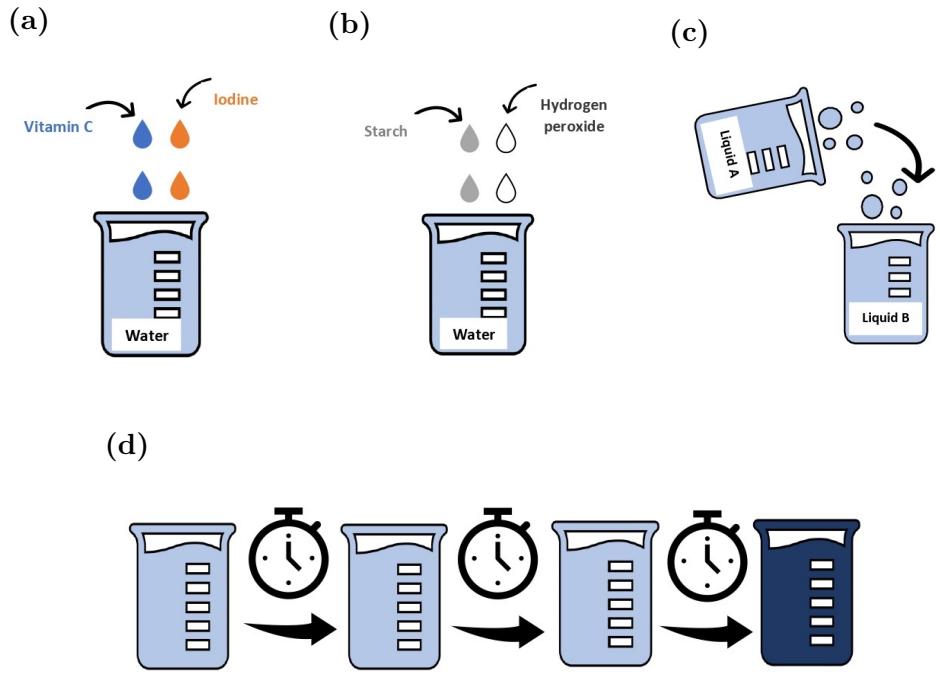

Figure 2.1: An illustration diagram of the vitamin C clock reaction, adapted from [10]. (a) Solution A: In the presence of vitamin C, a mixture of water and iodine, the solution appears clear. (b) Solution B: In the presence of hydrogen peroxide, a mixture of water and starch (which acts as an indicator, but is not directly involved in the chemical clock reaction), the solution appears clear. (c) A mixture of iodine and iodide to starch and hydrogen peroxide by pouring Solution A into Solution B. (d) The iodide gets converted to iodine, and the solution appears dark blue after the induction period.

2.3 Model Formulation

The model to be constructed is based on the multi-step reactions, via a system of nonlinear differential equations under the law of mass action. To build our model, we will focus on particular reactants that are essential to the clock chemical reactions ((2.1) and (2.2)), such as iodide, iodine, hydrogen peroxide and vitamin C. Reactants like the dehydroascobic acid, water and the isolated hydrogen ions will not be considered in our model. The amount of isolated hydrogen ions (H^+) produced does not significantly affect pH. Starch is used as an indicator to help with the appearance of the sudden change of color from clear to dark blue (as shown in Figure 2.1), and will not be explicitly incorporated into our model. In the first (slow) reaction: The total concentration of iodide at time t, denoted by $D(t)$, is converted to iodine (denoted by $I(t)$) in the presence of hydrogen peroxide (denoted by $P(t)$) at a rate given by $k_1[D][P]$. As has been previously reported in the literature [16, 31, 44], the rate of this reaction is linear in both I^- and H_2O_2 concentrations, based on experimental data. These studies have worked with hydrogen peroxide concentrations which are similar to the other substrates (while the study in [27] worked with hydrogen peroxide in great excess, so the first reaction rate is quadratic in I^- concentrations).

In this study, we assume that concentrations of hydrogen peroxide are similar to the other reactants, rather than in great excess. From this point forward, we express the reaction rate without square brackets for ease of notation. Therefore, the chemical reaction in the simplified form, is

$$2D + P \xrightarrow{k_1 DP} I. \tag{2.3}$$

In the second (fast) reaction: The total concentration of iodine at time t, denoted by $I(t)$, is converted to iodide (denoted by $D(t)$) in the presence of vitamin C (denoted by $C(t)$) at a rate of reaction given by k_2IC. Thus, the chemical reaction in the simplified form, is

$$I + C \xrightarrow{k_2IC} 2D. \tag{2.4}$$

The vitamin C clock reaction has been characterized as a *substrate-depletive* clock reaction [25, 27]. The substrate vitamin C (C) is consumed, causing the clock species iodine (I) to appear after a well-defined delay (induction period). The reaction mechanism is the *inhibition*: when the inhibitor vitamin C (C) is present, the fast reaction (2.4) dominates, and keeps the concentration of iodine (I) low in comparison to iodide (D). Eventually, vitamin C (C) is exhausted and the slower reaction (2.3) dominates, resulting in a rising concentration of iodine (I), and hence turning the solution to blue.

Applying the law of mass action to (2.3) and (2.4), the model is given by the following system of nonlinear differential equations (named, Model HPL referring to hydrogen peroxide linear):

$$\frac{dD}{dt} = 2k_2IC - 2k_1DP, \tag{2.5a}$$
$$\frac{dI}{dt} = -k_2IC + k_1DP, \tag{2.5b}$$
$$\frac{dC}{dt} = -k_2IC, \tag{2.5c}$$
$$\frac{dP}{dt} = -k_1DP, \tag{2.5d}$$

with initial conditions

$$D(0) = d_0, \quad I(0) = \iota_0, \quad C(0) = c_0, \quad P(0) = p_0. \tag{2.6}$$

The model (2.5) extends the work of Kerr et al., [27] by including hydrogen peroxide (P) in the model, and making the assumption that concentrations of hydrogen peroxide are similar to the other reactants, rather than in great excess. We observe that

$$\frac{dD}{dt} + 2\frac{dI}{dt} = 0, \tag{2.7}$$

which means that $D(t)+2I(t)$ is conserved (i.e., $D+2I =$ constant). We represent the initial concentration of (atomic) iodine by $m_0 = d_0 + 2\iota_0$. Hence,

$$D(t) = m_0 - 2I(t). \tag{2.8}$$

Therefore, we can eliminate the variable D from the model (2.5) by substituting (2.8) in (2.5), the system becomes

$$\frac{dI}{dt} = -k_2 IC - 2k_1 P(m_0 - 2I), \tag{2.9a}$$
$$\frac{dC}{dt} = -k_2 IC, \tag{2.9b}$$
$$\frac{dP}{dt} = -k_1 P(m_0 - 2I). \tag{2.9c}$$

It should be emphasized that the units of the reactants' concentrations (D, I, C, P) are moles per litres (mol/l), the units of time (t) are seconds (s), and the units of the reaction rates (k_1, k_2) are liters per moles per seconds (l/mol·s). The state variables and parameters of the model are tabulated in Table 2.1.

Table 2.1: Description of variables and parameters of the model (2.11)

Variables	Description	Units
D	Total concentration of iodide	mol/l
I	Total concentration of iodine	mol/l
C	Total concentration of Vitamin C	mol/l
P	Total concentration of Hydrogen peroxide	mol/l
t	Time	s
Parameter	**Description**	**Units**
k_1	The rate of the first (slow) reaction	l/mol·s
k_2	The rate of the second (fast) reaction	l/mol·s
m_0	The initial total concentration of iodine and iodide	mol/l
c_0	The initial concentration of vitamin C	mol/l
p_0	The initial concentration of hydrogen peroxide	mol/l
$\epsilon = k_1/k_2$	The reaction rate ratio	
$\rho = p_0/c_0$	The ratio of initial hydrogen peroxide to initial vitamin C	
$\sigma = m_0/c_0$	The ratio of initial atomic iodine to vitamin C	

2.4 Analysis of Vitamin C Clock Reaction Model HPL

Before analyzing the model (2.9), it is instructive to non-dimensionalize the system for simplicity by choosing the following scaling (in particular, we choose the timescale based on the fast reaction step of producing iodide),

$$I = m_0 I^*, \quad C = c_0 C^*, \quad P = p_0 P^*, \quad t = \frac{t^*}{k_2 c_0}, \tag{2.10}$$

where $*$ denotes a dimensionless quantity. There is no unique way for choosing the scaling factors when non-dimensionalizing a model. Multiple approaches can be valid depending on the objectives of the analysis. Substituting (2.10) into (2.9),

gives the following

$$\frac{dI^*}{dt^*} = -I^*C^* + \epsilon\rho P^*\left(1 - 2I^*\right), \tag{2.11a}$$

$$\frac{dC^*}{dt^*} = -\sigma I^*C^*, \tag{2.11b}$$

$$\frac{dP^*}{dt^*} = -\epsilon\sigma P^*\left(1 - 2I^*\right), \tag{2.11c}$$

where,

$$\epsilon = \frac{k_1}{k_2}, \quad \rho = \frac{p_0}{c_0}, \quad \sigma = \frac{m_0}{c_0}, \tag{2.12}$$

and the initial conditions become

$$I^*(0) = \frac{\iota_0}{m_0} =: \phi, \quad C^*(0) = 1, \quad P^*(0) = 1. \tag{2.13}$$

From this point forward, we drop stars for ease of notation. We note that (2.8) can also be nondimensionalised to give

$$D(t) = 1 - 2I(t), \tag{2.14}$$

where we see that the maximum value of $I(t)$ is $1/2$ (occurring when $D = 0$); this will be used in later analysis.

Figure 2.2 shows a typical simulation of the clock reaction model (2.11)-(2.13) where the clock species I appears only after depletion of the substrate C (making the reaction *substrate-depletive*), i.e. after the induction period.

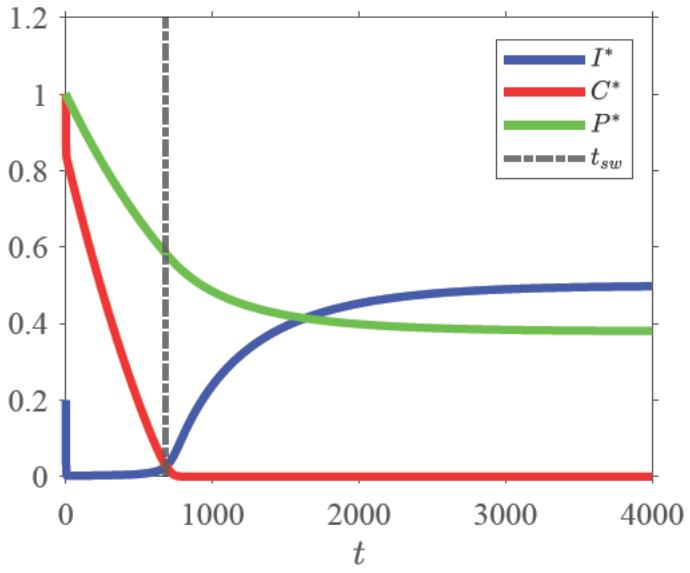

Figure 2.2: Numerical simulation of the model (2.11) illustrates the concentrations of the reactants as a function of time with initial conditions $I(0) = \phi$, $C(0) = 1$ and $P(0) = 1$, and the dimensionless parameter values are $\sigma = 0.8$, $\phi = 0.2$, $\rho = 2$ and $\epsilon = 0.001$. The clock reaction occurs after the induction period, with the dot-dashed line indicating the switchover time (t_{sw}).

2.4.1 Quasi-Steady State

Before proceeding with a time-dependent asymptotic analysis to derive a formula for the switchover (colour change) time, we show that a quasi-steady analysis can provide some insight into the induction period of the model (2.11) by using the fact that the clock chemical iodine (I) is only slowly fluctuating throughout the induction period. Using the quasi-steady-state hypothesis we set $dI/dt \approx 0$ in (2.11a), it follows that

$$IC \approx \epsilon\rho P(1-2I), \tag{2.15}$$

and hence,

$$\frac{IC}{\epsilon P(1-2I)} \approx \rho. \tag{2.16}$$

Dividing dC/dt by dP/dt in (2.11), to get

$$\frac{dC}{dP} = \frac{-\sigma IC}{-\epsilon\sigma P(1-2I)}, \tag{2.17}$$

substituting (2.16) into (2.17) leads to

$$\frac{dC}{dP} = \rho. \tag{2.18}$$

Using integration, therefore,

$$C = \rho P + b_1, \tag{2.19}$$

where b_1 is a constant. We leave determination of b_1 to Section 2.4.3 where we consider time periods before the quasi-steady. Since the clock chemical concentration (iodine; I) is small during the induction period, we take $I \approx 0$. In a later section, we will conduct a detailed analysis of a completed clock reaction, including the

induction period and the switchover time, as illustrated in Figure 2.3c. Hence, dP/dt in (2.11) can be simplified as

$$\frac{dP}{dt} = -\epsilon\sigma P, \tag{2.20}$$

which can be solved by separation of variables, leading to the solution

$$P = b_2 e^{-\epsilon\sigma t}, \tag{2.21}$$

where b_2 is a constant which again will be determined in Section 2.4.3, and we get

$$C(t) = \rho e^{-\epsilon\sigma t} + b_1, \tag{2.22}$$

as an approximation of Vitamin C during the induction period. In clock reactions, the quasi-steady state during the induction period means some chemicals stay constant while the reaction is actively progressing (i.e. the iodine is approximately constant while vitamin C and hydrogen peroxide are being consumed slowly). On the other hand, equilibrium refers to the balance between reactants and products, where no significant change is observed.

2.4.2 Lines of Equilibria

It is instructive to determine the number of possible equilibrium solutions that the model (2.11) can have. In chemical reaction models, an equilibrium refers to the state of a system in which the concentrations of the reactants and products do not change over time. The model (2.11) has three lines of equilibria, obtained by

setting the right-hand side of the equations in the model (2.11) to zero, given by

$$\left(\bar{I}, 0, 0\right), \quad \left(0, \bar{C}, 0\right), \quad \left(1/2, 0, \bar{P}\right), \tag{2.23}$$

where $\bar{I}, \bar{C}$ and $\bar{P}$ could be any positive values depending on the initial conditions used. $\left(\bar{I}, 0, 0\right)$ represents the situation in which only iodine (I) is present, and there is no vitamin C and no hydrogen peroxide (P); this means that the two chemical reactions (2.3) and (2.4) cannot happen. Moreover, the line of equilibria $\left(0, \bar{C}, 0\right)$ represents the situation in which there is no iodine (I) for vitamin C to activate, so it occurs when hydrogen peroxide (P) runs out before vitamin C does. In this situation, it means there is no substrate for the clock reaction so it stays trivial. Therefore, in both lines of equilibria $\left(\bar{I}, 0, 0\right)$ and $\left(0, \bar{C}, 0\right)$, the clock reaction has failed. From a mathematical view, the two lines of equilbria ($\left(\bar{I}, 0, 0\right)$ and $\left(0, \bar{C}, 0\right)$) are not interesting cases compared to the last case (the line of equilibria $\left(1/2, 0, \bar{P}\right)$).

The line of equilibria $\left(1/2, 0, \bar{P}\right)$ can be interpreted as the chemical reactions ((2.3) and (2.4)) no longer being able to take place because if $I = 1/2$, then there is no iodide to convert to iodine ($D = 0$ from (2.14)). In addition, if $C = 0$ then the iodine-to-iodide reaction (2.4) cannot occur. It is the ultimate state of the system: all iodide is converted to iodine and the solution appears blue.

Stability:

To study the linear stability of the lines of equilibria (non-trivial), we must find the eigenvalues of the linearized system using the Jacobian of the model (2.11),

$$J(I,C,P) = \begin{pmatrix} \frac{\partial I}{\partial I} & \frac{\partial I}{\partial C} & \frac{\partial I}{\partial P} \\ \frac{\partial C}{\partial I} & \frac{\partial C}{\partial C} & \frac{\partial C}{\partial P} \\ \frac{\partial P}{\partial I} & \frac{\partial P}{\partial C} & \frac{\partial P}{\partial P} \end{pmatrix}. \tag{2.24}$$

Or,

$$J(I,C,P) = \begin{pmatrix} -(C+2\epsilon\rho P) & -I & \epsilon\rho(1-2I) \\ -\sigma C & -\sigma I & 0 \\ 2\epsilon\sigma P & 0 & -\epsilon\sigma(1-2I) \end{pmatrix}. \tag{2.25}$$

We need to evaluate the Jacobian at each separate steady state. Consider the line of equilibria $\left(\bar{I},0,0\right)$, then

$$J\left(\bar{I},0,0\right) = \begin{pmatrix} 0 & -\bar{I} & \epsilon\rho\left(1-2\bar{I}\right) \\ 0 & -\sigma\bar{I} & 0 \\ 0 & 0 & -\epsilon\sigma\left(1-2\bar{I}\right) \end{pmatrix} \tag{2.26}$$

Therefore, the characteristic polynomial is as follows

$$\lambda\left(\lambda+\sigma\bar{I}\right)\left(-\epsilon\sigma\left(1-2\bar{I}\right)-\lambda\right)=0. \tag{2.27}$$

Hence, the eigenvalues are

$$\lambda_1 = 0, \quad \lambda_2 = -\sigma\bar{I}, \text{and} \quad \lambda_3 = -\epsilon\sigma\left(1-2\bar{I}\right). \tag{2.28}$$

Thus, the line of equilibria $\left(\bar{I}, 0, 0\right)$ has a zero eigenvalue, indicating a slow manifold [41], and negative eigenvalues since all the parameters and variables are positive and $0 < \bar{I} < 1/2$ (as stated after the non-dimensionalised model using (2.14)), which indicates a stable manifold [41].

Similarly, for the line of equilibria $\left(0, \bar{C}, 0\right)$ we have

$$J\left(0, \bar{C}, 0\right) = \begin{pmatrix} -\bar{C} & 0 & \epsilon\rho \\ -\sigma\bar{C} & 0 & 0 \\ 0 & 0 & -\epsilon\sigma \end{pmatrix} \tag{2.29}$$

The characteristic polynomial is given by

$$\lambda\left(\lambda + \bar{C}\right)\left(-\epsilon\sigma - \lambda\right) = 0. \tag{2.30}$$

Here, the eigenvalues are $\lambda_1 = 0$, where the zero eigenvalue indicates the slow manifold, and $\lambda_2 = -\bar{C}$, $\lambda_3 = -\epsilon\sigma$ are negative eigenvalues since all parameters and variables are positive which indicate the stable manifold.

Consider the Jacobian for the third line of equilibria, which is the most interesting case to study, $\left(1/2, 0, \bar{P}\right)$ which has the form

$$J\left(1/2, 0, \bar{P}\right) = \begin{pmatrix} -2\epsilon\rho\bar{P} & -1/2 & 0 \\ 0 & -\sigma/2 & 0 \\ 2\epsilon\sigma\bar{P} & 0 & 0 \end{pmatrix} \tag{2.31}$$

with the following characteristic polynomial

$$\lambda\left(\lambda + 2\epsilon\rho\bar{P}\right)\left(-\sigma/2 - \lambda\right) = 0, \tag{2.32}$$

and eigenvalues, $\lambda_1 = 0$, $\lambda_2 = -2\epsilon\rho\bar{P}$ and $\lambda_3 = -\sigma/2$. The eigenvalues λ_2 and λ_3 are negative since all parameters and variables are positive, therefore, the line of equilibria $\left(1/2, 0, \bar{P}\right)$ has a slow and stable manifold because of the zero and negative eigenvalues respectively. Note that all the three lines of equilibria have a zero eigenvalue; $\lambda = 0$ corresponds to the fact that the variables $\bar{I}, \bar{C}$ and $\bar{P}$ can take any value but also that the linear stability analysis has failed so further work needs to be done to verify the equilibria.

Numerical simulations of the model (2.11) in Figure 2.3, showing the concentrations of iodine, vitamin C and hydrogen peroxide as a function of time on logarithmic scale using various initial conditions, illustrate these three lines of equilibria (are the balance between the reactants and products with no visible change, while the quasi-steady state during the induction period keeps some reactants constant as the reaction continues). In Figure 2.3a, there is not enough vitamin C, so there is no induction period since the vitamin C is consumed already. In Figure 2.3b, there is not enough hydrogen peroxide, so the induction period starts but never ends because the hydrogen peroxide is used up before the vitamin C. In Figure 2.3c, the clock reaction is completed and both induction period and switchover time occur. Numerical analysis has been performed to solve the model (2.11) approximately using computational techniques in the MATLAB program with the ode45 solver. We will now show that asymptotic analysis studies can generate further insight into the model behaviour in the following section.

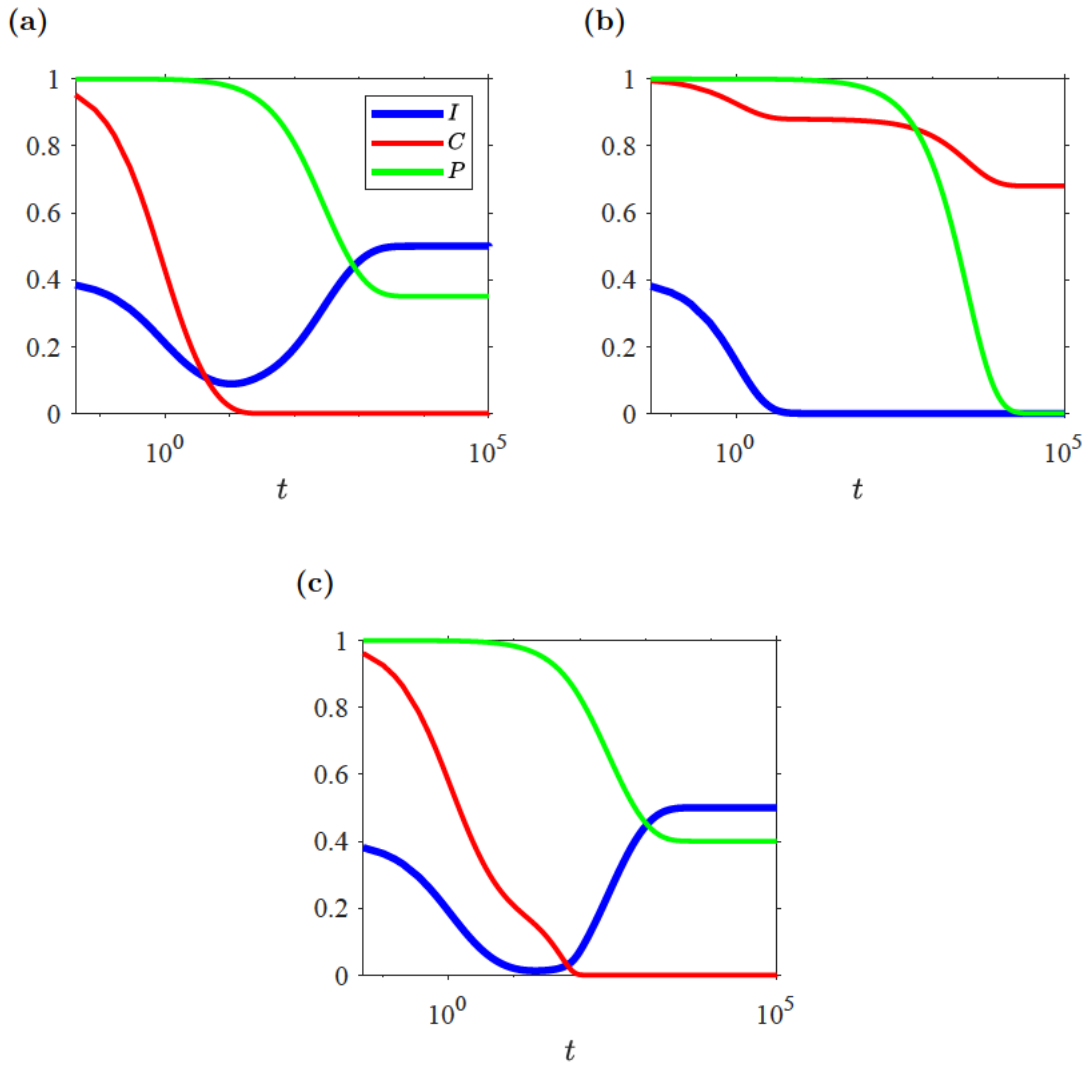

Figure 2.3: Numerical simulations of the model (2.11) illustrate the concentrations of iodine, vitamin C and hydrogen peroxide as a function of time on logarithmic scale using the initial conditions $(I(0) = 0.4,\ C(0) = 1,\ P(0) = 1)$ with $\epsilon = 0.001$ and various values for the dimensionless parameters ρ and σ. Even with fixed initial conditions, changes to parameter values can enable the system to achieve different equilibria. (a) The simulation shows the convergence to equilibrium $\left(\bar{I}, 0, 0\right) = (0.1, 0, 0)$ with parameter values $\rho = 0.2,\ \sigma = 3$. (b) The simulation shows the convergence to equilibrium $\left(0, \bar{C}, 0\right) = (0, 0.7, 0)$ with parameter values $\rho = 0.2,\ \sigma = 0.3$. (c) Simulation shows the convergence to the equilibrium $\left(1/2, 0, \bar{P}\right) = (0.5, 0, 0.4)$ with parameter values $\rho = 2,\ \sigma = 2$.

2.4.3 Asymptotic Analysis

Asymptotic analysis (more specifically here, matched asymptotic analysis) is the study of the limiting behaviour of models, leading to reduced (and therefore simpler) models that capture the behaviour of the full system in these limits, as terms have different magnitudes in different regimes. A similar approach was used by Billingham & Needham [8, 9], and Kerr et al., [27], We will see that the expression $\sigma\phi < 1$ is required (where $\sigma\phi = \iota_0/c_0 < 1$, so the initial concentration of vitamin C should be greater than the initial concentration of iodine) in order for vitamin C to survive the initial adjustment and therefore for the clock reaction to occur. There are four regions to be studied as detailed in the following sections.

Region I: Initial Adjustment

Reactants are mixed during Region I before the induction phase begins. Basically, it is described as where the dependent variables I, C, P are order 1 and the independent variable $t = O(1)$. Seeking a solution of the form (asymptotic expansions):

$$I = I_0 + \epsilon I_1 + \epsilon^2 I_2 + ..., \quad C = C_0 + \epsilon C_1 + \epsilon^2 C_2 + ..., \quad \text{and} \quad P = P_0 + \epsilon P_1 + \epsilon^2 P_2 + ... \tag{2.33}$$

we find that at leading order ($O(1)$),

$$\frac{dI_0}{dt} = -I_0 C_0, \tag{2.34a}$$

$$\frac{dC_0}{dt} = -\sigma I_0 C_0, \tag{2.34b}$$

$$\frac{dP_0}{dt} = 0, \tag{2.34c}$$

with the initial conditions:

$$I_0(0) = \phi \quad C_0(0) = 1 \quad \text{and} \quad P_0(0) = 1. \tag{2.35}$$

Note that

$$\sigma \frac{dI_0}{dt} - \frac{dC_0}{dt} = 0, \tag{2.36}$$

which means that the quantity $(\sigma I_0 - C_0)$ is a constant. Thus, $C_0 = \sigma\left(I_0 - \phi\right) + 1$. By substituting this result in (2.34b), this leads to

$$\frac{dI_0}{dt} = -I_0\left(\sigma\left(I_0 - \phi\right) + 1\right), \tag{2.37}$$

$$\frac{dP_0}{dt} = 0. \tag{2.38}$$

Using the separation of variables method:

$$\int \frac{dI_0}{-I_0\left(\sigma\left(I_0 - \phi\right) + 1\right)} = \int dt, \tag{2.39}$$

$$\int dP_0 = 0. \tag{2.40}$$

Thus,

$$P_0(t) = 1, \tag{2.41}$$

and solving for the variable I_0, we can use partial fraction decomposition for the left-hand side (LHS):

$$\int_{\phi}^{I_0} \frac{d\tilde{I}_0}{-\tilde{I}_0\left(\sigma\left(\tilde{I}_0 - \phi\right) + 1\right)} = -\int_{\phi}^{I_0} \left(\frac{A}{\tilde{I}_0} + \frac{B}{\left(\sigma\left(\tilde{I}_0 - \phi\right) + 1\right)}\right) d\tilde{I}_0, \tag{2.42}$$

where $A = 1/(1-\sigma\phi)$ and $B = -\sigma/(1-\sigma\phi)$. This allows us to integrate both sides in (2.39)

$$\frac{1}{(\sigma\phi - 1)} \left[\ln \frac{\tilde{I}_0}{\sigma\left(\tilde{I}_0 - \phi\right) + 1} \right]_{\phi}^{I_0} = t, \tag{2.43}$$

where the sign of the argument of the natural logarithm is positive (i.e., $\tilde{I}_0/\sigma\left(\tilde{I}_0 - \phi\right) + 1 > 0$). Using the natural logarithm properties and the fact that the natural logarithm is the inverse of the exponential function, solving for I_0 leads to

$$I_0 = \frac{\phi\,(1-\sigma\phi)\,e^{(\sigma\phi-1)t}}{1-\sigma\phi e^{(\sigma\phi-1)t}}, \tag{2.44}$$

where the condition $1 - \sigma\phi > 0$ is needed. Substituting the expression of (2.44) into $C_0 = \sigma\,(I_0 - \phi) + 1$, gives us that

$$C_0 = \frac{\sigma\phi\,(1-\sigma\phi)\,e^{(\sigma\phi-1)t}}{1-\sigma\phi e^{(\sigma\phi-1)t}} + 1 - \sigma\phi. \tag{2.45}$$

Hence, as $t \to \infty$, $I_0 \to 0$ and $C_0 \to 1 - \sigma\phi$. It turns out that the condition $1 - \sigma\phi > 0$ is needed in order to have enough vitamin C. During the initial adjustment, we are therefore able to see that approximately $\sigma\phi = \iota_0/c_0$ (the initial concentration of iodine per the initial concentration of vitamin C) of the initial quantity of the inhibitor C is used up.

Therefore, the asymptotic solutions in Region I are as follows:

$$I(t) = \frac{\phi\,(1-\sigma\phi)\,e^{-(1-\sigma\phi)t}}{1-\sigma\phi e^{-(1-\sigma\phi)t}} + O(\epsilon), \tag{2.46a}$$

$$C(t) = \frac{\sigma\phi\,(1-\sigma\phi)\,e^{-(1-\sigma\phi)t}}{1-\sigma\phi e^{-(1-\sigma\phi)t}} + 1 - \sigma\phi + O(\epsilon), \tag{2.46b}$$

$$P(t) = 1 + O(\epsilon). \tag{2.46c}$$

Region II: Induction

As the induction period begins, the two chemical reactions (2.3) and (2.4) keep the concentration of iodine (I) low. As iodide (D) is produced rapidly in the fast (second) chemical reaction (2.4), it removes iodine (I) from the system faster than it can be produced. Due to these two reactions, the concentrations of vitamin C (C) and hydrogen peroxide (P) are slowly being consumed. Thus, $I(t) = O(\epsilon)$ and $T = \epsilon t$ whereas C and P are still of order 1. We re-scale $\hat{I}(T) = I(T/\epsilon)/\epsilon$, with $\hat{C}(T) = C(T/\epsilon)$, $\hat{P}(T) = P(T/\epsilon)$, the system becomes

$$\epsilon\frac{d\hat{I}}{dT} = -\hat{I}\hat{C} + \rho\hat{P}\left(1 - 2\epsilon\hat{I}\right), \tag{2.47}$$

$$\frac{d\hat{C}}{dT} = -\sigma\hat{I}\hat{C}, \tag{2.48}$$

$$\frac{d\hat{P}}{dT} = -\sigma\hat{P}\left(1 - 2\epsilon\hat{I}\right). \tag{2.49}$$

Similar to Region I, looking for asymptotic expansions:

$$\hat{I} = \hat{I}_0 + \epsilon\hat{I}_1 + ..., \quad \hat{C} = \hat{C}_0 + \epsilon\hat{C}_1 + ..., \quad \text{and} \quad \hat{P} = \hat{P}_0 + \epsilon\hat{P}_1 + ..., \tag{2.50}$$

the leading order problem is at quasi-steady state:

$$\epsilon \frac{d\hat{I}_0}{dT} = 0, \tag{2.51a}$$

$$-\hat{I}_0\hat{C}_0 + \rho\hat{P}_0\left(1 - 2\epsilon\hat{I}_0\right) = 0, \tag{2.51b}$$

$$\hat{I}_0\hat{C}_0 = \rho\hat{P}_0\left(1 - 2\epsilon\hat{I}_0\right), \tag{2.51c}$$

and,

$$\frac{d\hat{C}_0}{dT} = -\sigma\hat{I}_0\hat{C}_0. \tag{2.52}$$

Substituting the expression (2.51c) in (2.52) gives

$$\frac{d\hat{C}_0}{dT} = -\sigma\left[\rho\hat{P}_0\left(1 - 2\epsilon\hat{I}_0\right)\right]. \tag{2.53}$$

The clock chemical reaction is small during the induction period ($\hat{I}_0 \approx 0$) giving

$$\frac{d\hat{C}_0}{dT} = -\sigma\rho\hat{P}_0, \tag{2.54}$$

$$\frac{d\hat{P}_0}{dT} = -\sigma\hat{P}_0. \tag{2.55}$$

Hence,

$$\frac{d\hat{C}_0}{d\hat{P}_0} = \rho, \tag{2.56}$$

using separation of variables

$$\int d\hat{C}_0 = \rho\int d\hat{P}_0. \tag{2.57}$$

Thus,

$$\hat{C_0} = \rho \hat{P_0} + b_1, \tag{2.58}$$

and,

$$\hat{P_0} = b_2 e^{-\sigma T}, \tag{2.59}$$

where b_1 and b_2 are constants that can be found by taking $T \to 0$ (using the initial condition), and matching to the Region I solution as $t \to \infty$:

$$b_1 = 1 - \sigma\phi - \rho, \tag{2.60}$$

$$b_2 = 1. \tag{2.61}$$

The variable $\hat{I_0}$ could be found from (2.51c), it follows

$$\hat{I_0} = \frac{\rho \hat{P_0}}{\hat{C_0}}. \tag{2.62}$$

Therefore, in the original dimensionless variables, the leading order solutions in Region II are as follows:

$$I(t) = \frac{\epsilon\rho e^{-\epsilon\sigma t}}{\rho e^{-\epsilon\sigma t} + (1 - \sigma\phi - \rho)} + O(\epsilon^2), \tag{2.63a}$$

$$C(t) = \rho e^{-\epsilon\sigma t} + (1 - \sigma\phi - \rho) + O(\epsilon), \tag{2.63b}$$

$$P(t) = e^{-\epsilon\sigma t} + O(\epsilon). \tag{2.63c}$$

The Region II solution provides a prediction for the time point at which the balance between fast and slow reactions changes, referred to as the switchover time.

Switchover Time:

When vitamin C becomes small, the fast reaction no longer dominates and t_{sw} can be defined as the solution of $C_0(t) = 0$ in (2.63b)). This leads to

$$t_{sw} = \frac{1}{\epsilon\sigma} \ln\left(\frac{\rho}{\rho + \sigma\phi - 1}\right). \tag{2.64}$$

We need the condition that $\rho > 1 - \sigma\phi$ (where $\rho = p_0/c_0$ and $\sigma\phi = \iota_0/c_0$), then the expression $\rho - (1 - \sigma\phi) = O(1)$ is assumed to be order 1. The amount of vitamin C left after region I (initial adjustment) is $1 - \sigma\phi$. Physically, $\rho > 1 - \sigma\phi$ means that there should be enough hydrogen peroxide (P) in the system to drive the vitamin C to zero.

In dimensional variables, recall,

$$t = \frac{t^*}{k_2 c_0}, \quad \rho = \frac{p_0}{c_0}, \quad \sigma = \frac{m_0}{c_0}, \quad \phi = \frac{\iota_0}{m_0}, \quad \text{and} \quad \epsilon = \frac{k_1}{k_2}. \tag{2.65}$$

The switchover time is consequently illustrated by,

$$t_{sw} = \frac{t^*}{k_2 c_0}, \quad \text{when} \quad t^* \to \frac{1}{\epsilon\sigma} \ln\left(\frac{\rho}{\rho + \sigma\phi - 1}\right), \tag{2.66}$$

hence (in dimensional variables),

$$t_{sw} = \frac{1}{k_1 m_0} \ln\left(\frac{p_0}{p_0 + \phi m_0 - c_0}\right). \tag{2.67}$$

Equation (2.67) states that enough hydrogen peroxide (p_0) and molecular iodine (m_0) must be provided initially to drive the vitamin C concentration (c_0) to zero before hydrogen peroxide runs out, i.e. $p_0 + \phi m_0 > c_0$. As the vitamin C concen-

tration (c_0) increases, the expression in the denominator $p_0 + \phi m_0 - c_0$ decreases, and therefore the switchover time (t_{sw}) increases logarithmically as the vitamin C concentration (c_0) grows. When vitamin C concentration (c_0) is small, the expression $p_0 + \phi m_0 - c_0$ is close to $p_0 + \phi m_0$, and the switchover time (t_{sw}) remains low. A large molecular iodine concentration (m_0) effectively slows the increase in the switchover time (t_{sw}). Thus, we are able to express the switchover time simply in terms of initial concentrations and the slow reaction rate. Significantly, a similar equation to the switchover time formula (2.67) was given in a recent study by Parra Cordova and Peña [40] through a quasi-steady argument with appropriate assumptions, without including the ϕm_0 term in the denominator.

Region III: Corner

Region III corresponds to the transition from the rapid color change during the induction period to the stable long-term state, where all reactants have settled. This phase occurs when the two reactions, both slow and fast, occur in similar magnitudes. The most appropriate structured balance is achieved when $I = C = O(\epsilon^{1/2})$ and $P = O(1)$ with the shifted time coordinate here being $\bar{t} = \epsilon^{-1/2}(\epsilon t - T_{sw})$. We re-scale $\bar{I} = \epsilon^{-1/2} I$, $\bar{C} = \epsilon^{-1/2} C$, and $\bar{P} = P$. Therefore, the Model HPL (2.11) takes the following form at the leading order terms of the asymptotic expansions,

$$\frac{d\bar{I}}{d\bar{t}} = -\bar{I}\bar{C} + \rho\bar{P}\left(1 - 2\epsilon^{1/2}\bar{I}\right), \tag{2.68}$$

$$\frac{d\bar{C}}{d\bar{t}} = -\sigma\bar{I}\bar{C}, \tag{2.69}$$

$$\frac{d\bar{P}}{d\bar{t}} = -\epsilon^{1/2}\sigma\bar{P}\left(1 - 2\epsilon^{1/2}\bar{I}\right). \tag{2.70}$$

As above, we look for asymptotic expansions:

$$\bar{I} = \bar{I}_0 + \epsilon^{1/2}\bar{I}_1 + ..., \quad \bar{C} = \bar{C}_0 + \epsilon^{1/2}\bar{C}_1 + ..., \quad \text{and} \quad \bar{P} = \bar{P}_0 + \epsilon^{1/2}\bar{P}_1 + ..., \tag{2.71}$$

and, the leading order problem is

$$\frac{d\bar{I}_0}{d\bar{t}} = -\bar{I}_0\bar{C}_0 + \rho\bar{P}_0, \tag{2.72a}$$

$$\frac{d\bar{C}_0}{d\bar{t}} = -\sigma\bar{I}_0\bar{C}_0, \tag{2.72b}$$

$$\frac{d\bar{P}_0}{d\bar{t}} = 0, \tag{2.72c}$$

hence, $\bar{P}_0 = b_5$ is a constant, which can be found by the matching condition of $P(T_{sw})$ to Region II yielding

$$b_5 = \frac{\rho + \sigma\phi - 1}{\rho}. \tag{2.73}$$

We also seek the lower order correction term for the variable $\bar{P}$:

$$\epsilon^{1/2}\frac{d\bar{P}_1}{dt} = -\epsilon^{1/2}\sigma\bar{P}_0, \tag{2.74}$$

$$\int d\bar{P}_1 = -\sigma\bar{P}_0 \int dt, \tag{2.75}$$

thus,

$$\bar{P}_1 = -\sigma b_5\bar{t} + b_8, \tag{2.76}$$

the constant $b_8 = 0$ by matching condition to Region II solutions, giving

$$\bar{P} = \bar{P}_0 + \epsilon^{1/2}\bar{P}_1, \tag{2.77}$$

$$= b_5 - \epsilon^{1/2}\sigma b_5 \bar{t}. \tag{2.78}$$

Now, multiplying (2.72a) by σ, and then subtracting (2.72b), it follows that

$$\sigma\frac{d\bar{I}_0}{d\bar{t}} - \frac{d\bar{C}_0}{d\bar{t}} = -\sigma\bar{I}_0\bar{C}_0 + \rho b_5 + \sigma\bar{I}_0\bar{C}_0 = \rho b_5. \tag{2.79}$$

Integrating both sides,

$$\sigma\bar{I}_0 = \bar{C}_0 + \rho b_5\bar{t} + b_6, \quad \text{where} \quad b_6 \quad \text{is a constant.} \tag{2.80}$$

Substituting the expression (2.80) in the equation (2.72b) gives

$$\frac{d\bar{C}_0}{d\bar{t}} = -\left(\bar{C}_0 + \rho b_5\bar{t} + b_6\right)\bar{C}_0. \tag{2.81}$$

Note that (2.81) is the Riccati equation [8, 13], which can be solved by seeking a solution of the form $\bar{C}_0 = u'/u$, which means satisfying

$$\bar{C}_0' = -\bar{C}_0^2 - \left(\rho b_5\bar{t} + b_6\right)\bar{C}_0. \tag{2.82}$$

Thus,

$$\frac{d}{d\bar{t}}\left(\frac{u'}{u}\right) = -\left(\rho b_5 \bar{t} + b_6 + \frac{u'}{u}\right)\frac{u'}{u}, \tag{2.83}$$

$$\frac{uu'' - u'^2}{u^2} = -\left(\frac{u'}{u}\right)^2 - \left(\rho b_5 \bar{t} + b_6\right)\left(\frac{u'}{u}\right), \tag{2.84}$$

$$\frac{u''}{u} - \left(\frac{u'}{u}\right)^2 = -\left(\frac{u'}{u}\right)^2 - \left(\rho b_5 \bar{t} + b_6\right)\left(\frac{u'}{u}\right), \tag{2.85}$$

leads to

$$u'' = -\left(\rho b_5 \bar{t} + b_6\right) u'. \tag{2.86}$$

Equation (2.86) is a second-order differential equation with the following solution

$$u' = \exp\left[-\int \left(\rho b_5 \bar{t} + b_6\right) d\bar{t}\right], \tag{2.87}$$

$$= \exp\left[-\bar{t}\left(\rho b_5 \frac{\bar{t}}{2} + b_6\right)\right], \tag{2.88}$$

and,

$$u = \int u', \tag{2.89}$$

$$= \int_0^{\bar{t}} \exp\left[-s\left(\rho b_5 \frac{s}{2} + b_6\right)\right] ds + b_7. \tag{2.90}$$

Recall $\bar{C}_0 = u'/u$, and hence

$$\bar{C}_0 = \frac{\exp\left[-\bar{t}\left(\rho b_5 \frac{\bar{t}}{2} + b_6\right)\right]}{\int_0^{\bar{t}} \exp\left[-s\left(\rho b_5 \frac{s}{2} + b_6\right)\right] ds + b_7}, \tag{2.91}$$

which can be expressed in terms of the error function (by completing the square) as

$$\bar{C}_0 = \frac{\sigma \exp\left[-\bar{t}\left(\rho b_5 \frac{\bar{t}}{2} + b_6\right)\right]}{\frac{\sqrt{\pi}}{2} \exp\left(b_6^2/(2\rho b_5)\right)\left[\mathrm{erf}\left(\frac{\rho b_5 \bar{t} + b_6}{\sqrt{2\rho b_5}}\right) + b_7\right]}. \tag{2.92}$$

For the simplicity of notation, we denote $f(\bar{t}) = \left(\rho b_5 \bar{t} + b_6\right)/(\sqrt{2\rho b_5})$. Using the asymptotic expansion form of the error function as follows

$$\mathrm{erf}(f(\bar{t})) \sim 1 - \frac{\exp\left(-f(\bar{t})^2\right)}{\sqrt{\pi}\, f(\bar{t})}\left(1 + O(f(\bar{t}))^{-2}\right), \quad \text{as} \quad \bar{t} \to \infty, \tag{2.93}$$

and the fact that it is an odd function: $\mathrm{erf}(f(\bar{t})) = -\mathrm{erf}(-f(\bar{t}))$ as $-\bar{t} \to \infty$, it follows

$$\mathrm{erf}(f(\bar{t})) = -1 - \frac{\exp\left(-f(\bar{t})^2\right)}{\sqrt{\pi}\, f(\bar{t})}\left(1 + O(f(\bar{t}))^{-2}\right), \quad \text{as} \quad \bar{t} \to -\infty. \tag{2.94}$$

Hence,

$$\exp\left(-f(\bar{t})^2\right) = \frac{\exp\left[-\bar{t}\left(\rho b_5 \frac{\bar{t}}{2} + b_6\right)\right]}{\exp\left(b_6^2/(2\rho b_5)\right)}, \tag{2.95}$$

therefore,

$$\bar{C}_0(\bar{t}) = \frac{\sigma \exp\left(-f(\bar{t})^2\right)}{\frac{\sqrt{\pi}}{2}\left[-1 - \frac{\exp(-f(\bar{t})^2)}{\sqrt{\pi}\, f(\bar{t})}\left(1 + O(f(\bar{t}))^{-2}\right) + b_7\right]}, \tag{2.96}$$

and we assume that $\bar{C}_0(\bar{t})$ tends to a non-zero limit since $f(\bar{t}) \to -\infty$ as $\bar{t} \to -\infty$, which means that $b_7 = 1$. Thus, the asymptotic behaviour is

$$\bar{C}_0(\bar{t}) = -2\sigma f(\bar{t})\left(1 + O(f(\bar{t}))^{-2}\right), \tag{2.97}$$

$$= -\sigma\sqrt{\frac{2}{\rho b_5}}\left(\rho b_5 \bar{t} + b_6\right)\left(1 + O(f(\bar{t}))^{-2}\right). \tag{2.98}$$

In the Region II variables, we have

$$C(T) = -\sigma\sqrt{2\rho b_5}\,T + \sqrt{2\rho b_5}\,\ln\left(\frac{\rho+\sigma\phi-1}{\rho}\right) - \sigma\sqrt{\frac{2}{\rho b_5}}\,\epsilon^{1/2}\,b_6 + O(\epsilon), \quad (2.99)$$

hence, the constant $b_6 = 0$ by matching to the region II solution. Therefore, the approximate solution (with $\bar{t} = \epsilon^{-1/2}(\epsilon t - T_{sw})$) in Region III can be written as

$$I(t) = \epsilon^{1/2}\,\frac{\exp\left(\frac{-\rho b_5}{2}\,\epsilon^{-1}\,(\epsilon t - T_{sw})^2\right)}{\frac{\sqrt{\pi}}{2}\left[\operatorname{erf}\left(\sqrt{\frac{\rho b_5}{2}}\,\epsilon^{-1/2}\,(\epsilon t - T_{sw})\right)+1\right]} + \frac{\rho b_5}{\sigma}\,(\epsilon t - T_{sw}) + O(\epsilon) \quad (2.100a)$$

$$C(t) = \epsilon^{1/2}\,\frac{\sigma\,\exp\left(\frac{-\rho b_5}{2}\,\epsilon^{-1}\,(\epsilon t - T_{sw})^2\right)}{\frac{\sqrt{\pi}}{2}\left[\operatorname{erf}\left(\sqrt{\frac{\rho b_5}{2}}\,\epsilon^{-1/2}\,(\epsilon t - T_{sw})\right)+1\right]} + O(\epsilon) \quad (2.100b)$$

$$P(t) = b_5 - \sigma b_5\,(\epsilon t - T_{sw}) + O(\epsilon). \quad (2.100c)$$

Region IV: Long-term State

Region IV illustrates the system's long-term behavior, indicating that solutions will gradually approach equilibrium over time, and some reactants are expected to remain even after the reaction reaches its end point. We will address the long-term analysis, in which $I(t) = O(1)$ and $t = O(\epsilon^{-1})$. Denoting, $\breve{I}(T) = I(T/\epsilon)$, with

$\breve{C}(T) = C(T/\epsilon)$, and $\breve{P}(T) = P(T/\epsilon)$, thus, the system becomes

$$\epsilon \frac{d\breve{I}}{dT} = -\breve{I}\breve{C} + \epsilon\rho\breve{P}\left(1 - 2\breve{I}\right), \tag{2.101}$$

$$\epsilon \frac{d\breve{C}}{dT} = -\sigma\breve{I}\breve{C}, \tag{2.102}$$

$$\epsilon \frac{d\breve{P}}{dT} = -\epsilon\sigma\breve{P}\left(1 - 2\breve{I}\right). \tag{2.103}$$

Seeking asymptotic expansions, again

$$\breve{I} = \breve{I}_0 + \epsilon\breve{I}_1 + \epsilon^2\breve{I}_2 + ..., \quad \breve{C} = \breve{C}_0 + \epsilon\breve{C}_1 + \epsilon^2\breve{C}_2 + ..., \quad \text{and} \quad \breve{P} = \breve{P}_0 + \epsilon\breve{P}_1 + \epsilon^2\breve{P}_2 + ... \tag{2.104}$$

We must have that $\breve{I}_0\breve{C}_0 = 0$, and hence $\breve{C}_0 = 0$, and moreover at $O(\epsilon^n)$

$$\frac{d\breve{C}_{n-1}}{dT} = -\sigma\left(\breve{I}_0\breve{C}_n + ... + \breve{I}_n\breve{C}_0\right). \tag{2.105}$$

By induction it follows that $\breve{C}_0$ for all n (we will provide this proof in more detail in Chapter 4). Hence,

$$\frac{d\breve{I}}{dT} = \rho\breve{P}\left(1 - 2\breve{I}\right), \tag{2.106a}$$

$$\frac{d\breve{P}}{dT} = -\sigma\breve{P}\left(1 - 2\breve{I}\right), \tag{2.106b}$$

and,

$$\frac{d\breve{I}}{d\breve{P}} = \frac{\rho}{-\sigma}, \tag{2.107}$$

which has the solution,

$$\breve{I} = \frac{-\rho}{\sigma}\breve{P} + b_3, \tag{2.108}$$

b_3 being a constant. The matching condition $\breve{I}(T) \to 0$ as $T \to T_{sw}$ (where $T_{sw} = -(\ln(\rho + \sigma\phi - 1) - \ln\rho)/\sigma$) yields

$$b_3 = \frac{\rho}{\sigma} e^{-\sigma T_{sw}}. \tag{2.109}$$

By substituting (2.108) into (2.106b), therefore

$$\frac{d\breve{P}}{dT} = -\sigma\breve{P}\left[1 - \frac{2\rho}{\sigma}\left(e^{-\sigma T_{sw}} - \breve{P}\right)\right], \tag{2.110}$$

$$= \breve{P}\left[-2\rho\breve{P} + \sigma(2b_3 - 1)\right], \tag{2.111}$$

by using the separation of variables gives

$$\int \frac{d\breve{P}}{\breve{P}\left(-2\rho\breve{P} + \sigma(2b_3 - 1)\right)} = \int dT, \tag{2.112}$$

the left-hand side (LHS) can be solved using the partial fraction decomposition, which leads to

$$\frac{-1}{\sigma(2b_3 - 1)} \ln\left|\frac{\sigma(2b_3 - 1)}{\breve{P}} - 2\rho\right| = T + b_4, \tag{2.113}$$

where b_4 is a constant. Hence, the definition for the absolute value of the function $\left|\frac{\sigma(2b_3-1)}{\breve{P}} - 2\rho\right|$ is given by

$$\left|\frac{\sigma(2b_3 - 1)}{\breve{P}} - 2\rho\right| = \begin{cases} \left(\frac{\sigma(2b_3-1)}{\breve{P}} - 2\rho\right), & \text{if} \quad \left(\frac{\sigma(2b_3-1)}{\breve{P}} - 2\rho\right) \geq 0 \\ -\left(\frac{\sigma(2b_3-1)}{\breve{P}} - 2\rho\right), & \text{if} \quad \left(\frac{\sigma(2b_3-1)}{\breve{P}} - 2\rho\right) < 0 \end{cases} \tag{2.114}$$

Note that $\left(\frac{\sigma(2b_3-1)}{\breve{P}} - 2\rho\right) < 0$ since $\frac{\sigma(2b_3-1)}{\breve{P}} < -2\rho < 0$, it follows that

$|\frac{\sigma(2b_3-1)}{\breve{P}} - 2\rho| = -\left(\frac{\sigma(2b_3-1)}{\breve{P}} - 2\rho\right)$. Using the natural logarithm properties and the fact that the natural logarithm is the inverse of the exponential function, gives

$$\frac{-\sigma\left(2b_3-1\right)+2\rho\breve{P}}{\breve{P}} = e^{-\sigma(2b_3-1)(T+b_4)}, \tag{2.115}$$

and then solving for $\breve{P}$ gives

$$\breve{P} = \frac{-\sigma\left(2b_3-1\right)}{e^{-\sigma(2b_3-1)(T+b_4)} - 2\rho}. \tag{2.116}$$

The constant b_4 can be found by the matching condition $\breve{P}(T) \to e^{-\sigma T_{sw}}$ as $T \to T_{sw}$ yielding

$$b_4 = \frac{-1}{\sigma\left(2b_3-1\right)} \ln\left(\frac{-\sigma\left(2b_3-1\right)}{e^{-\sigma T_{sw}}} + 2\rho\right) - T_{sw}. \tag{2.117}$$

In the original variables, the leading order solutions in Region IV are as follows:

$$I(t) = \frac{-\rho}{\sigma}\left[\frac{-\sigma\left(2b_3-1\right)}{e^{-\sigma(2b_3-1)(\epsilon t+b_4)} - 2\rho}\right] + b_3 + O(\epsilon), \tag{2.118a}$$

$$C(t) = 0 + O(\epsilon^n) \quad \text{for all} \quad n > 0, \tag{2.118b}$$

$$P(t) = \frac{-\sigma\left(2b_3-1\right)}{e^{-\sigma(2b_3-1)(\epsilon t+b_4)} - 2\rho} + O(\epsilon). \tag{2.118c}$$

Comparison Of Asymptotic And Numerical Approximations

To validate the asymptotic solutions in each region, Matlab (*ode45* solver) was used to calculate a numerical solution with initial conditions $I(0) = \phi$, $C(0) = 1$, and $P(0) = 1$, and the dimensionless parameter values set to $\rho = 2$, $\sigma = 0.8$, $\phi = 0.2$ (iodide: iodine ratio) and $\epsilon = 0.001$ (the reaction rate ratio), these values

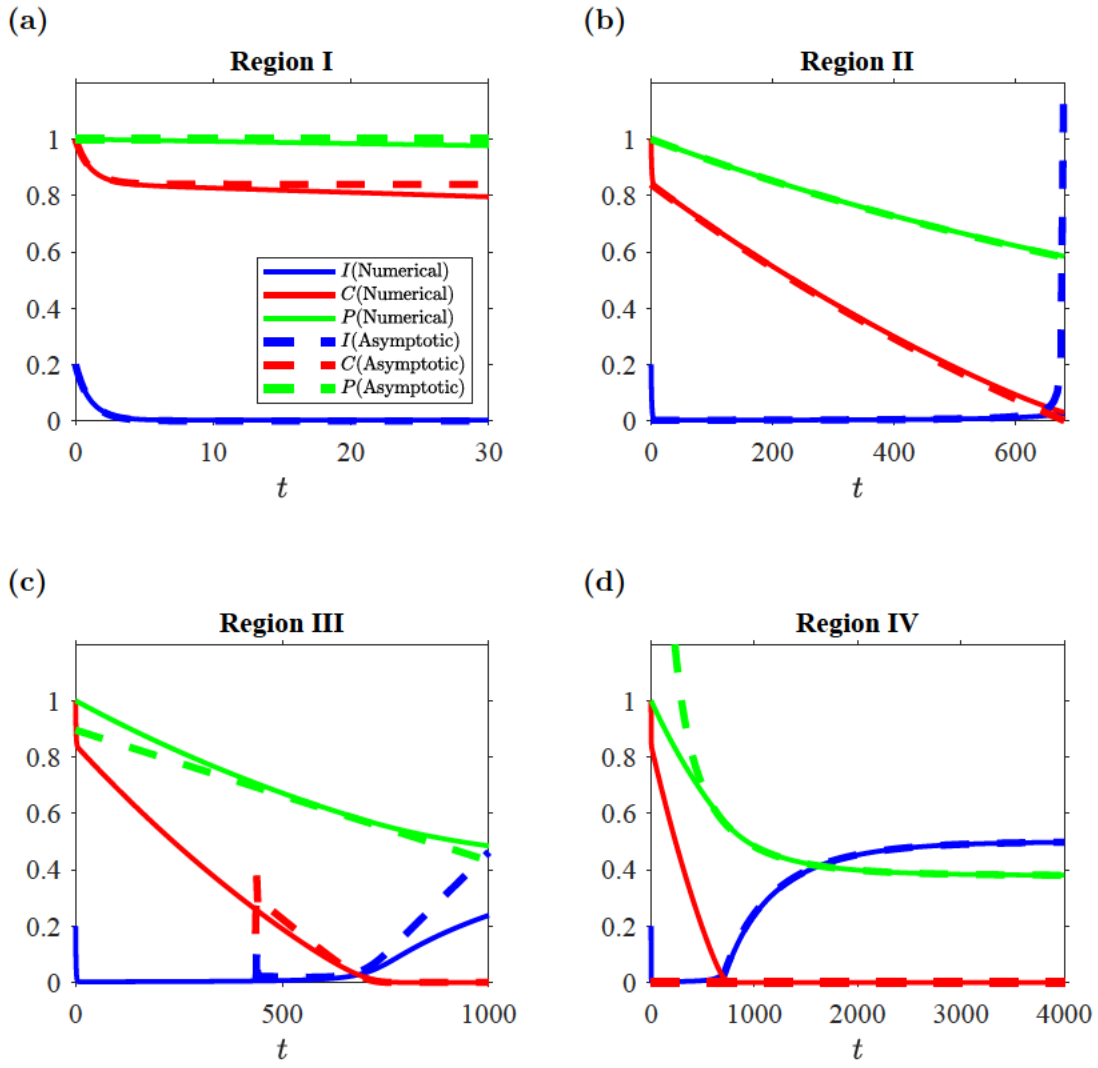

Figure 2.4: Comparison between numerical and asymptotic solutions of the model (2.11) with initial conditions $I(0) = \phi$, $C(0) = 1$ and $P(0) = 1$, and the dimensionless parameter values are $\rho = 2$, $\sigma = 0.8$, $\phi = 0.2$ and $\epsilon = 0.001$. (a) Region I, (b) Region II, (c) Region III, (d) Region IV.

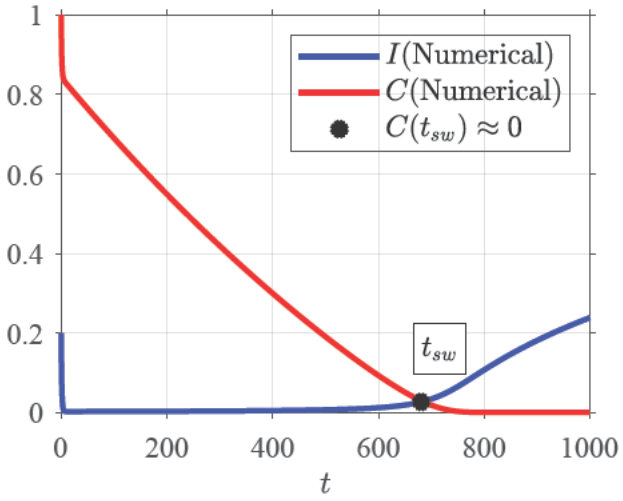

Figure 2.5: Numerical solutions for $C(t)$ and $I(t)$ of the model (2.11) shown alongside the value of the switchover time (intersecting point) calculated by the approximate formula (2.64), with initial conditions $P(0) = 1$, $C(0) = 1$ and $I(0) = \phi$, and the dimensionless parameter values are $\rho = 2$, $\sigma = 0.8$, $\phi = 0.2$ and $\epsilon = 0.001$.

are chosen arbitrarily. A comparison of the asymptotic and numerical solution of the model (2.11) is shown in Figure 2.4. The Region I solutions follow the numerical approximation very closely up to around $t = 30$. The Region II solution then follows the numerical solution up to around $t = 600$. At the end of Region II (induction period), the switchover time point occurs when the concentration of the clock chemical reaction iodine (I) increases after the concentration of vitamin C (C) has been used (around $t = 680$), the blow up of the iodine concentration (I) appears as a nearly vertical dashed line in Figure 2.4b. The Region III solution then closely follows the numerical solution around the switchover time $t = 680$, up to around $t = 800$. After that, the asymptotic and numerical solutions are in excellent agreement in Region IV. Furthermore, the matching between the numerical and asymptotic solutions improves for smaller values of ϵ (examples not shown for brevity).

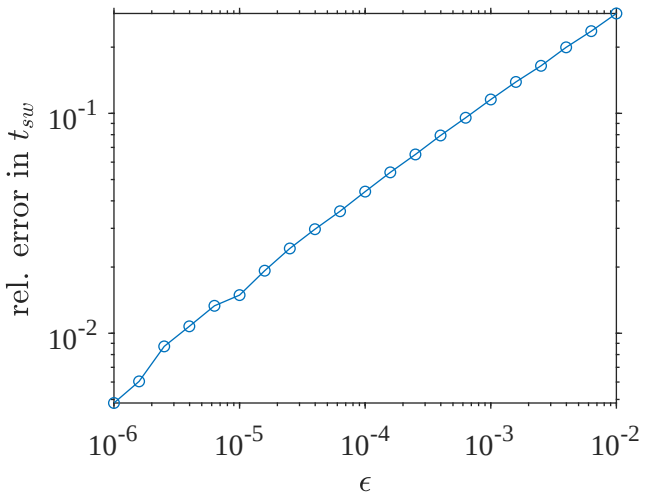

Figure 2.6: Relative error between the asymptotic approximation for switchover time formula (2.64) of the model (2.11) and the point at which the numerical solution falls below a threshold value of ϵ, as a function of the parameter ϵ. The dimensionless parameter values are $\rho = 2$, $\sigma = 0.8$ and $\phi = 0.2$.

Figure 2.5 shows that the approximate switchover time (t_{sw}) matches the intersecting point of the numerical solution of the model (2.11) for I and C well. Figure 2.6 plots the relative error between the asymptotic approximation of the switchover time formula (2.64) and the switchover time point computed from the numerical solution of the model (2.11), as a function of ϵ. A log-log plot provides an estimate for the order of the error in ϵ. Specifically, the relative errors have been calculated by

$$\frac{|t_{num} - t_{asymp}|}{t_{asymp}},$$

where t_{num} is the switchover time point computed from the numerical solution of the model (2.11) and t_{asymp} is the switchover time formula derived through asymptotic analysis, given in (2.64). The convergence of the error as $\epsilon \to 0$ is approximately sublinear, and the gradient on a log-log scale approaches approxi-

mately 0.5 (can be calculated based on the last two points of smaller ϵ values from the log-log plot using MATLAB).

2.5 Conclusion

This chapter discussed and analysed the simple clock reaction (fast and slow) model by extending the work of Kerr et al. [27], to include hydrogen peroxide in the model explicitly and assuming that the rate of the slow reaction is linear in both iodine and hydrogen peroxide concentrations based on experimental findings in this regime [16]. The asymptotic solutions and numerical simulations showed good agreement within the specified time regions. Furthermore, we developed a switchover time formula to identify the key event when the clock reaction occurs and the dark blue appears. The formula can be viewed as a refinement of a result contained in the recent paper of Parra Cordova and Peña [40], additionally taking account of the effect of the initial molecular iodine level.

The next chapter will explore how the hydrogen peroxide levels influence whether the slow reaction kinetics are effectively quadratic or linear. To gain insight into this process, we analyse the slow reaction in isolation.

Chapter 3

Model ISR: Slow Reaction Model In Isolation With Moderate and High Hydrogen Peroxide

3.1 Motivation

As previously described, recent work by Kerr et al. [27] conducted the clock reaction experiments using concentrations of hydrogen peroxide (P) in great excess compared to the other reactants. The authors showed that a mathematical model where the slow reaction rate was proportional to D^2 matched the data (using the law of mass action, rate $\propto D^2$). However, Copper and Koubek [16] found linear kinetics in experiments with moderate hydrogen peroxide (P) concentration (due to the rate-limiting step in the slow reaction, the rate $\propto DP$). This chapter will address the question of when the chemical slow reaction converting iodide to iodine should be quadratic in iodide or linear and the potential role of hydrogen peroxide

concentration. By focusing on the slow reaction in more detail, we demonstrate how the order of the ratio of hydrogen peroxide to iodide determines when linear kinetics apply and when quadratic kinetics apply. As a result, when the ratio of hydrogen peroxide to iodide is order 1, then the rate of change of iodine (I) is linear in terms of the concentration of hydrogen peroxide (P) and iodide (D). When the ratio of hydrogen peroxide to iodide is order ϵ^{-1} then the overall iodide to iodine reaction will emerge as being quadratic.

3.2 Extended Model Formulation For The Slow Reaction

As stated in Chapter 2, there are two chemical reactions that occur in the vitamin C clock reaction: the slow reaction when iodide ions are converted to iodine molecules in the presence of hydrogen peroxide, and the fast reaction when vitamin C (*the inhibitor*) converts iodine to iodide. The main objective of this chapter is to investigate the slow reaction in isolation and break this down in more detail to understand the effect of hydrogen peroxide concentration on kinetics. We consider the modified iodine clock reaction described by [16] for the slow (first) reaction (2.1),

$$2H^+ + 2I^- + H_2O_2 \rightarrow I_2 + 2H_2O, \tag{3.1}$$

which is a result of the following pair of chemical reactions:

$$I^- + H_2O_2 \xrightarrow{k_3} HOI + OH^-, \tag{3.2a}$$

$$I^- + HOI \xrightarrow{k_4} I_2 + OH^-. \tag{3.2b}$$

We will focus on particular reactants that are essential to the slow chemical reaction, (3.2), in order to construct our model. In the chemical reaction (3.2a), the total concentration of iodide (I^-) at time t, denoted by $D(t)$ in the model, is converted to hypoiodous acid (HOI), denoted by $Q(t)$, in the presence of hydrogen peroxide (H_2O_2), denoted by $P(t)$, at a rate given by k_3DP. The parameter k_3 is named as the nucleophilic attack rate [16]. In the second chemical reaction (3.2b), the iodide (I^-), denoted by $D(t)$, is converted to iodine (I_2), denoted by $I(t)$, in the presence of hypoiodous acid (HOI), denoted by $Q(t)$, at a rate given by k_4DQ. Based on [16] we infer that $k_3 \ll k_4$ and so step (3.2a) is rate limiting in the overall reaction unless the concentration of hydrogen peroxide is increased to compensate. Our hypothesis, which we will assess through mathematical modelling, is that the rate limiting nature of (3.2a) in the situation of moderate hydrogen peroxide results in overall linear rate kinetics, whereas when the hydrogen peroxide concentration is much greater than other reactants, both steps (i.e., (3.2a) and (3.2b)) are important in governing the overall rate, resulting in the quadratic kinetics that would follow from applying the law of mass action to the overall reaction $2I^- + H_2O_2 \rightarrow I_2 + 2OH^-$. We, therefore, have in simplified form,

$$D + P \xrightarrow{k_3DP} Q, \tag{3.3a}$$

$$D + Q \xrightarrow{k_4DQ} I. \tag{3.3b}$$

Several studies have investigated the chemical reactions (3.2) [4, 5, 30, 34, 45, 46, 57]. It has been found that hypoiodous acid (HOI) can be transformed by three pathways:

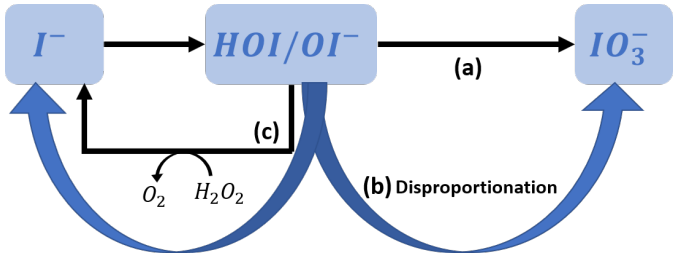

Figure 3.1: Schematic diagram of the transformation pathways of hypoiodous acid (HOI): (a) oxidation to iodate (IO_3^-), (b) disproportionation to iodide (I^-) and (IO_3^-) and (c) reduction to (I^-) by hydrogen peroxide (H_2O_2), adapted from [45].

(a) oxidation to iodate (IO_3^-) which is the iodine oxoanion,

(b) disproportionation to iodide (I^-) and iodate (IO_3^-),

(c) reduction to iodide (I^-) by hydrogen peroxide (H_2O_2).

Figure 3.1 represents a diagram of the transformation pathways of iodide and hypoiodous acid. In this study, we are not interested in iodate (IO_3^-), so we consider only the third transformation pathway, where hypoiodous acid (HOI) reduces to iodide (I^-) by hydrogen peroxide (H_2O_2), which is the reverse reaction as described in [45]:

$$HOI + H_2O_2 \rightarrow I^-. \tag{3.4}$$

In the reverse chemical reaction (3.4), the total concentration of hypoiodous acid (HOI) at time t, denoted by $Q(t)$, is converted to the iodide (I^-), denoted by $D(t)$, in the presence of hydrogen peroxide (H_2O_2), denoted by $P(t)$, at a rate given by k_5QP. The simplified form is

$$Q + P \xrightarrow{k_5QP} D. \tag{3.5}$$

Thus, the slow (first) chemical reaction (2.1) is a combination of (3.2) and (3.4), given by

$$D + P \xrightarrow{k_3 DP} Q, \tag{3.6a}$$

$$D + Q \xrightarrow{k_4 DQ} I, \tag{3.6b}$$

$$Q + P \xrightarrow{k_5 QP} D. \tag{3.6c}$$

Based on the above formulations and applying the law of mass action to (3.6), the model is given by the following system of nonlinear differential equations (named Model ISR referring to isolated slow reaction):

$$\frac{dD}{dt} = -k_3 DP - k_4 DQ + k_5 QP, \tag{3.7a}$$

$$\frac{dP}{dt} = -k_3 DP - k_5 QP, \tag{3.7b}$$

$$\frac{dQ}{dt} = k_3 DP - k_4 DQ - k_5 QP, \tag{3.7c}$$

$$\frac{dI}{dt} = k_4 DQ, \tag{3.7d}$$

with initial conditions

$$D(0) = d_0, \quad P(0) = p_0, \quad Q(0) = q_0, \quad I(0) = \iota_0. \tag{3.8}$$

We observe that the three equations ((3.7a), (3.7c), (3.7d)) for iodide, hypoiodous acid and iodine yield the following conservation law,

$$\frac{d}{dt}\left(D + Q + 2I\right) = 0. \tag{3.9}$$

We deduce that $D(t)+Q(t)+2I(t)$ is conserved. We represent the total concentration of iodine atoms in the reaction by $n_0 = d_0 + q_0 + 2\iota_0$. Hence, the variable $I(t)$ will be eliminated from the model (3.7) by substituting $I(t) = 1/2\big[n_0 - D(t) - Q(t)\big]$ into (3.7), thus the Model ISR can be reduced to

$$\frac{dD}{dt} = -k_3 DP - k_4 DQ + k_5 QP, \tag{3.10a}$$
$$\frac{dP}{dt} = -k_3 DP - k_5 QP, \tag{3.10b}$$
$$\frac{dQ}{dt} = k_3 DP - k_4 DQ - k_5 QP. \tag{3.10c}$$

It is instructive to non-dimensionalize the system by choosing the following scalings (in particular, we choose the timescale based on the final step producing iodine),

$$D = n_0 D^*, \quad P = p_0 P^*, \quad Q = n_0 Q^*, \quad t = \frac{t^*}{k_4 n_0}, \tag{3.11}$$

where $*$ denotes a dimensionless quantity. Substituting (3.11) into (3.10) leads to the dimensionless system,

$$\frac{dD^*}{dt^*} = -\epsilon\alpha D^* P^* - D^* Q^* + \epsilon\beta\alpha Q^* P^*, \tag{3.12a}$$
$$\frac{dP^*}{dt^*} = -\epsilon D^* P^* - \epsilon\beta Q^* P^*, \tag{3.12b}$$
$$\frac{dQ^*}{dt^*} = \epsilon\alpha D^* P^* - D^* Q^* - \epsilon\beta\alpha Q^* P^*, \tag{3.12c}$$

where the dimensionless parameters are

$$\epsilon = \frac{k_3}{k_4}, \quad \epsilon\beta = \frac{k_5}{k_4} \quad \text{and} \quad \alpha = \frac{p_0}{n_0}. \tag{3.13}$$

As mentioned earlier that $k_3 \ll k_4$, the reaction converting iodide (D) to hypoiodous acid (Q) is much slower than the reaction converting iodide (D) to iodine (I), therefore, $\epsilon \ll 1$. The parameter β is order 1, and the magnitude of the parameter α determines whether the situation is moderate or high hydrogen peroxide. The initial conditions become

$$D^*(0) = d_0^*, \quad P^*(0) = 1, \quad Q^*(0) = q_0^*, \tag{3.14}$$

with

$$d_0^* = \frac{d_0}{n_0}, \quad q_0^* = \frac{q_0}{n_0}. \tag{3.15}$$

We consider the specific situation in which all the initial substrate is in the iodide (D) form and the product (I) and intermediate (Q) are absent. Thus, $N_0 \approx D_0$, and it follows that $D^*(0) = 1$ and $Q^*(0) = 0$, and hence $\alpha = p_0/d_0$. Figure 3.2 shows the numerical simulation of the model (3.12) with different values of ϵ.

From this point forward, we drop stars for ease of notation. The primary distinction between the HPL Model (2.11) (stated in Chapter 2) and the ISR Model (3.12) is that the HPL Model explicitly incorporates hydrogen peroxide at moderate concentrations of the simple clock reaction (slow and fast reactions), while the ISR Model is structured to examine the affects of hydrogen peroxide on kinetics by analyzing the slow reaction in isolation. One of the main objectives of this study is to demonstrate how numerical simulations and asymptotic analysis can reveal the key features of a chemical reaction model and lead to a simplified model that captures the observed dynamics of the full chemical reaction model. In Section 3.3, we will study the situation of moderate hydrogen peroxide concentration and, in Section 3.4, the high hydrogen peroxide concentration to determine the overall

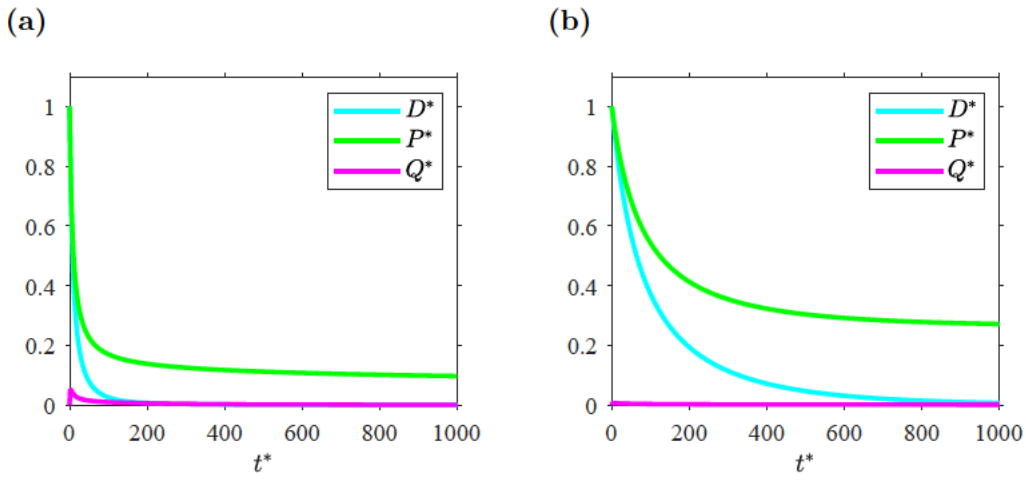

Figure 3.2: Numerical simulation for the model (3.12) of the moderate hydrogen peroxide case with initial conditions $D^*(0) = 1$, $P^*(0) = 1$ and $Q^*(0) = 0$, and dimensionless parameter values $\alpha = 0.7$ and $\beta = 0.9$. (a) with $\epsilon = 0.1$, and (b) with $\epsilon = 0.01$.

effective kinetics. Briefly, the ratio of the initial concentration of hydrogen peroxide to the initial concentration of iodide (i.e., $\alpha = p_0/d_0$) for the model (3.12) will be studied: (1) when hydrogen peroxide (p_0) is similar in concentration to iodide (d_0), so $\alpha = O(1)$, and (2) when there is an excess of hydrogen peroxide (p_0), so $\alpha = O(\epsilon^{-1})$. More details are given in the following sections.

3.3 Case 1 (when $\alpha = O(1)$):

In this section, we will study the qualitative analysis for the model (3.12) when initial hydrogen peroxide (P) is similar in concentration to iodide (D), so $\alpha = p_0/d_0 = O(1)$. Since $Q(0) = 0$ and we can see in Figure 3.2 that $Q(t)$ remains low, this motivates us to initially scale $Q = \epsilon\tilde{Q}$, where $\tilde{Q} = O(1)$. Looking at the equation (3.12c), the positive term is $O(\epsilon)$ and the negative terms are linear in Q,

so if Q starts at 0 then it would be expected to be no larger than $O(\epsilon)$. In addition, Figure 3.2 illustrates that hydrogen peroxide (P) concentration is decreasing to stay low whereas iodide (D) concentration is decreasing, eventually, going to zero.

3.3.1 Asymptotic Analysis

As in Chapter 2, we will apply the technique of matched asymptotic expansion to construct approximate solutions of the model (3.12).

Region I: Initial Adjustment

The first region can be described as where the independent variable t is order 1 ($t = O(1)$), the dependent variables D, P are order 1, and Q is order ϵ ($D, P = O(1)$ and $Q = O(\epsilon)$, so $Q = \epsilon\tilde{Q}$). It follows that the model (3.12) with variables rescaled, the system in Region I, takes the form

$$\frac{dD}{dt} = -\epsilon\alpha DP - \epsilon D\tilde{Q} + \epsilon^2\beta\alpha\tilde{Q}P, \tag{3.16a}$$

$$\frac{dP}{dt} = -\epsilon DP - \epsilon^2\beta\tilde{Q}P, \tag{3.16b}$$

$$\epsilon\frac{d\tilde{Q}}{dt} = \epsilon\alpha DP - \epsilon D\tilde{Q} - \epsilon^2\beta\alpha\tilde{Q}P. \tag{3.16c}$$

Seeking a solution of the form (asymptotic expansions):

$$D = D_0+\epsilon D_1+\epsilon^2 D_2+..., \quad P = P_0+\epsilon P_1+\epsilon^2 P_2+..., \quad \text{and} \quad \tilde{Q} = \tilde{Q}_0+\epsilon\tilde{Q}_1+\epsilon^2\tilde{Q}_2+..., \tag{3.17}$$

we find that at the leading order,

$$\frac{dD_0}{dt} = 0, \tag{3.18a}$$

$$\frac{dP_0}{dt} = 0, \tag{3.18b}$$

$$\frac{d\tilde{Q}_0}{dt} = \alpha D_0 P_0 - D_0 \tilde{Q}_0, \tag{3.18c}$$

with the initial conditions:

$$D_0(0) = 1 \quad P_0(0) = 1 \quad \text{and} \quad \tilde{Q}_0(0) = 0. \tag{3.19}$$

Equations (3.18a) and (3.18b) combined with the initial conditions (3.19) immediately yield

$$D_0 = 1 \quad \text{and} \quad P_0 = 1 \quad \text{for all} \quad t. \tag{3.20}$$

By substituting (3.20) into (3.18c), we obtain

$$\frac{d\tilde{Q}_0}{dt} = \alpha - \tilde{Q}_0. \tag{3.21}$$

Using the separation of variables method with the initial conditions in (3.19) gives

$$\tilde{Q}_0 = \alpha \left(1 - e^{-t}\right). \tag{3.22}$$

Therefore, the asymptotic solutions in Region I are as follows:

$$D(t) = 1 + O(\varepsilon), \tag{3.23a}$$

$$P(t) = 1 + O(\varepsilon), \tag{3.23b}$$

$$\tilde{Q}(t) = \alpha\left(1 - e^{-t}\right) + O(\varepsilon). \tag{3.23c}$$

It is clear from equation (3.22) that $\tilde{Q}_0$ rapidly approaches α, corresponding to balance (quasi-equilibrium) in the production and removal of $\tilde{Q}$ at leading order. Hence, as $t \to \infty$, $D_0 \to 1$, $P_0 \to 1$ and $\tilde{Q}_0 \to \alpha$. In terms of the chemical species in Region I, we are seeing the establishment of a quasi-equilibrium before the slower process of conversion of D to I can take place in multi-step reactions (3.6).

Region II: Long-term Behaviour

The conversion of D to I takes place on a longer timescale $O(1/\epsilon)$; we refer to this process as Region II. We will address the long-term analysis for the model (3.12), in which $t = O(\epsilon^{-1})$. Denoting, $\tau = \epsilon t$ with $\breve{D}(\tau) = D(\tau/\epsilon)$, $\breve{P}(\tau) = P(\tau/\epsilon)$, and $\breve{Q}(\tau) = \tilde{Q}(\tau/\epsilon)$ where $\tilde{Q} = \epsilon^{-1}Q$, the system becomes

$$\epsilon\frac{d\breve{D}}{d\tau} = -\epsilon\alpha\breve{D}\breve{P} - \epsilon\breve{D}\breve{Q} + \epsilon^2\beta\alpha\breve{Q}\breve{P}, \tag{3.24a}$$

$$\epsilon\frac{d\breve{P}}{d\tau} = -\epsilon\breve{D}\breve{P} - \epsilon^2\beta\breve{Q}\breve{P}, \tag{3.24b}$$

$$\epsilon^2\frac{d\breve{Q}}{d\tau} = \epsilon\alpha\breve{D}\breve{P} - \epsilon\breve{D}\breve{Q} - \epsilon^2\beta\alpha\breve{Q}\breve{P}. \tag{3.24c}$$

Again, seeking a solution in the form of the asymptotic expansions:

$$\breve{D} = \breve{D}_0 + \epsilon\breve{D}_1 + ..., \quad \breve{P} = \breve{P}_0 + \epsilon\breve{P}_1 + ..., \quad \text{and} \quad \breve{Q} = \breve{Q}_0 + \epsilon\breve{Q}_1 + ..., \tag{3.25}$$

we find that at leading order,

$$\frac{d\breve{D}_0}{d\tau} = -\alpha\breve{D}_0\breve{P}_0 - \breve{D}_0\breve{Q}_0, \tag{3.26a}$$

$$\frac{d\breve{P}_0}{d\tau} = -\breve{D}_0\breve{P}_0, \tag{3.26b}$$

$$0 = \alpha\breve{D}_0\breve{P}_0 - \breve{D}_0\breve{Q}_0. \tag{3.26c}$$

Solving (3.26c) for $\breve{Q}_0$ gives

$$\breve{Q}_0 = \alpha\breve{P}_0, \tag{3.27}$$

and substituting (3.27) into (3.26a) yields

$$\frac{d\breve{D}_0}{d\tau} = -2\alpha\breve{D}_0\breve{P}_0, \tag{3.28}$$

and, hence, dividing (3.28) by (3.26b) yields

$$\frac{d\breve{D}_0}{d\breve{P}_0} = 2\alpha. \tag{3.29}$$

By matching to Region I solutions in (3.23) to find the constant of integration, we have,

$$\breve{D}_0 = 2\alpha\breve{P}_0 + (1 - 2\alpha)\,. \tag{3.30}$$

Substituting (3.30) into (3.26b) yields

$$\frac{d\breve{P}_0}{d\tau} = -\breve{P}_0 \left[2\alpha\breve{P}_0 + (1-2\alpha)\right]. \tag{3.31}$$

The equation (3.31) has two equilibria

$$\breve{P}_0 = 0 \quad \text{and} \quad \breve{P}_0 = 1 - \frac{1}{2\alpha}. \tag{3.32}$$

We are interested in the equilibrium $\breve{P}_0 = 1 - 1/2\alpha$ which is asymptotically stable when the slope of the equation (3.31) at the equilibrium $\breve{P}_0 = 1 - 1/2\alpha$ is negative (i.e., $(1-2\alpha) < 0$ if $\alpha > 1/2$). Equation (3.31) has the following solution

$$\frac{1}{(1-2\alpha)} \ln \left| \frac{2\alpha\breve{P}_0 + (1-2\alpha)}{\breve{P}_0} \right| = \tau + c_5, \tag{3.33}$$

and the constant of integration can be determined from the matching condition ($c_5 = 0$). We constrain $\alpha > 1/2$, then we note that the term in the modulus sign starts out positive when $\breve{P}_0 = 1$ and remains positive until the asymptotically stable equilibrium $\breve{P}_0 = 1 - 1/2\alpha$ is reached. We can therefore restrict to the positive case only. It yields

$$\left| \frac{2\alpha\breve{P}_0 + (1-2\alpha)}{\breve{P}_0} \right| = \frac{2\alpha\breve{P}_0 + (1-2\alpha)}{\breve{P}_0} \quad \text{if} \quad \alpha > 1/2, \tag{3.34}$$

and, hence,

$$\ln \left(\frac{2\alpha\breve{P}_0 + (1-2\alpha)}{\breve{P}_0} \right) = (1-2\alpha)\,\tau, \tag{3.35}$$

or equivalently

$$\frac{2\alpha\breve{P}_0 + (1-2\alpha)}{\breve{P}_0} = e^{(1-2\alpha)\tau}. \tag{3.36}$$

Solving for $\breve{P}_0$ (where $\alpha > 1/2$) yields

$$\breve{P}_0 = \frac{(2\alpha-1)}{2\alpha - e^{-(2\alpha-1)\tau}}. \tag{3.37}$$

Now, substituting (3.37) back into (3.30) and (3.27) to find $\breve{D}_0$ and $\breve{Q}_0$:

$$\breve{D}_0 = \frac{2\alpha\,(2\alpha-1)}{2\alpha - e^{-(2\alpha-1)\tau}} - (2\alpha-1)\,, \tag{3.38a}$$

$$\breve{Q}_0 = \frac{\alpha\,(2\alpha-1)}{2\alpha - e^{-(2\alpha-1)\tau}}. \tag{3.38b}$$

Therefore, the asymptotic solutions in Region II are as follows:

$$\breve{D}(\tau) = \frac{2\alpha\,(2\alpha-1)}{2\alpha - e^{-(2\alpha-1)\tau}} - (2\alpha-1) + O(\varepsilon), \tag{3.39a}$$

$$\breve{P}(\tau) = \frac{(2\alpha-1)}{2\alpha - e^{-(2\alpha-1)\tau}} + O(\varepsilon), \tag{3.39b}$$

$$\breve{Q}(\tau) = \frac{\alpha\,(2\alpha-1)}{2\alpha - e^{-(2\alpha-1)\tau}} + O(\varepsilon). \tag{3.39c}$$

Hence, if $\alpha > 1/2$, then as $\tau \to \infty$: $\breve{D}_0 \to 0$, $\breve{P}_0 \to (2\alpha-1)/2\alpha$, and $\breve{Q}_0 \to (2\alpha-1)/2$, which means once the iodide (D) is exhausted, then the slow chemical reaction (3.6) can no longer occur as there is no remaining reactant.

Significantly, substituting the expression (3.27) into (3.7d), we find that at leading order the asymptotic analysis in Region II leads to

$$\frac{dI}{dt} \propto DP. \tag{3.40}$$

Hence, the main conclusion that can be drawn is that when $\alpha = p_0/d_0$ is order 1, the rate of change of iodine (I) is linear in terms of the concentration of hydrogen peroxide (P) and iodide (D). Importantly, this result is consistent with the experimental data in [16], and validates the model used in Chapter 2 of this thesis.

Comparison Of Asymptotic And Numerical Approximations

The Matlab *ode45* solver is utilized for computing a numerical solution given initial conditions $D(0) = 1$, $P(0) = 1$ and $\tilde{Q}(0) = 0$, along with dimensionless parameters $\alpha = 0.7$ and $\beta = 0.9$ incorporating the reaction rate ratio ϵ, these values are chosen arbitrarily. Figure 3.3 depicts how the matching between the asymptotic approximation solution in (3.23) and numerical simulation for the model (3.16) gets better for smaller values of ϵ. For more quantitative analysis, Figure 3.4 illustrates the errors (difference between the numerical solution and asymptotic approximation for each variable) as a function of ϵ on a log-log scale. The log-log plot is a useful tool for visualizing how the errors decrease as the parameter ϵ gets smaller and analyzing the slope of the errors curves to understand the convergence behaviour. In this case, the absolute errors have been calculated by the infinity norm (defined as the maximum absolute value), $\|y_{num} - y_{asymp}\|_\infty = \max|y_{num} - y_{asymp}|$, from the time points outputted by *ode45*. It yields

$$\log \|y_{num} - y_{asymp}\|_\infty = c + b \log \epsilon. \tag{3.41}$$

Hence,

$$\|y_{num} - y_{asymp}\|_\infty = a\epsilon^b. \tag{3.42}$$

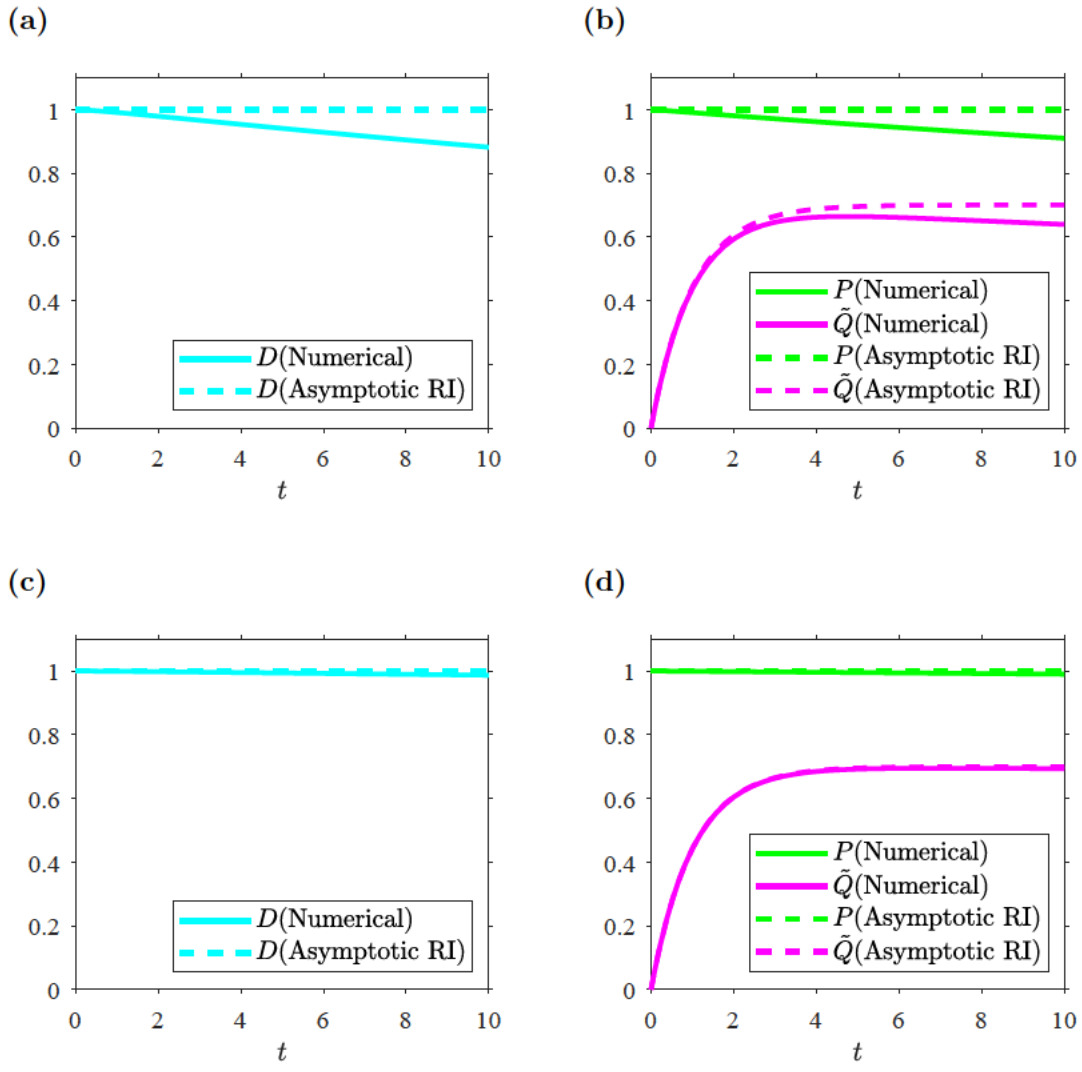

Figure 3.3: Comparison between asymptotic approximation in (3.23) and numerical solutions of the model (3.12). The match gets better for smaller values of ϵ, with initial conditions $D(0) = 1$, $P(0) = 1$ and $\tilde{Q}(0) = 0$. The dimensionless parameter values are $\alpha = 0.7$ and $\beta = 0.9$. (a, b) $\epsilon = 0.01$ and (c, d) $\epsilon = 0.001$.

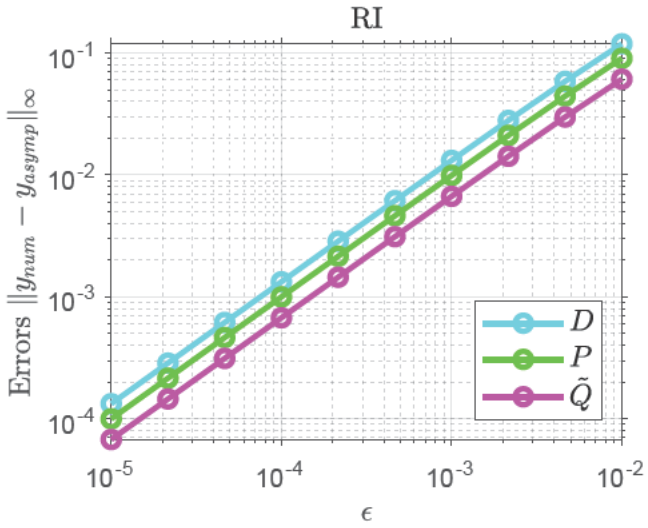

Figure 3.4: The difference between numerical solution of the model (3.16) and asymptotic approximation in (3.23) for each variable as a function of ϵ values on a log-log scale, over period of time $[0, 10]$. The initial conditions are $D(0) = 1$, $P(0) = 1$ and $\tilde{Q}(0) = 0$, and dimensionless parameter values $\beta = 0.9$ and $\alpha = 0.7$.

where $a = e^c$ is the y-axis intercept, and b is the slope (gradient), and hence $b \approx 1$ (can be calculated based on any two points from log-log plot using MATLAB code). Therefore,

$$\|y_{num} - y_{asymp}\|_\infty \approx \epsilon^1, \tag{3.43}$$

which means

$$\|y_{num} - y_{asymp}\|_\infty = O(\epsilon). \tag{3.44}$$

This result is consistent with the asymptotic expansion approach $\|y - y_0\|_\infty = O(\epsilon)$, where y is the model and y_0 is the leading order asymptotic solution of the model. Comparison between the analytical solution in (3.39) and the numerical simulation of the model (3.24) is presented in Figure 3.5. Figure 3.6 illustrates the errors (difference between numerical solution and asymptotic approximation for each variable) as a function of ϵ on a log-log scale. Similarly, the absolute errors have

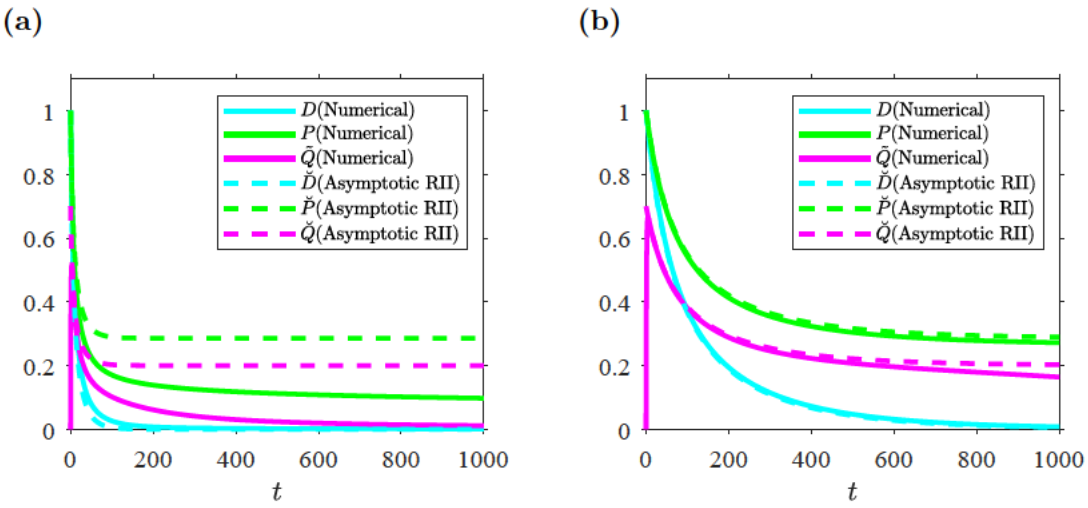

Figure 3.5: Comparison between asymptotic approximation (3.39) and numerical solutions of the model (3.12) with initial conditions $D(0) = 1$, $P(0) = 1$ and $\tilde{Q}(0) = 0$, and dimensionless parameter values $\beta = 0.9$ and $\alpha = 0.7$. The results representative of case (a) when $\epsilon = 0.1$, and case (b) when $\epsilon = 0.01$.

been calculated by the infinity norm (defined as the maximum absolute value), $\|y_{num} - y_{asymp}\|_\infty = \max |y_{num} - y_{asymp}|$ from the time points outputted by ode45. The gradient is also approximately 1 (can be calculated based on any two points from log-log plot using MATLAB code), which implies

$$\|y_{num} - y_{asymp}\|_\infty = O(\epsilon). \tag{3.45}$$

3.4 Case 2 (when $\alpha = O(\epsilon^{-1})$):

In §3.3 when $\alpha = O(1)$, hydrogen peroxide concentration was assumed to be similar to the other substrates. We observed that the rate (3.40) is linear in both iodide

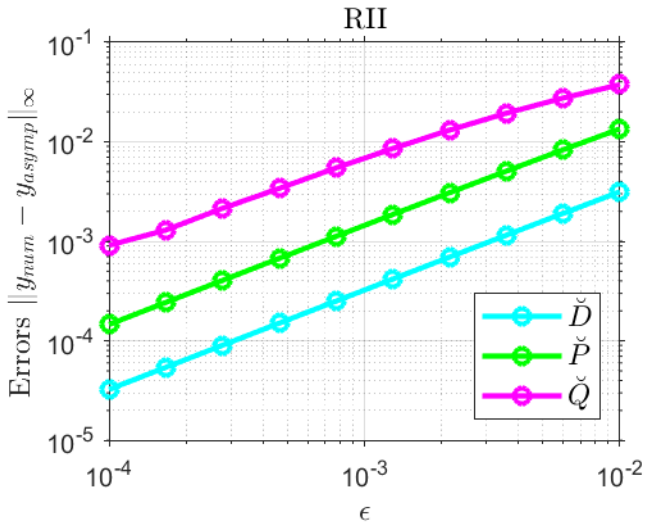

Figure 3.6: The difference between numerical solution of the model (3.24) and asymptotic approximation in (3.39) for each variable as a function of ϵ values on a log-log scale, over period of time $[0, 1000]$. The initial conditions $\breve{D}(0) = 1$, $\breve{P}(0) = 1$ and $\breve{Q}(0) = \alpha$, and dimensionless parameter values $\beta = 0.9$ and $\alpha = 0.7$.

(D) and hydrogen peroxide (P) concentrations. In this section, we will be looking at the qualitative analysis of the model (3.12) when there is an excess of hydrogen peroxide (P) concentration in the model (3.12), so $\alpha = O(\epsilon^{-1})$.

3.4.1 Asymptotic Analysis

Denoting, $\hat{\alpha} = \epsilon\alpha$ (i.e., $\hat{\alpha} = O(1)$), the system becomes

$$\frac{dD}{dt} = -\hat{\alpha}DP - DQ + \hat{\alpha}\beta QP, \tag{3.46a}$$

$$\frac{dP}{dt} = -\epsilon DP - \epsilon\beta QP, \tag{3.46b}$$

$$\frac{dQ}{dt} = \hat{\alpha}DP - DQ - \hat{\alpha}\beta QP. \tag{3.46c}$$

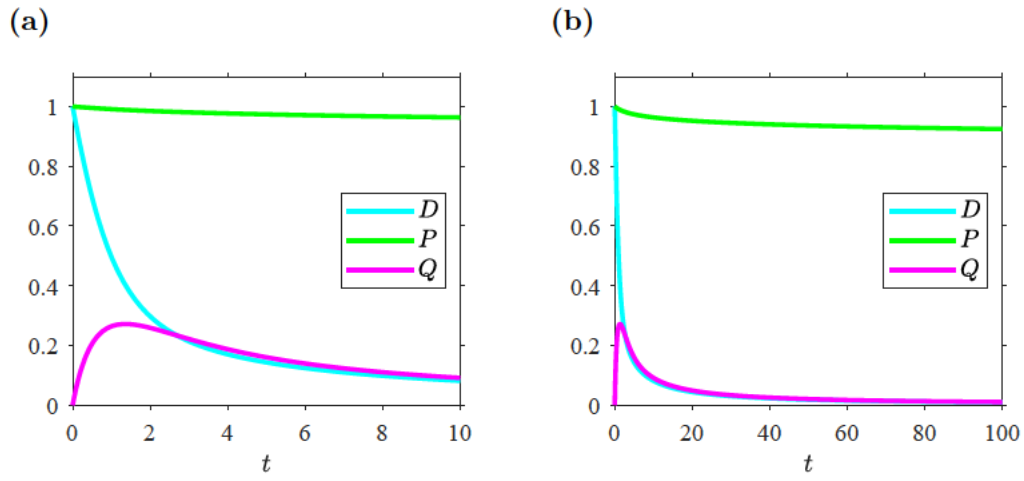

Figure 3.7: Numerical simulation for the model (3.46) (hydrogen peroxide in excess) with initial conditions $D(0) = 1$, $P(0) = 1$ and $Q(0) = 0$, and dimensionless parameter values $\hat{\alpha} = 0.7$ (i.e., $\alpha = 70$), $\beta = 0.9$ and $\epsilon = 0.01$. (a) for $t = [0, 10]$. (b) for $t = [0, 100]$.

Figure 3.7 shows the numerical solutions of the model (3.46) for different time periods. It reveals that hydrogen peroxide (P) concentration stays high whereas iodide (D) concentration drops fast to zero and hypoiodous acid (Q) concentration remains low when $\alpha = O(\epsilon^{-1})$. By comparing this result when $\alpha = O(\epsilon^{-1})$ to the first case (when $\alpha = O(1)$ in Figure 3.2 and model (3.12)), it must be pointed out that the hydrogen peroxide (P) now stays high.

Region I: Initial Adjustment

In the first region, the independent variable t is order 1, and the dependent variables D, P, Q are of order 1. Using the asymptotic expansions:

$$D = D_0+\epsilon D_1+\epsilon^2 D_2+..., \quad P = P_0+\epsilon P_1+\epsilon^2 P_2+..., \quad \text{and} \quad Q = Q_0+\epsilon Q_1+\epsilon^2 Q_2+..., \tag{3.47}$$

yields the following leading order behaviour

$$\frac{dD_0}{dt} = -\hat{\alpha}D_0P_0 - D_0Q_0 + \hat{\alpha}\beta Q_0P_0, \tag{3.48a}$$

$$\frac{dP_0}{dt} = 0, \tag{3.48b}$$

$$\frac{dQ_0}{dt} = \hat{\alpha}D_0P_0 - D_0Q_0 - \hat{\alpha}\beta Q_0P_0. \tag{3.48c}$$

We can solve equation (3.48b) directly, obtaining the solution $P_0 = 1$. Hence,

$$\frac{dD_0}{dt} = -\hat{\alpha}D_0 - D_0Q_0 + \hat{\alpha}\beta Q_0, \tag{3.49a}$$

$$\frac{dQ_0}{dt} = \hat{\alpha}D_0 - D_0Q_0 - \hat{\alpha}\beta Q_0. \tag{3.49b}$$

As we have been unable to solve (3.49) analytically, we instead explore its numerical solution to determine the behaviour of these variables that will enable us to determine the appropriate scalings for the next regime. Solving the above equations in (3.49) numerically is illustrated in Figure 3.8. It demonstrates the proportional relationship between the two variables: ($Q_0 \propto D_0$). As Q_0 increases, D_0 increases at the same rate, and the constant of proportionality is the value that relates the two amounts. The ratio of Q_0 to D_0 is equivalent to $1/\beta$ when $D_0 \leq 0.025$. In addition, Table 3.1 indicates the proportional relationship between the two variables Q_0 and D_0. Since the relationship is proportional, we can write an equation in the form $Q_0 \sim D_0/\beta$ to represent it when $D_0 \leq 0.025$. That motivates the study of the quasi-steady-state.

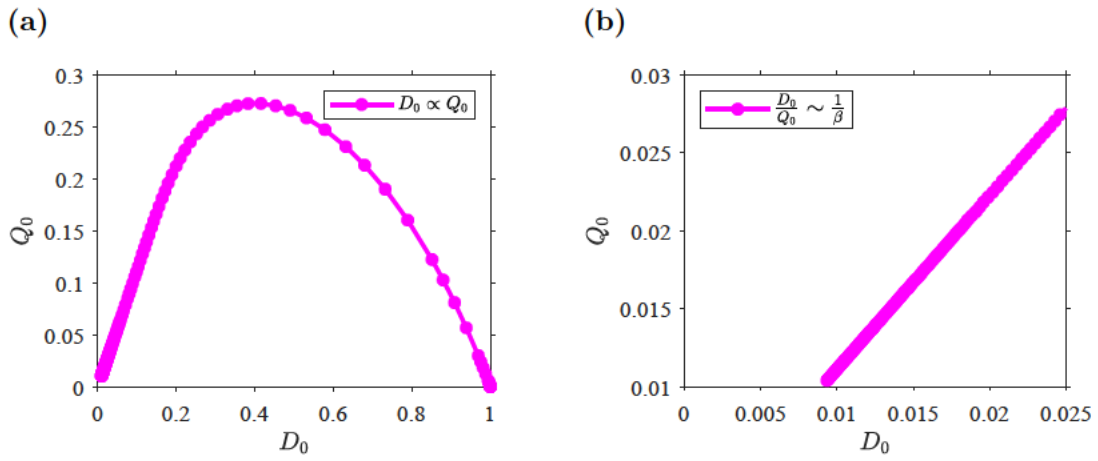

Figure 3.8: Numerical simulation of the proportional relationship behaviour D_0 and Q_0 functions of the equations (3.49) ($D_0 \propto Q_0$) with initial conditions $D(0) = 1$ and $Q(0) = 0$, and dimensionless parameter values $\hat{\alpha} = 0.7$, $\beta = 0.9$ and $\epsilon = 0.001$, and (b) scaled to show $D_0 \leq 0.025$.

$\hat{\alpha}$	β	D_0	Q_0	$Q_0/D_0 \sim 1/\beta$
0.7	0.9	0.0251 0.0246 0.0188 0.0127	0.0280 0.0274 0.0210 0.0141	1.11
0.7	1.1	0.0252 0.0225 0.0157	0.0229 0.0204 0.0143	0.91
0.9	0.9	0.0252 0.0221 0.0148	0.0281 0.0245 0.0165	1.11

Table 3.1: Numerical findings on the relationship between the two variables Q_0 and D_0. For every data pair, the ratio of Q_0 to D_0 is equivalent to $1/\beta$, which is the constant of proportionality (rounding off to the nearest hundredths) when $D_0 \leq 0.025$.

long-term behaviour on Region I:

Since we have been unable to obtain an analytical solution to (3.49), we instead consider its long-term behaviour to aid with scaling to the next timescale. We use the scaling $D_0 = Q_0 = O(\delta)$ and $t = O(1/\delta)$, where $\delta = O(\epsilon)$. Denoting $D_0 = \delta\tilde{D}_0$, $Q_0 = \delta\tilde{Q}_0$ and $\tilde{t} = \delta t$.

$$\frac{d\tilde{D}_0}{d\tilde{t}} = -\hat{\alpha}\delta\tilde{D}_0 - \delta^2\tilde{D}_0\tilde{Q}_0 + \hat{\alpha}\beta\delta\tilde{Q}_0, \tag{3.50a}$$

$$\frac{d\tilde{Q}_0}{d\tilde{t}} = \hat{\alpha}\delta\tilde{D}_0 - \delta^2\tilde{D}_0\tilde{Q}_0 - \hat{\alpha}\beta\delta\tilde{Q}_0. \tag{3.50b}$$

This implies that $d\tilde{D}_0/d\tilde{t} \approx 0 \approx d\tilde{Q}_0/d\tilde{t}$, and considering only the leading order contributions to the variables, it follows that

$$0 = -\hat{\alpha}\delta\tilde{D}_0 - \delta^2\tilde{D}_0\tilde{Q}_0 + \hat{\alpha}\beta\delta\tilde{Q}_0, \tag{3.51a}$$

$$0 = \hat{\alpha}\delta\tilde{D}_0 - \delta^2\tilde{D}_0\tilde{Q}_0 - \hat{\alpha}\beta\delta\tilde{Q}_0. \tag{3.51b}$$

Neglecting the δ^2 term in (3.51a), we deduce that

$$\tilde{D}_0 \approx \beta\tilde{Q}_0, \tag{3.52}$$

as we anticipated from our earlier numerical investigations. Adding the two equations (3.50a) and (3.50b) gives

$$\frac{d}{d\tilde{t}}\left(\tilde{D}_0 + \tilde{Q}_0\right) = -2\delta^2\tilde{D}_0\tilde{Q}_0, \tag{3.53}$$

hence,

$$\frac{d}{d\tilde{t}}\left(\tilde{D}_0 + \tilde{Q}_0\right) \propto -\tilde{D}_0\tilde{Q}_0. \tag{3.54}$$

Substituting (3.52) into (3.54) leads to

$$\frac{d}{d\tilde{t}}\left(\beta\tilde{Q}_0 + \tilde{Q}_0\right) \propto -\beta\tilde{Q}_0^2, \tag{3.55a}$$

$$(\beta+1)\frac{d\tilde{Q}_0}{d\tilde{t}} \propto -\beta\tilde{Q}_0^2. \tag{3.55b}$$

Using the separation of variables method for integration,

$$\int \frac{d\tilde{Q}_0}{\tilde{Q}_0^2} \propto \int \frac{-\beta}{(\beta+1)} d\tilde{t}, \tag{3.56}$$

yields,

$$\frac{-1}{\tilde{Q}_0} \propto \frac{-\beta}{(\beta+1)}\tilde{t}. \tag{3.57}$$

Solving for $\tilde{Q}_0$ in (3.57), we have

$$\tilde{Q}_0 \propto \frac{1}{\tilde{t}}, \tag{3.58}$$

and from (3.52), $\tilde{D}_0 \propto 1/\tilde{t}$ also.

Region II: Long-term State

In this section, we will take a look at the long-term analysis for the model (3.46), in which $t = O(\epsilon^{-1})$. Denoting, $\tau = \epsilon t$ with $\breve{D} = O(\epsilon)$, $\breve{P} = O(1)$, and $\breve{Q} = O(\epsilon)$,

thus, the system becomes

$$\epsilon^2 \frac{d\breve{D}}{d\tau} = -\epsilon\hat{\alpha}\breve{D}\breve{P} - \epsilon^2\breve{D}\breve{Q} + \epsilon\hat{\alpha}\beta\breve{Q}\breve{P}, \tag{3.59a}$$

$$\epsilon \frac{d\breve{P}}{d\tau} = -\epsilon^2\breve{D}\breve{P} - \epsilon^2\beta\breve{Q}\breve{P}, \tag{3.59b}$$

$$\epsilon^2 \frac{d\breve{Q}}{d\tau} = \epsilon\hat{\alpha}\breve{D}\breve{P} - \epsilon^2\breve{D}\breve{Q} - \epsilon\hat{\alpha}\beta\breve{Q}\breve{P}. \tag{3.59c}$$

We are going to be looking at the leading order of asymptotic analysis as follows

$$0 = -\hat{\alpha}\breve{D}_0\breve{P}_0 + \hat{\alpha}\beta\breve{Q}_0\breve{P}_0, \tag{3.60a}$$

$$\frac{d\breve{P}_0}{d\tau} = 0, \tag{3.60b}$$

$$0 = \hat{\alpha}\breve{D}_0\breve{P}_0 - \hat{\alpha}\beta\breve{Q}_0\breve{P}_0. \tag{3.60c}$$

Hence,

$$\breve{P}_0 = 1, \tag{3.61}$$

and substituting (3.61) into (3.60a) leads to

$$\hat{\alpha}\breve{D}_0 = \hat{\alpha}\beta\breve{Q}_0, \tag{3.62}$$

yielding,

$$\breve{Q}_0 = \frac{1}{\beta}\breve{D}_0. \tag{3.63}$$

We now consider how this affects the rate of change of iodine in this high peroxide regime. Substituting the expression (3.63) into (3.7d), we find that at the leading

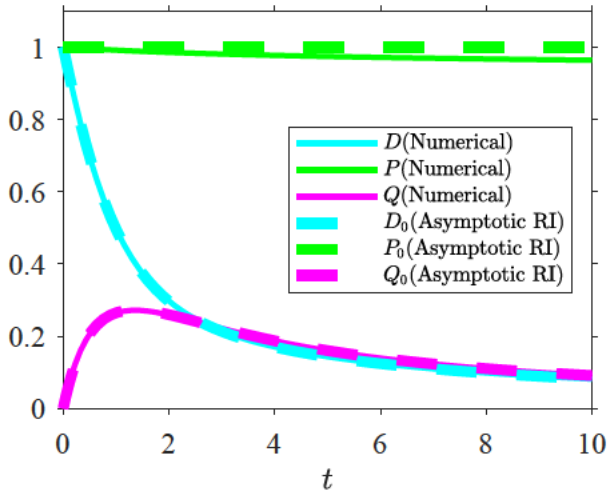

Figure 3.9: Numerical simulation shows the match between numerical solutions of the model (3.46) and the leading order asymptotic approximation (3.48), with initial conditions $D(0) = 1$, $P(0) = 1$, and $Q(0) = 0$. The dimensionless parameter values are $\hat{\alpha} = 0.7$ (i.e., $\alpha = 70$), $\beta = 0.9$ and $\epsilon = 0.01$.

order of asymptotic analysis in Region II

$$\frac{dI}{dt} \propto D^2. \tag{3.64}$$

Our results demonstrated that when $\alpha = p_0/d_0$ is order ϵ^{-1} then the rate of change of iodine (I) is quadratic rate in terms of the iodide (D) concentration. Overall this validates the model used by Kerr et al. [27].

Comparison Of Asymptotic And Numerical Approximations

Figure 3.9 illustrates the matching between numerical solutions of the model (3.46) and the leading order asymptotic approximation (3.48) on region I. Figure 3.10a displays the matching between the numerical solution of the variable Q_0 function (3.48c) and the long-term behaviour of $\tilde{Q}_0$ function (3.58) on Region II. It shows

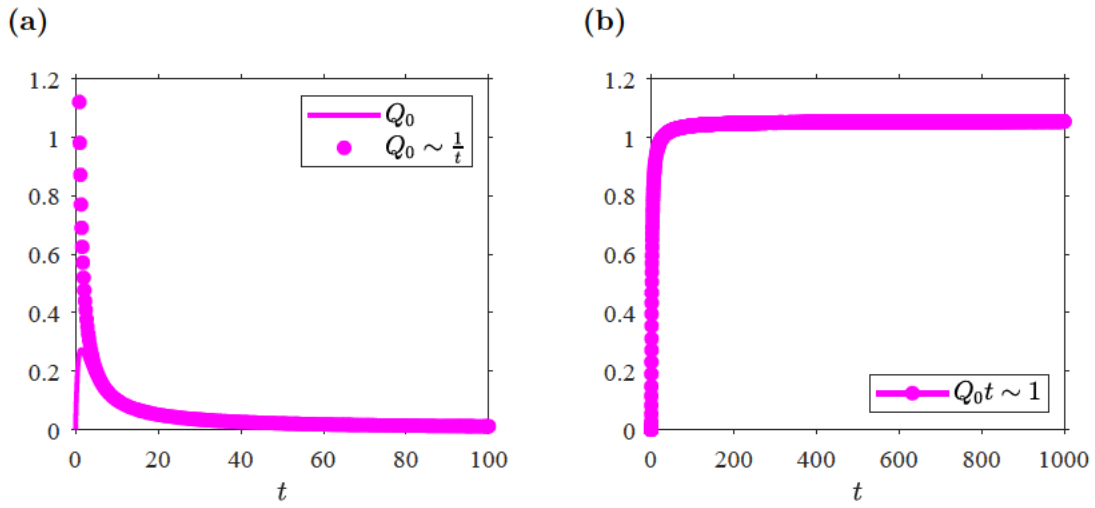

Figure 3.10: Numerical simulation of the variable Q_0 at the leading order equation (3.49b) and the long-term behaviour of Q_0 function (3.58) when $t = \delta^{-1}\tilde{t}$ with initial conditions $D_0(0) = 1$ and $Q_0(0) = 0$, and parameter values are $\hat{\alpha} = 0.7$, $\beta = 0.9$ and $\epsilon = 0.001$, where (a) Q_0 decays slowly and it matches to $Q_0 \sim 1/t$, and (b) $Q_0 t \sim 1$.

that Q_0 decays and it matches to $\tilde{Q}_0 \sim 1/\tilde{t}$, with this relationship being confirmed in Figure 3.10b.

	$\alpha = p_0/d_0$ is order 1:	$\alpha = p_0/d_0$ is order ϵ^{-1}:
Assumption:	Hydrogen peroxide concentration (P) is **similar (moderate levels)** to the other reactants in the slow chemical reaction.	Hydrogen peroxide concentration (P) is in **great excess (high levels)** compared to the other reactants in the slow chemical reaction.
Region I:	Approximation Solutions At Leading Order: $$D_0(t) = 1,$$ $$P_0(t) = 1, \quad (3.65)$$ $$\tilde{Q}_0(t) = \alpha\left(1 - e^{-t}\right).$$	Leading Order Behaviour: $$\text{As} \quad t \to \infty \begin{cases} P_0 & = 1, \\ \frac{D_0}{Q_0} & \sim \beta, \\ Q_0 & \sim \frac{1}{t}. \end{cases} \quad (3.66)$$
Region II:	Approximation Solutions At Leading Order: $$D_0(\tau) = \frac{2\alpha(1-2\alpha)}{-2\alpha + e^{(1-2\alpha)\tau}} + (1 - 2\alpha),$$ $$P_0(\tau) = \frac{(1-2\alpha)}{-2\alpha + e^{(1-2\alpha)\tau}}, \quad (3.67)$$ $$\tilde{Q}_0(\tau) = \frac{\alpha(1-2\alpha)}{-2\alpha + e^{(1-2\alpha)\tau}}.$$	Leading Order Behaviour: $$\breve{P}_0(\tau) = 1,$$ $$\breve{Q}_0(\tau) = \frac{1}{\beta}\breve{D}_0. \quad (3.68)$$
Results:	**Linear Kinetics** apply in both (D) and (P) concentrations, $$\frac{dI}{dt} \propto DP. \quad (3.69)$$ This result is consistent with the experimental data in Copper and Koubek [16].	**Quadratic Kinetics** apply in (D) concentration, $$\frac{dI}{dt} \propto D^2. \quad (3.70)$$ This result is consistent with the asymptotic and experimental analysis in Kerr et al [27].

Table 3.2: Summary table of our results and how they compare with previous studies.

3.5 Conclusion

This chapter studied the slow reaction in isolation to understand the effect of the concentration of hydrogen peroxide on the kinetics by including the hypoiodous acid reactant and reverse reaction. We exhibited how the order of the ratio of hydrogen peroxide to iodide determines whether the reaction kinetics are effectively linear or quadratic, and explains the discrepancies between the two previous studies by Copper and Koubek [16] and Kerr et al [27]. The main contributions of this chapter are summarised in Table 3.2.

For the next chapter, we will be incorporating the multi-step model of the slow reaction with the fast reaction associated with vitamin C to formulate a unified model of the chemical clock reaction valid for both moderate and hydrogen peroxide cases. We will again develop an asymptotic analysis, elucidating how the moderate and hydrogen peroxide regimes differ, leading to approximate switchover time formulae in each case.

Chapter 4

Model FCR: Full Model Of Chemical Clock Reaction With Moderate and High Hydrogen Peroxide

4.1 Motivation

The kinetics of the chemical clock reaction (including the slow and fast reactions) must be fully understood. In Chapter 3, we analysed the slow reaction in isolation to understand the effect of hydrogen peroxide concentration on the kinetics (i.e., Model ISR), by including the hypoiodous acid reactant and reverse reaction. We now perform asymptotic analysis on the full model of the chemical clock reaction (slow and fast) with this reverse reaction and associated vitamin C (will be named, Model FCR), by combining Model ISR and the fast reaction. The analysis will

enable us to obtain an approximate formula for the dependence of the switchover time on the initial concentration of the reactants for both the moderate and high hydrogen peroxide regimes (from one unified model). This will empower the comparison of the full clock reaction model results (Model FCR) to Model HPL (the simple model with moderate hydrogen peroxide in Chapter 2) which has linear kinetics based on experimental data by Copper and Koubek [16], and to the model with high hydrogen peroxide by Kerr et al., [27] which has quadratic kinetics.

4.2 Model Formulation

The aim of this chapter is to investigate the full model of the chemical clock reaction with reverse reaction and associated vitamin C and hydrogen peroxide as follows: The slow (first) reaction is a result of the three reactions (as stated earlier in Chapter 3, Model ISR) taking the following form

$$2D + P \xrightarrow{k_1} I \begin{cases} D + P \xrightarrow{k_3} Q, \\ D + Q \xrightarrow{k_4} I, \\ Q + P \xrightarrow{k_5} D, \end{cases} \tag{4.1}$$

and the form of the fast (second) reaction (as stated earlier in Chapter 2) is given by

$$I + C \xrightarrow{k_2} 2D. \tag{4.2}$$

Based on the above formulations and applying the law of mass action, the model is given by the following system of nonlinear differential equations (named Model

FCR referring to full clock reaction):

$$\frac{dD}{dt} = -k_3DP - k_4DQ + k_5QP + 2k_2IC, \tag{4.3a}$$
$$\frac{dP}{dt} = -k_3DP - k_5QP, \tag{4.3b}$$
$$\frac{dQ}{dt} = k_3DP - k_4DQ - k_5QP, \tag{4.3c}$$
$$\frac{dC}{dt} = -k_2IC, \tag{4.3d}$$
$$\frac{dI}{dt} = k_4DQ - k_2IC, \tag{4.3e}$$

with initial conditions

$$P(0) = p_0, \quad Q(0) = q_0, \quad C(0) = c_0, \quad I(0) = \iota_0. \tag{4.4}$$

We note that the equations for iodide (D), hypoiodous acid (Q) and iodine (I) obey the following conservation law,

$$\frac{d}{dt}\left(D + Q + 2I\right) = 0. \tag{4.5}$$

We deduce that $D(t) + Q(t) + 2I(t) = d_0 + q_0 + 2\iota_0 = n_0$, where n_0 is the total concentration of iodine atoms. Eliminating the variable D (i.e., $D = n_0 - Q - 2I$)

in (4.3) we have the reduced system

$$\frac{dP}{dt} = -k_3\left(n_0 - Q - 2I\right)P - k_5 QP, \tag{4.6a}$$
$$\frac{dQ}{dt} = k_3\left(n_0 - Q - 2I\right)P - k_4\left(N_0 - Q - 2I\right)Q - k_5 QP, \tag{4.6b}$$
$$\frac{dC}{dt} = -k_2 IC, \tag{4.6c}$$
$$\frac{dI}{dt} = k_4\left(n_0 - Q - 2I\right)Q - k_2 IC. \tag{4.6d}$$

It should be emphasized that the units of the reactants' concentrations (P, Q, C, I) are moles per litres (mol/l), the units of time (t) are seconds (s), and the units of the reaction rates (k_2, k_3, k_4, k_5) are liters per moles per seconds (l/mol·s). It is instructive to non-dimensionalize the system by choosing the following scalings (in particular, we choose the timescale based on the final step producing iodine),

$$P = p_0 P^*, \quad Q = n_0 Q^*, \quad C = c_0 C^*, \quad I = n_0 I^*, \quad t = \frac{t^*}{k_2 c_0}, \tag{4.7}$$

where $*$ denotes a dimensionless quantity. Substituting (4.7) into (4.6) leads to the dimensionless system,

$$\frac{dP^*}{dt^*} = -\epsilon^2\sigma\left(1 - Q^* - 2I^*\right)P^* - \epsilon^2\beta\sigma Q^* P^*, \tag{4.8a}$$
$$\frac{dQ^*}{dt^*} = \epsilon^2\rho\left(1 - Q^* - 2I^*\right)P^* - \epsilon\gamma\sigma\left(1 - Q^* - 2I^*\right)Q^* - \epsilon^2\beta\rho Q^* P^*, \tag{4.8b}$$
$$\frac{dC^*}{dt^*} = -\sigma I^* C^*, \tag{4.8c}$$
$$\frac{dI^*}{dt^*} = \epsilon\gamma\sigma\left(1 - Q^* - 2I^*\right)Q^* - I^* C^*, \tag{4.8d}$$

where the dimensionless parameters are

$$\sigma = \frac{n_0}{c_0}, \quad \rho = \frac{p_0}{c_0}, \quad \epsilon^2 = \frac{k_3}{k_2}, \quad \epsilon^2\beta = \frac{k_5}{k_2}, \quad \epsilon\gamma = \frac{k_4}{k_2}, \quad \phi = \frac{\iota_0}{n_0}. \tag{4.9}$$

It should be mentioned that the reaction converting iodide (D) to hypoiodous acid (Q) and the reverse reaction converting hypoiodous acid (Q) to iodide (D) are much slower than the reaction converting iodide (D) to iodine (I), so $k_3, k_5 \ll k_4$. Furthermore, $k_4 \ll k_2$, because the reaction converting iodide (D) to iodine (I) is much slower than the fast reaction converting iodine (I) to iodide (D), therefore, the reaction rate ratio $\epsilon^2 \ll 1$. The parameters β and γ are order 1, and the magnitude of the parameter ρ determines whether we are considering moderate or high hydrogen peroxide. The initial conditions become

$$P^*(0) = 1, \quad Q^*(0) = q_0^*, \quad C^*(0) = 1, \quad I^*(0) = \iota_0^*, \tag{4.10}$$

with

$$q_0^* = \frac{q_0}{n_0}, \quad \iota_0^* = \frac{\iota_0}{n_0}. \tag{4.11}$$

We consider the specific situation in which Q is absent initially. It follows that $Q^*(0) = 0$ and $I^*(0) = \iota_0/n_0 = \phi$. We drop the stars for easier notation. The main difference between the ISR Model and FCR Model lies on their focus: The ISR Model (3.7), as stated in Chapter 3, focus on the slow reaction in isolation to understand the effect of the concentration of hydrogen peroxide on the kinetics by including the hypoiodous acid reactant and reverse reaction. The FCR Model (4.8) focus on the full clock reaction incorporating the multi-step model of the slow reaction with the fast reaction associated with vitamin C to formulate a unified

model valid for both moderate and hydrogen peroxide cases.

4.3 Asymptotic Analysis

Due to the small reaction rate ratio ϵ^2 (i.e., $\epsilon^2 \ll 1$), we can generate an approximate solution to Model FCR (4.8) via matched asymptotic expansions. The asymptotic analysis will be divided into four regions and we must also consider hydrogen peroxide (P) concentration. In this chapter, we look at the Model FCR (4.8) in two cases: (1) with moderate hydrogen peroxide, named Model FCR-M-HP. Note that we use 'moderate' here to signify hydrogen peroxide is present in a similar concentration to other reactants; (2) with high hydrogen peroxide, named Model FCR-H-HP, through asymptotic analysis. Figure 4.1 illustrates the concentrations of the reactants as a function of time for both cases of the model (4.8). The clock reaction (in which iodine (I) appears after the induction period) occurs when vitamin C is totally consumed. A logarithmic scale for time in Figure 4.2 exhibits the timescales spanning several orders of magnitude.

4.3.1 Model FCR-M-HP: The Full Model With Moderate Hydrogen Peroxide

We first consider that there are similar levels of hydrogen peroxide (P) concentration in the system to the other reactants. Thus, we assume that ρ is order 1 in the Model FCR (4.8), where $\rho = p_0/c_0$. Since Q remains low as shown in Figure 4.2a, we initially scale $Q = \epsilon\tilde{Q}$ where $\tilde{Q} = O(1)$.

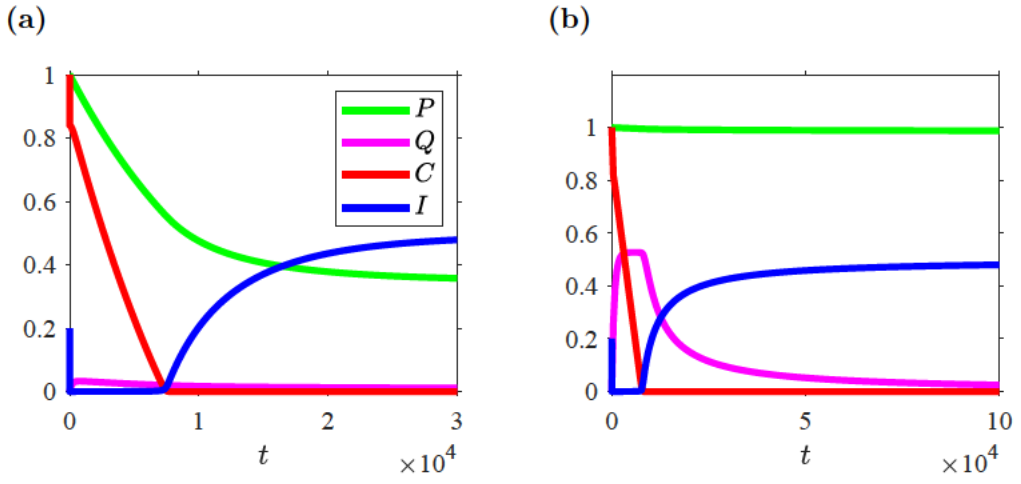

Figure 4.1: Numerical simulation of the model (4.8) illustrates the concentrations of the reactants as a function of time with initial conditions $P(0) = 1$, $Q(0) = 0$, $C(0) = 1$ and $I(0) = \phi$, and the dimensionless parameter values (chosen arbitrarily) are $\beta = 0.6$, $\gamma = 0.7$, $\sigma = 0.8$ and $\phi = 0.2$. (4.1a) First case with moderate hydrogen peroxide where $\rho = 2$ and $\epsilon = 0.01$. (4.1b) Second case with high hydrogen peroxide where $\rho = 900$ and $\epsilon = 0.001$. The clock reaction appears after the induction period.

We obtain the following model, named Model FCR-M-HP:

$$\frac{dP}{dt} = -\epsilon^2\sigma\left(1 - \epsilon\tilde{Q} - 2I\right)P - \epsilon^3\beta\sigma\tilde{Q}P, \tag{4.12a}$$

$$\frac{d\tilde{Q}}{dt} = \epsilon\rho\left(1 - \epsilon\tilde{Q} - 2I\right)P - \epsilon\gamma\sigma\left(1 - \epsilon\tilde{Q} - 2I\right)\tilde{Q} - \epsilon^2\beta\rho\tilde{Q}P, \tag{4.12b}$$

$$\frac{dC}{dt} = -\sigma IC, \tag{4.12c}$$

$$\frac{dI}{dt} = \epsilon^2\gamma\sigma\left(1 - \epsilon\tilde{Q} - 2I\right)\tilde{Q} - IC. \tag{4.12d}$$

The initial conditions are:

$$P(0) = 1, \quad \tilde{Q}(0) = 0, \quad C(0) = 1, \quad I(0) = \phi. \tag{4.13}$$

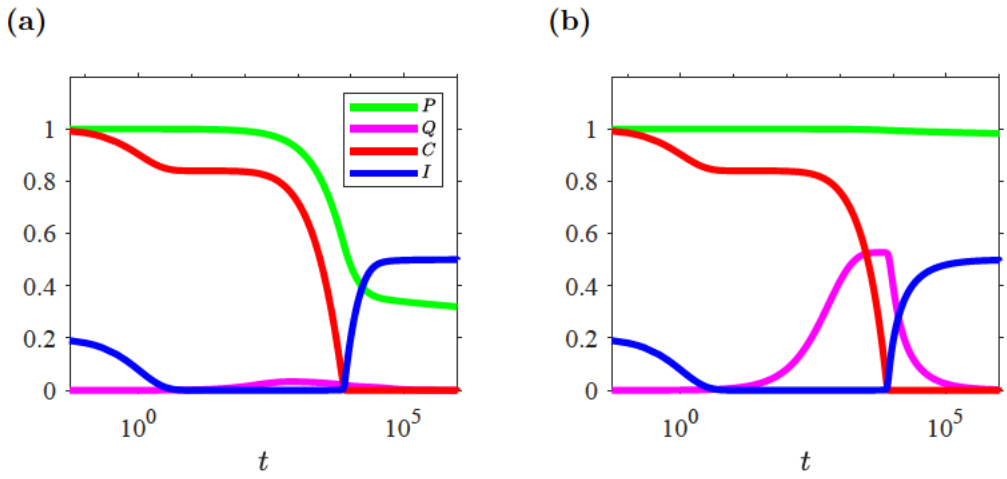

Figure 4.2: Numerical solutions of the concentrations of the reactants as a function of time on a log scale, of the model (4.8), with initial conditions $P(0) = 1$, $Q(0) = 0$, $C(0) = 1$ and $I(0) = \phi$, and the dimensionless parameter values (chosen arbitrarily) are $\beta = 0.6$, $\gamma = 0.7$, $\sigma = 0.8$, $\phi = 0.2$. (4.2a) First case with moderate hydrogen peroxide where $\rho = 2$ and $\epsilon = 0.01$. (4.2b) Second case with high hydrogen peroxide where $\rho = 900$ and $\epsilon = 0.001$.

The Model FCR-M-HP (4.12) will be studied through five asymptotic regions in detail in the following sections.

Region I: Initial Adjustment

During Region I, the reactants are mixed before the induction phase begins. It can be described as where the dependent variables I, C, P are order 1 and the independent variable $t = O(1)$. The leading order terms for the asymptotic expansion

of the Model FCR-M-HP (4.12) are:

$$\frac{dP_0}{dt} = 0, \tag{4.14a}$$

$$\frac{d\tilde{Q}_0}{dt} = 0, \tag{4.14b}$$

$$\frac{dC_0}{dt} = -\sigma I_0 C_0, \tag{4.14c}$$

$$\frac{dI_0}{dt} = -I_0 C_0, \tag{4.14d}$$

with the initial conditions:

$$P_0(0) = 1, \quad \tilde{Q}_0(0) = 0, \quad C_0(0) = 1, \quad I_0(0) = \phi. \tag{4.15}$$

Equations (4.14a) and (4.14b), alongside their initial conditions yield

$$P_0 = 1, \tag{4.16}$$

$$\tilde{Q}_0 = 0. \tag{4.17}$$

Dividing (4.14c) by (4.14d) gives the following

$$\frac{dC_0}{dI_0} = \sigma. \tag{4.18}$$

Using the separation of variables method, and the initial conditions, yields

$$C_0 = \sigma\left(I_0 - \phi\right) + 1, \tag{4.19}$$

and hence,

$$\frac{dI_0}{dt} = -I_0 \left[\sigma \left(I_0 - \phi\right) + 1\right]. \tag{4.20}$$

Using the separation of variables and the partial fraction decomposition for integration (with ϕ as the lower limit of the integral) leads to

$$\ln \left| \frac{I_0}{\sigma \left(I_0 - \phi\right) + 1} \right| - \ln(\phi) = -\left(1 - \sigma\phi\right) t. \tag{4.21}$$

The sign of the argument of natural log is positive because $I_0 - \phi > 0$. Hence,

$$\frac{I_0}{\sigma I_0 + (1 - \sigma\phi)} = \phi e^{-(1-\sigma\phi)t}, \tag{4.22}$$

yielding,

$$I_0 = \frac{\phi \left(1 - \sigma\phi\right) e^{-(1-\sigma\phi)t}}{1 - \sigma\phi e^{-(1-\sigma\phi)t}}, \tag{4.23}$$

and substituting (4.23) into (4.19) leads to

$$C_0 = \frac{\sigma\phi \left(1 - \sigma\phi\right) e^{-(1-\sigma\phi)t}}{1 - \sigma\phi e^{-(1-\sigma\phi)t}} + \left(1 - \sigma\phi\right). \tag{4.24}$$

It follows that the approximate solutions on Region I are:

$$P(t) = 1 + O(\epsilon), \tag{4.25a}$$

$$Q(t) = 0 + O(\epsilon), \tag{4.25b}$$

$$C(t) = \frac{\sigma\phi \left(1 - \sigma\phi\right) e^{-(1-\sigma\phi)t}}{1 - \sigma\phi e^{-(1-\sigma\phi)t}} + (1 - \sigma\phi) + O(\epsilon), \tag{4.25c}$$

$$I(t) = \frac{\phi \left(1 - \sigma\phi\right) e^{-(1-\sigma\phi)t}}{1 - \sigma\phi e^{-(1-\sigma\phi)t}} + O(\epsilon). \tag{4.25d}$$

As $t \to \infty$ we observe that $(P_0(t), Q_0(t), C_0(t), I_0(t)) \to (1, 0, 1-\sigma\phi, 0)$. During the initial adjustment behaviour, approximately $\sigma\phi$ (which in dimensional terms is ι_0/c_0, i.e., the initial concentration of iodine per the initial concentration of vitamin C) of the initial quantity of the inhibitor C is used up. The condition $1-\sigma\phi > 0$ (i.e, $\iota_0/c_0 < 1$) is essential in order to have enough vitamin C. The initial adjustment therefore corresponds to consumption of a proportion $\sigma\phi$ of the initial vitamin C concentration via the fast reaction, which results in converting the majority of the initial iodine concentration to iodide in order 1 time; the slow reaction is subleading in this region. In particular, note that $I_0(t)$ is exponentially decaying.

Region Ia: Quasi Equilibrium Established for Q

Following the exponential decay of iodine and vitamin C, the fast reaction no longer dominates and the slow reaction becomes of comparable importance. A distinctive feature of the Model FCR-M-HP case as opposed to the Model FCR-H-HP case is the existence of a region intermediate between the initial adjustment and the induction period, during which the hypoiodous acid concentration reaches quasi-equilibrium. This process corresponds to the two forward steps in the slow reaction balancing in their production and removal of hypoiodous acid (i.e., $D + P \to Q$ and $D + Q \to I$). Therefore, we consider the following scaling: $P = C = O(1)$, $I = O(\epsilon^2)$ and $t = O(\epsilon^{-1})$. Denoting $\tau = \epsilon t$ and $I = \epsilon^2 \tilde{I}$, then the system takes the form at leading order (substituting the asymptotic expansions into Model FCR-

M-HP (4.12)):

$$\frac{dP_0}{d\tau} = 0, \tag{4.26a}$$

$$\frac{d\tilde{Q}_0}{d\tau} = \rho P_0 - \gamma\sigma\tilde{Q}_0, \tag{4.26b}$$

$$\frac{dC_0}{d\tau} = 0, \tag{4.26c}$$

$$0 = \gamma\sigma\tilde{Q}_0 - \tilde{I}_0 C_0, \tag{4.26d}$$

with the matching conditions to the Region I solution:

$$P_0(0) = 1, \quad \tilde{Q}_0(0) = 0, \quad C_0(0) = 1 - \sigma\phi, \quad \tilde{I}_0(0) = 0. \tag{4.27}$$

Hence,

$$P_0 = 1, \tag{4.28}$$

$$C_0 = 1 - \sigma\phi. \tag{4.29}$$

Substituting (4.28) into (4.26b) leads to

$$\frac{d\tilde{Q}_0}{d\tau} = \rho - \gamma\sigma\tilde{Q}_0. \tag{4.30}$$

Using the separation of variables for integration to solve (4.30):

$$\int \frac{d\tilde{Q}_0}{\rho - \gamma\sigma\tilde{Q}_0} = \int d\tau, \tag{4.31}$$

yields,

$$\frac{-1}{\gamma\sigma}\ln\left|\gamma\sigma\left(\frac{\rho}{\gamma\sigma}-\tilde{Q}_0\right)\right| = \tau + c_1, \tag{4.32}$$

where c_1 is a constant that can be found by matching to Region I,

$$c_1 = \frac{-\ln(\rho)}{\gamma\sigma}. \tag{4.33}$$

Taking into account the quasi-steady state of (4.30), we see that $\tilde{Q}_0 \approx \rho/\gamma\sigma$, and hence $\rho/\gamma\sigma - \tilde{Q}_0 > 0$. Therefore, (4.32) and (4.33) give

$$\tilde{Q}_0 = \frac{\rho}{\gamma\sigma}\left(1-e^{-\gamma\sigma\tau}\right). \tag{4.34}$$

Substituting (4.29) and (4.34) into (4.26d) yields

$$\tilde{I}_0 = \frac{\rho}{1-\sigma\phi}\left(1-e^{-\gamma\sigma\tau}\right). \tag{4.35}$$

It should be noted that as $\tau \to \infty$:

$$\left(P_0(\tau), \tilde{Q}_0(\tau), C_0(\tau), \tilde{I}_0(\tau)\right) \to \left(1, \frac{\rho}{\gamma\sigma}, 1-\sigma\phi, \frac{\rho}{1-\sigma\phi}\right).$$

It follows that the approximate solutions for Region Ia are:

$$P(t) = 1 + O(\epsilon), \tag{4.36a}$$

$$Q(t) = \frac{\epsilon\rho}{\gamma\sigma}\left(1-e^{-\epsilon\gamma\sigma t}\right) + O(\epsilon^2), \tag{4.36b}$$

$$C(t) = 1 - \sigma\phi + O(\epsilon), \tag{4.36c}$$

$$I(t) = \frac{\epsilon^2\rho}{1-\sigma\phi}\left(1-e^{-\epsilon\gamma\sigma t}\right) + O(\epsilon^3). \tag{4.36d}$$

Region II: Induction Period

Following the establishment of quasi-equilibrium within the slow reaction, the system enters the induction period, which is the distinguishing feature of a clock reaction. During the induction period, the two chemical reactions (4.1) and (4.2) keep the concentration of iodine (I) low. As iodide (D) is produced rapidly in the fast (second) chemical reaction (4.2), it removes iodine (I) from the system faster than it can be produced. As a result of these two reactions, the concentrations of vitamin C (C) and hydrogen peroxide (P) are slowly being consumed. Thus, I is order ϵ^2 and t is order ϵ^{-2} whereas P and C are still of order 1. We rescale $T = \epsilon^2 t$ and $I = \epsilon^2 \tilde{I}$ (i.e., $t = O(\epsilon^{-2})$ and $I = O(\epsilon^2)$). Therefore, the Model FCR-M-HP (4.12) takes the following form at the leading order of the asymptotic expansions,

$$\frac{dP_0}{dT} = -\sigma P_0, \tag{4.37a}$$

$$0 = \rho P_0 - \gamma\sigma\tilde{Q}_0, \tag{4.37b}$$

$$\frac{dC_0}{dT} = -\sigma \tilde{I}_0 C_0, \tag{4.37c}$$

$$0 = \gamma\sigma\tilde{Q}_0 - \tilde{I}_0 C_0, \tag{4.37d}$$

with the matching conditions to Region Ia:

$$P_0(0) = 1, \quad \tilde{Q}_0(0) = \frac{\rho}{\gamma\sigma}, \quad C_0(0) = 1 - \sigma\phi, \quad \tilde{I}_0(0) = \frac{\rho}{1-\sigma\phi}. \tag{4.38}$$

We can solve equation (4.37a) directly, obtaining the solution

$$P_0 = e^{-\sigma T}. \tag{4.39}$$

Substituting (4.39) into (4.37b) and (4.37d) yields

$$\tilde{Q}_0 = \frac{\rho}{\gamma\sigma} e^{-\sigma T}, \tag{4.40}$$

and, hence,

$$\tilde{I}_0 C_0 = \rho e^{-\sigma T}. \tag{4.41}$$

Combining (4.41) and (4.37c) leads to

$$\frac{dC_0}{dT} = -\sigma\rho e^{-\sigma T}. \tag{4.42}$$

Equations (4.41) and (4.42) can be solved to give

$$C_0 = \rho e^{-\sigma T} + (1 - \sigma\phi - \rho), \tag{4.43}$$

and,

$$\tilde{I}_0 = \frac{\rho e^{-\sigma T}}{\rho e^{-\sigma T} + (1 - \sigma\phi - \rho)}. \tag{4.44}$$

The approximate solutions in Region II are, therefore,

$$P(t) = e^{-\epsilon^2\sigma t} + O(\epsilon), \tag{4.45a}$$

$$Q(t) = \frac{\epsilon\rho}{\gamma\sigma} e^{-\epsilon^2\sigma t} + O(\epsilon^2), \tag{4.45b}$$

$$C(t) = \rho e^{-\epsilon^2\sigma t} + (1 - \sigma\phi - \rho) + O(\epsilon), \tag{4.45c}$$

$$I(t) = \frac{\epsilon^2\rho e^{-\epsilon^2\sigma t}}{\rho e^{-\sigma T} + (1 - \sigma\phi - \rho)} + O(\epsilon^3). \tag{4.45d}$$

One intriguing aspect of the clock reaction model is the exploration of the

switchover time formula, which reveals the precise moment when the system transitions from one chemical state to another.

Switchover Time:

We can approximate the switchover time T_{sw} as being when vitamin C is all consumed at leading order, i.e. $C_0(T_{sw}) = 0$ in (4.45)) This leads to

$$\rho e^{-\sigma T_{sw}} + (1 - \sigma\phi - \rho) \approx 0, \tag{4.46}$$

which can be rearranged to give

$$T_{sw} = \frac{1}{\sigma} \ln\left(\frac{\rho}{\rho + \sigma\phi - 1}\right). \tag{4.47}$$

In dimensional variables (recall (4.7) and (4.9)), we have that the switchover time is

$$t_{sw} = \frac{1}{k_2 c_0} \frac{1}{\epsilon^2 \frac{n_0}{c_0}} \ln\left(\frac{\frac{p_0}{c_0}}{\frac{p_0}{c_0} + \frac{n_0}{c_0}\frac{\iota_0}{n_0} - 1}\right), \tag{4.48}$$

or equivalently (using $\epsilon^2 = k_3/k_2$),

$$t_{sw} = \frac{1}{k_3 n_0} \ln\left(\frac{p_0}{p_0 + \phi n_0 - c_0}\right). \tag{4.49}$$

We consider the sign of $(\rho + \sigma\phi - 1)$ from (4.47) (where $\rho = p_0/c_0$ and $\sigma\phi = \iota_0/c_0$). For this to be positive, it follows that $\rho > 1 - \sigma\phi$ which satisfies $p_0 + \iota_0 > c_0$. Thus, there is enough hydrogen peroxide (P) to drive the vitamin C to zero.

A key result here is that the switchover time formula given in (4.47) is the same as the simplified linear kinetics model HPL shown earlier in Chapter 2, namely

equation (2.67).

Region III: Corner

Region III matches the behaviour at the end of the induction period, after the rapid colour change, with the beginning of the long-term state where all reactants settle. Region III connects regions II and IV together. Region III occurs when the two reactions (fast and slow) are in balance (same order of magnitude). The most suitable structured balance is found when $P = O(1)$ and $Q = C = I = O(\epsilon)$, with the shifted time coordinate $\bar{t} = \epsilon^{-1}(\epsilon^2 t - T_{sw})$. The re-scaled variables are $\bar{C} = \epsilon^{-1}C$ and $\bar{I} = \epsilon^{-1}I$. Thus, the Model FCR-M-HP (4.12) at leading order becomes

$$\frac{dP_0}{d\bar{t}} = 0, \tag{4.50a}$$

$$\frac{d\tilde{Q}_0}{d\bar{t}} = \rho P_0 - \gamma\sigma\tilde{Q}_0, \tag{4.50b}$$

$$\frac{d\bar{C}_0}{d\bar{t}} = -\sigma\bar{I}_0\bar{C}_0, \tag{4.50c}$$

$$\frac{d\bar{I}_0}{d\bar{t}} = \gamma\sigma\tilde{Q}_0 - \bar{I}_0\bar{C}_0. \tag{4.50d}$$

Equation (4.50a) indicates that the concentration of hydrogen peroxide (P) stays constant between the induction period (Region II) and the long-term state (Region IV) of the Model FCR-M-HP (4.12) at leading order. We find the following solution for P_0 through the matching condition with Region II (i.e., $P(t_{sw})$),

$$P_0 = \frac{\rho + \sigma\phi - 1}{\rho}. \tag{4.51}$$

We can also derive the correction term for the variable P:

$$\epsilon^2 \frac{\bar{P}_1}{d\bar{t}} = -\epsilon^2 \sigma \bar{P}_0, \tag{4.52}$$

giving

$$\bar{P}_1 = -\sigma P_0 \bar{t} + a_1, \tag{4.53}$$

the constant $a_1 = 0$ by matching condition to Region II solutions. This leads to

$$P = \bar{P}_0 + \epsilon \bar{P}_1, \tag{4.54}$$

$$= \frac{\rho + \sigma\phi - 1}{\rho} - \frac{\epsilon\sigma\left(\rho + \sigma\phi - 1\right)}{\rho}\bar{t}. \tag{4.55}$$

Substituting (4.51) into equation (4.50b) gives

$$\frac{d\tilde{Q}_0}{d\bar{t}} = (\rho + \sigma\phi - 1) - \gamma\sigma\tilde{Q}_0, \tag{4.56}$$

yielding,

$$\frac{-1}{\gamma\sigma} \ln \left| \gamma\sigma \left(\frac{(\rho + \sigma\phi - 1)}{\gamma\sigma} - \tilde{Q}_0 \right) \right| = \bar{t} + c_1, \tag{4.57}$$

where c_1 is a constant of integration. Considering the quasi-steady-state of (4.56) gives

$$\tilde{Q}_0 \approx \frac{(\rho + \sigma\phi - 1)}{\gamma\sigma}, \tag{4.58}$$

and substituting (4.58) into (4.50d) yields

$$\frac{d\bar{I}_0}{d\bar{t}} = (\rho + \sigma\phi - 1) - \bar{I}_0\bar{C}_0. \tag{4.59}$$

Hence, we obtain the following system

$$\frac{d\bar{C}_0}{d\bar{t}} = -\sigma \bar{I}_0 \bar{C}_0, \tag{4.60a}$$

$$\frac{d\bar{I}_0}{d\bar{t}} = (\rho + \sigma\phi - 1) - \bar{I}_0 \bar{C}_0. \tag{4.60b}$$

The quantity $(\rho + \sigma\phi - 1)$ is a positive constant, leading to the expression

$$\frac{d}{d\bar{t}} \left(\sigma \bar{I}_0 - \bar{C}_0\right) = \sigma \left(\rho + \sigma\phi - 1\right), \tag{4.61}$$

and, hence,

$$\sigma \bar{I}_0 - \bar{C}_0 = \sigma \left(\rho + \sigma\phi - 1\right) \bar{t} + c_2, \tag{4.62}$$

where c_2 is a constant of integration. Equation (4.60a) becomes the Riccati Equation [8, 27]:

$$\frac{d\bar{C}_0}{d\bar{t}} = -\left(\sigma \left(\rho + \sigma\phi - 1\right) \bar{t} + c_2 + \bar{C}_0\right) \bar{C}_0. \tag{4.63}$$

We seek a solution of the form $\bar{C}_0 = u'/u$. By applying the quotient rule and integration, we come up with the separable differential equation

$$u'' = -\left(\sigma \left(\rho + \sigma\phi - 1\right) \bar{t} + c_2\right) u'. \tag{4.64}$$

Solving the differential equation, we find the solution

$$u' = \exp\left[-\bar{t} \left(\frac{\sigma \left(\rho + \sigma\phi - 1\right) \bar{t}}{2} + c_2 \right) \right]. \tag{4.65}$$

In order to find a solution of $\bar{C}_0$, we substitute (4.65) into $\bar{C}_0 = u'/u$ and find

$$\bar{C}_0 = \frac{\exp\left[-\bar{t}\left(\sigma\left(\rho+\sigma\phi-1\right)\bar{t}/2+c_2\right)\right]}{\int_0^{\bar{t}} \exp\left[-s\left(\sigma\left(\rho+\sigma\phi-1\right)s/2+c_2\right)\right]ds + c_3}. \tag{4.66}$$

We can express the solution using the error function, where the error function, denoted by erf, is defined as,

$$\text{erf}(z) = \frac{2}{\sqrt{\pi}}\int_0^z e^{-t^2}dt, \tag{4.67}$$

and, hence,

$$\bar{C}_0 = \frac{\exp\left[-\bar{t}\left(\sigma\left(\rho+\sigma\phi-1\right)\bar{t}/2+c_2\right)\right]}{\sqrt{\pi/2\sigma\left(\rho+\sigma\phi-1\right)}\exp\left[c_2^2/2\sigma\left(\rho+\sigma\phi-1\right)\right]\left[\text{erf}(f(\bar{t})+c_4\right]}, \tag{4.68}$$

where,

$$f(\bar{t}) = \sqrt{\frac{\sigma\left(\rho+\sigma\phi-1\right)}{2}}\left[\bar{t}+\frac{c_2}{\sigma\left(\rho+\sigma\phi-1\right)}\right]. \tag{4.69}$$

The constant c_4 can be found by analysing the asymptotic form of the error function [27, 48], which is

$$\text{erf}(x) \sim 1 - e^{-x^2}x^{-1}\pi^{-1/2}\left(1+O(x^{-2})\right), \quad \text{as} \quad x\to\infty,$$

since the error function is odd,

$$\text{erf}(-x) = -\text{erf}(x) \sim -\left(1 - e^{-x^2}x^{-1}\pi^{-1/2}\left(1+O(x^{-2})\right)\right).$$

Hence,

$$\text{erf}(f(\bar{t})) \sim -1 - \frac{\exp\left(-f(\bar{t})^2\right)}{f(\bar{t})\sqrt{\pi}}\left(1 + O(f(\bar{t})^{-2})\right) \quad \text{as} \quad \bar{t} \to -\infty. \tag{4.70}$$

Consequently, substituting (4.70) into (4.68)

$$\bar{C}_0 = \frac{\sqrt{2\sigma\left(\rho + \sigma\phi - 1\right)}\exp\left(-f(\bar{t})^2\right)}{\sqrt{\pi}\big[-1 - \exp\left(-f(\bar{t})^2\right)/f(\bar{t})\sqrt{\pi}\left(1 + O(f(\bar{t})^{-2})\right) + c_4\big]},$$

where,

$$\exp\left(-f(\bar{t})^2\right) = \frac{\exp\left[-\bar{t}\left(\sigma\left(\rho + \sigma\phi - 1\right)\bar{t}/2 + c_2\right)\right]}{\exp\left[c_2^2/2\sigma\left(\rho + \sigma\phi - 1\right)\right]}.$$

Note that as $\bar{t} \to -\infty$, $f(\bar{t}) \to -\infty$ and for $\bar{C}_0$ to have a non-zero limit, we must have $c_4 = 1$. Therefore, the solution can be rearranged as

$$\bar{C}_0 = -\sqrt{2\sigma\left(\rho + \sigma\phi - 1\right)}f(\bar{t})\left(1 + O(f(\bar{t})^{-2})\right), \tag{4.71}$$

and by substituting (4.69) into (4.71) gives

$$\bar{C}_0 = -\sqrt{2\sigma\left(\rho + \sigma\phi - 1\right)}\left(\sqrt{\frac{\sigma\left(\rho + \sigma\phi - 1\right)}{2}}\left[\bar{t} + \frac{c_2}{\sigma\left(\rho + \sigma\phi - 1\right)}\right]\right) \cdot \left(1 + O(f(\bar{t})^2)\right). \tag{4.72}$$

The constant c_2 can be found through matching to Region II. In the Region II variables, we then have

$$C(T) = -\sqrt{2\sigma\left(\rho + \sigma\phi - 1\right)}\left(\sqrt{\frac{\sigma\left(\rho + \sigma\phi - 1\right)}{2}}\left[(T - T_{sw}) + \frac{\epsilon c_2}{\sigma\left(\rho + \sigma\phi - 1\right)}\right]\right),$$

hence, $c_2 = 0$. The solution for $\bar{C}_0$ is

$$\bar{C}_0 = \frac{\exp\left[-\sigma\left(\rho + \sigma\phi - 1\right)\bar{t}^2/2\right]}{\sqrt{\pi/2\sigma\left(\rho + \sigma\phi - 1\right)}\left[\mathrm{erf}\left(\sqrt{\sigma\left(\rho + \sigma\phi - 1\right)/2} \quad \bar{t}\right) + 1\right]}. \tag{4.73}$$

Substituting (4.73) into (4.62), the solution for $\bar{I}_0$ is

$$\bar{I}_0 = \frac{\exp\left[-\sigma\left(\rho + \sigma\phi - 1\right)\bar{t}^2/2\right]}{\sigma\sqrt{\pi/2\sigma\left(\rho + \sigma\phi - 1\right)}\left[\mathrm{erf}\left(\sqrt{\sigma\left(\rho + \sigma\phi - 1\right)/2} \quad \bar{t}\right) + 1\right]} + \left(\rho + \sigma\phi - 1\right)\bar{t}. \tag{4.74}$$

The approximate solutions in Region III in the original variables are, therefore,

$$P(t) = \frac{\rho + \sigma\phi - 1}{\rho} - \frac{\sigma\left(\rho + \sigma\phi - 1\right)}{\rho}\left(\epsilon^2 t - T_{sw}\right), \tag{4.75a}$$

$$Q(t) = \frac{\epsilon\left(\rho + \sigma\phi - 1\right)}{\gamma\sigma}, \tag{4.75b}$$

$$C(t) = \frac{\epsilon\sqrt{2\sigma\left(\rho + \sigma\phi - 1\right)}\exp\left[-\sigma\left(\rho + \sigma\phi - 1\right)\epsilon^{-2}\left(\epsilon^2 t - T_{sw}\right)^2/2\right]}{\sqrt{\pi}\left[\mathrm{erf}\left(\sqrt{\sigma\left(\rho + \sigma\phi - 1\right)/2} \quad \epsilon^{-1}\left(\epsilon^2 t - T_{sw}\right)\right) + 1\right]}, \tag{4.75c}$$

$$I(t) = \frac{\epsilon\sqrt{2\sigma\left(\rho + \sigma\phi - 1\right)}\exp\left[-\sigma\left(\rho + \sigma\phi - 1\right)\epsilon^{-2}\left(\epsilon^2 t - T_{sw}\right)^2/2\right]}{\sigma\sqrt{\pi}\left[\mathrm{erf}\left(\sqrt{\sigma\left(\rho + \sigma\phi - 1\right)/2} \quad \epsilon^{-1}\left(\epsilon^2 t - T_{sw}\right)\right) + 1\right]} + \left(\rho + \sigma\phi - 1\right)\left(\epsilon^2 t - T_{sw}\right). \tag{4.75d}$$

Region IV: Long-term State

Region IV characterises the long-term state of the system. Our predictions are that the solutions will tend towards the equilibrium point as $t \to \infty$ and there will be some of the reactants left over from the reactions after the colour change. All the reactants return to being of $O(1)$, however, $t = O(\epsilon^{-2})$, indicating $T = \epsilon^2 t$. Then the system is composed as follows at the leading order of asymptotic analysis:

$$\frac{dP_0}{dT} = -\sigma\left(1 - 2I_0\right)P_0, \tag{4.76a}$$

$$0 = \rho\left(1 - 2I_0\right)P_0 - \gamma\sigma\left(1 - 2I_0\right)\tilde{Q}_0, \tag{4.76b}$$

$$0 = -\sigma I_0 C_0, \tag{4.76c}$$

$$\frac{dI_0}{dT} = \gamma\sigma\left(1 - 2I_0\right)\tilde{Q}_0. \tag{4.76d}$$

We will prove that $C_n = 0$ for all $n = 0, 1, 2, ...$ by induction. We substitute the asymptotic expansions into (4.76c) before the leading-order terms are taken:

$$\epsilon^2\left(\frac{dC_0}{dT} + \epsilon\frac{dC_1}{dT} + \epsilon^2\frac{dC_2}{dT} + ...\right) = -\sigma\left(I_0 + \epsilon I_1 + \epsilon^2 I_2 + ...\right) \cdot \left(C_0 + \epsilon C_1 + \epsilon^2 C_2 + ...\right), \tag{4.77}$$

We assume that $I_0 \neq 0$ (which is clear from the numerical solutions). For the case $n = 0$,

$$0 = -\sigma I_0 C_0, \tag{4.78}$$

we must have that $C_0 = 0$ as $I_0 \neq 0$. For the case $n = 1$,

$$0 = -\sigma\left(\epsilon I_0 C_1 + \epsilon I_1 C_0\right), \tag{4.79}$$

we must have that $C_1 = 0$ since $C_0 = 0$ and $I_0 \neq 0$. In general at $O(\epsilon^n)$,

$$\frac{dC_{n-2}}{dT} = -\sigma \left(I_0 C_n + ... + I_n C_0 \right). \tag{4.80}$$

Hence $C_0 = ... = C_{n-2} = 0$ implies $C_n = 0$. By induction, we have found $C_n = 0$ for all n. As a result, $C \approx 0$ at all orders of ϵ when $I = O(1)$ and $t = O(\epsilon^{-2})$. This result implies that the vitamin C reactant in Region IV has the asymptotic approximation solution as

$$C(T) = 0. \tag{4.81}$$

Rewriting (4.76b) obtains

$$\rho \left(1 - 2I_0\right) P_0 = \gamma\sigma \left(1 - 2I_0\right) \tilde{Q}_0, \tag{4.82}$$

yielding,

$$\frac{\rho}{\gamma\sigma} P_0 = \tilde{Q}_0. \tag{4.83}$$

Substituting (4.82) into (4.76d) gives,

$$\frac{dI_0}{dT} = \rho \left(1 - 2I_0\right) P_0, \tag{4.84}$$

and dividing (4.76a) by (4.84) gives

$$\frac{dP_0}{dI_0} = \frac{-\sigma}{\rho},$$

which has the following solution

$$P_0 = \frac{-\sigma}{\rho} I_0 + b_1, \tag{4.85}$$

where b_1 is a constant that can be found by matching the condition to Region II ($P_0(T_{sw}) = e^{-\sigma T_{sw}}$):

$$b_1 = e^{-\sigma T_{sw}}.$$

(where T_{sw} is given in (4.47)). Hence,

$$b_1 = \frac{(\rho + \sigma\phi - 1)}{\rho}. \tag{4.86}$$

We will retain the notation b_1 for the rest of the calculation for shortness. Substituting (4.85) into (4.76a),

$$\frac{dP_0}{dT} = -\sigma P_0 \left[1 - \frac{2\rho}{\sigma} \left(-P_0 + b_1 \right) \right], \tag{4.87}$$

which when rearranged leads to

$$\frac{dP_0}{dT} = P_0 \left[-2\rho P_0 + (2\rho b_1 - \sigma) \right]. \tag{4.88}$$

Using the separation of variables and the partial fraction decomposition, the equation (4.88) can be solved to give:

$$\frac{-1}{(2\rho b_1 - \sigma)} \ln \left| \frac{2\rho P_0 - (2\rho b_1 - \sigma)}{P_0} \right| = T + b_2, \tag{4.89}$$

where b_2 is a constant that could be found by matching the condition to Region II (where $P_0(T_{sw}) = b_1$). Noting that $P_0 \gg 0$ and $P_0 = b_1 > 0$, it follows that the term inside the modulus sign is initially positive, so we deduce that

$$\ln\left[\frac{2\rho P_0 - (2\rho b_1 - \sigma)}{P_0}\right] = -\left(2\rho b_1 - \sigma\right)\left(T + b_2\right). \tag{4.90}$$

The constant b_2 is then calculated to be,

$$b_2 = \frac{1}{(2\rho b_1 - \sigma)} \ln\left(\frac{b_1}{\sigma}\right) - T_{sw}. \tag{4.91}$$

Using the natural logarithm properties and the fact that the natural logarithm is the inverse of the exponential function, and then solving for P_0 in equation (4.90) gives

$$P_0 = \frac{(2\rho b_1 - \sigma)}{2\rho - e^{-(2\rho b_1 - \sigma)(T + b_2)}}, \tag{4.92}$$

substituting (4.92) into (4.83) and (4.85) yields

$$\tilde{Q}_0 = \frac{\rho}{\gamma\sigma}\left[\frac{(2\rho b_1 - \sigma)}{2\rho - e^{-(2\rho b_1 - \sigma)(T + b_2)}}\right], \tag{4.93}$$

$$I_0 = \frac{\rho}{\sigma}\left[\frac{-\left(2\rho b_1 - \sigma\right)}{2\rho - e^{-(2\rho b_1 - \sigma)(T + b_2)}} + b_1\right]. \tag{4.94}$$

Moreover, substituting (4.91) into (4.92), then the long-timescale solution for hydrogen peroxide can be expressed as follows:

$$P_0(T) = \frac{2\rho b_1 - \sigma}{2\rho - (\sigma/b_1)\exp\left[-\left(2\rho b_1 - \sigma\right)\left(T - T_{sw}\right)\right]}, \tag{4.95}$$

and, hence,

$$I_0(T) = \rho b_1 \left\{ \frac{1 - \exp\left[-(2\rho b_1 - \sigma)(T - T_{sw}) \right]}{2\rho b_1 - \sigma \exp\left[-(2\rho b_1 - \sigma)(T - T_{sw}) \right]} \right\}. \tag{4.96}$$

Two cases can be distinguished in equations (4.95) and (4.96). The first case is if $(2\rho b_1 - \sigma) > 0$, i.e. there is sufficient hydrogen peroxide remaining following the switchover time, then in the limit as $T \to \infty$,

$$P_0(T) \sim \frac{2\rho b_1 - \sigma}{2\rho} = \frac{2(\rho - 1) + \sigma(2\phi - 1)}{2\rho}, \tag{4.97a}$$

$$I_0(T) \sim \frac{1}{2}, \tag{4.97b}$$

as a result, it means that all of the iodide and hypoiodous acid is converted to molecular iodine.

The second case is if however $(2\rho b_1 - \sigma) < 0$, i.e. there is insufficient hydrogen peroxide remaining following the switchover time, then in the limit as $T \to \infty$,

$$P_0(T) \sim 0, \tag{4.98a}$$

$$I_0(T) \sim \frac{\rho b_1}{\sigma} = \frac{\rho + \sigma\phi - 1}{\sigma}. \tag{4.98b}$$

We consider the first case, where there must be sufficient hydrogen peroxide to convert all iodide to iodine by the end of the whole process of the clock reaction. The condition $(2\rho b_1 - \sigma) > 0$ is required and equivalent to $p_0 > (n_0/2) + c_0 - \iota_0$ in dimensional variables. In summary, the leading order of Region IV solutions

which represent the long-term evolution of the system are,

$$P_0(T) = \frac{2(\rho-1)+\sigma(2\phi-1)}{2\rho - \left(\frac{\sigma\rho}{\rho+\sigma\phi-1}\right)\exp\left[-(2(\rho-1)+\sigma(2\phi-1))(T-T_{sw})\right]}, \tag{4.99a}$$

$$\tilde{Q}_0(T) = \frac{\rho}{\gamma\sigma}\left(\frac{2(\rho-1)+\sigma(2\phi-1)}{2\rho - \left(\frac{\sigma\rho}{\rho+\sigma\phi-1}\right)\exp\left[-(2(\rho-1)+\sigma(2\phi-1))(T-T_{sw})\right]}\right), \tag{4.99b}$$

$$C_0(T) = 0, \tag{4.99c}$$

$$\begin{aligned} I_0(T) = {} & (\rho+\sigma\phi-1)(1-\exp[-(2(\rho-1)+\sigma(2\phi-1))(T-T_{sw})]) \\ & \cdot((\rho+\sigma\phi-1)-\sigma\exp[-(2(\rho-1)+\sigma(2\phi-1))(T-T_{sw})])^{-1}, \end{aligned} \tag{4.99d}$$

where T_{sw} is given in equation (4.47). Alternatively, in the original variables, the approximate solutions in Region IV are, therefore,

$$P(t) = \frac{(2\rho b_1-\sigma)}{2\rho - e^{-(2\rho b_1-\sigma)(\epsilon^2 t+b_2)}} + O(\epsilon), \tag{4.100a}$$

$$Q(t) = \frac{\epsilon\rho}{\gamma\sigma}\left[\frac{(2\rho b_1-\sigma)}{2\rho - e^{-(2\rho b_1-\sigma)(\epsilon^2 t+b_2)}}\right] + O(\epsilon^2), \tag{4.100b}$$

$$C(t) = 0 + O(\epsilon^n), \text{ for all } n > 0, \tag{4.100c}$$

$$I(t) = \frac{\rho}{\sigma}\left[\frac{-(2\rho b_1-\sigma)}{2\rho - e^{-(2\rho b_1-\sigma)(\epsilon^2 t+b_2)}} + b_1\right] + O(\epsilon), \tag{4.100d}$$

where the constants b_1 and b_2 are given in equations (4.86) and (4.91).

Comparison Of Asymptotic And Numerical Approximations Of Model FCR-M-HP

Matlab (*ode45* solver) is used to calculate a numerical solution with initial conditions $P(0) = 1$, $Q(0) = 0$, $C(0) = 1$ and $I(0) = \phi$, and the dimensionless parameter values are $\gamma = 0.7$, $\beta = 0.6$, $\rho = 2$, $\sigma = 0.8$, $\phi = 0.2$ (iodide:iodine ratio) and $\epsilon = 0.01$ (the reaction rate ratio), these values are chosen arbitrarily. The numerical solutions are compared with the asymptotic solutions found for each region.

A comparison of the asymptotic and numerical solution of the model (4.12) is shown in Figure 4.3. The Region I and Region I-a solutions follow the numerical approximation very closely up to around $t = 400$. The Region II solution then follows the numerical solution up to around $t = 5,000$. At the end of Region II (induction period), the switchover time point occurs when the concentration of the clock chemical reaction iodine (I) increases after the concentration of vitamin C (C) has been used. It illustrates that $t = 7,000$. The Region III solution then closely follows the numerical solution around the switchover time $t = 7,000$, up to around $t = 8,000$. After that, the agreement between the numerical and asymptotic solutions is excellent, using the shifted time coordinate $t = \epsilon^{-2}(\epsilon\bar{t} + T_{sw})$, in Region IV. Importantly, the matching between the numerical and asymptotic solutions is becoming more adequate for smaller values of ϵ (examples not shown for brevity).

Figure 4.4 depicts the intersecting point of C and I from the numerical solution of the model (4.12) and the evaluated switchover time (t_{sw}); there is excellent

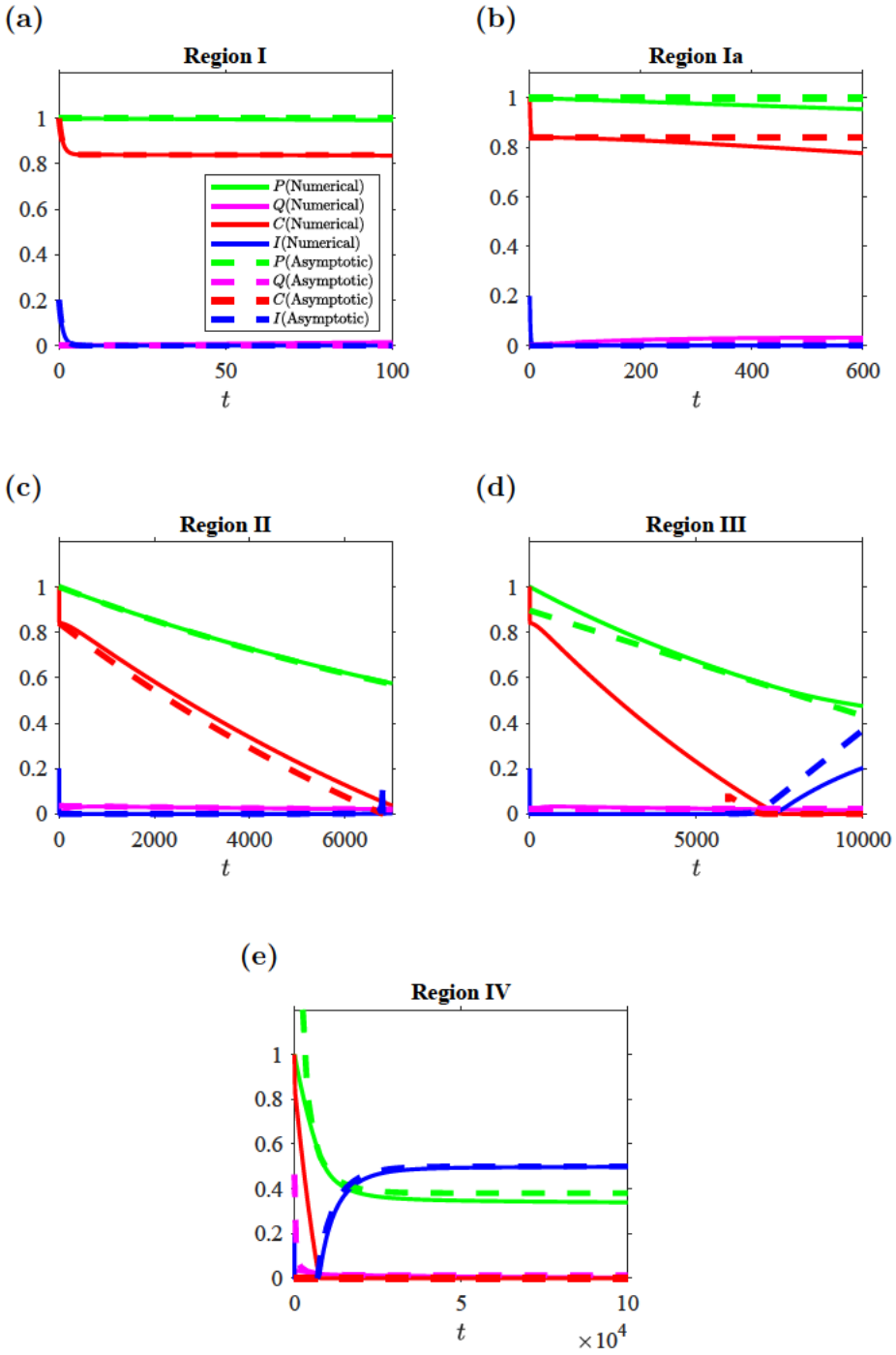

Figure 4.3: Comparison between numerical and asymptotic solutions of the Model FCR-M-HP (4.12) for all regions with initial conditions $P(0) = 1$, $Q(0) = 0$, $C(0) = 1$ and $I(0) = \phi$, and the dimensionless parameter values are $\gamma = 0.7$, $\beta = 0.6$, $\rho = 2$, $\sigma = 0.8$, $\phi = 0.2$ and $\epsilon = 0.01$.

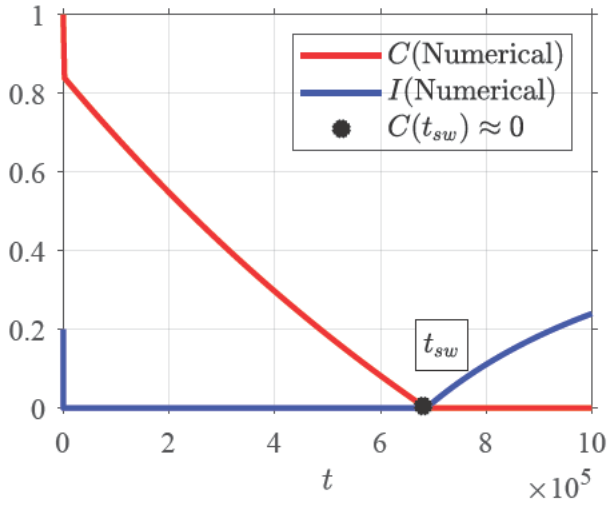

Figure 4.4: Numerical solutions for $C(t)$ and $I(t)$ of the model (4.12) shown alongside the value of the switchover time (intersecting point) calculated by the approximate formula (4.47), with initial conditions $P(0) = 1$, $Q(0) = 0$, $C(0) = 1$ and $I(0) = \phi$, and the dimensionless parameter values are $\gamma = 0.7$, $\beta = 0.6$, $\rho = 2$, $\sigma = 0.8$, $\phi = 0.2$ and $\epsilon = 0.001$.

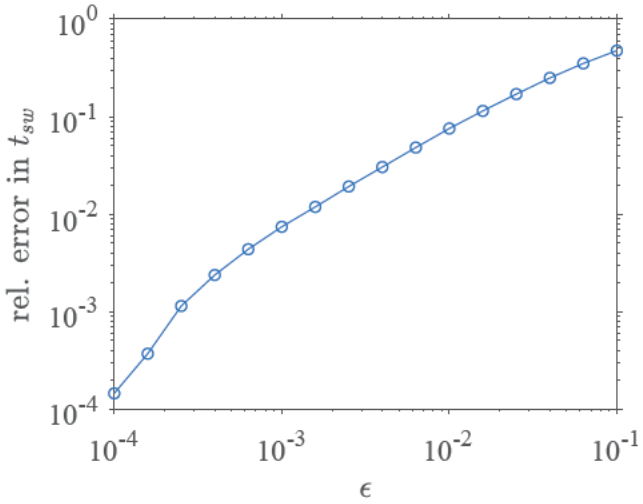

Figure 4.5: Relative error between the asymptotic approximation for the switchover time formula (4.47) of the model (4.12) and the point at which the numerical solution falls below a threshold value of ϵ, as a function of the parameter ϵ. The dimensionless parameter values are $\gamma = 0.7$, $\beta = 0.6$, $\rho = 2$, $\sigma = 0.8$ and $\phi = 0.2$.

agreement. Figure 4.5 plots the relative error between the asymptotic approximation of the switchover time formula (4.47) and the switchover time point computed from the numerical solution of the model (4.12), as a function of ϵ. The convergence of the error as $\epsilon \to 0$ is approximately linear, and the gradient on a log-log scale is approximately 1.

A log-log plot can be used to visualize how errors decrease as ϵ decreases. In this case, the relative errors have been calculated by

$$\frac{|T_{num} - T_{asymp}|}{T_{asymp}},$$

where T_{num} represents the switchover time point computed from the numerical solution of the model (4.12) and T_{asymp} represents the switchover time formula derived through asymptotic analysis, given in (4.47). It yields

$$\frac{|T_{num} - T_{asymp}|}{T_{asymp}} \approx \epsilon^1,$$

because the slope (gradient) on a log-log scale is ≈ 1 (is calculated based on the last two points of smaller ϵ values from the log-log plot using MATLAB). This result is consistent with taking only the leading-order terms of the asymptotic expansion approach, as we expected the convergence to be $O(\epsilon)$.

4.3.2 Model FCR-H-HP: The Full Model With High Hydrogen Peroxide

We consider, now, that there is a high hydrogen peroxide (P) concentration in the system. Thus, we assume that ρ is order ϵ^{-1} in the Model FCR (4.8), where

$\rho = p_0/c_0$, denoting $\hat{\rho} = \epsilon\rho$. We obtain the following model, named Model FCR-H-HP:

$$\frac{dP}{dt} = -\epsilon^2\sigma\left(1 - Q - 2I\right)P - \epsilon^2\beta\sigma QP, \tag{4.101a}$$

$$\frac{dQ}{dt} = \epsilon\hat{\rho}\left(1 - Q - 2I\right)P - \epsilon\gamma\sigma\left(1 - Q - 2I\right)Q - \epsilon\beta\hat{\rho}QP, \tag{4.101b}$$

$$\frac{dC}{dt} = -\sigma IC, \tag{4.101c}$$

$$\frac{dI}{dt} = \epsilon\gamma\sigma\left(1 - Q - 2I\right)Q - IC. \tag{4.101d}$$

The initial conditions are as follows:

$$P(0) = 1, \quad Q(0) = 0, \quad C(0) = 1, \quad I(0) = \phi. \tag{4.102}$$

Figure 4.1b illustrates the concentrations of the reactants as a function of time, for the high hydrogen peroxide model (4.101). The clock reaction (in which iodine (I) appears after the induction period) occurs when vitamin C is totally consumed. It reveals when $\rho = O(\epsilon^{-1})$, the hydrogen peroxide (P) concentration stays high whereas hypoiodous acid (Q) concentration is not low at the beginning of the reaction, however, it decreases slowly, and eventually goes to zero. Similar to the previous section, Model FCR-H-HP (4.101) will be analysed through four asymptotic regions in detail in the following sections.

Region I: Initial Adjustment

The first region can be defined as where the dependent variables I, C, P are order 1, Q is order ϵ and the independent variable $t = O(1)$. Re-scaling $Q = \epsilon\tilde{Q}$. The leading order terms for the asymptotic expansion of the Model FCR-H-HP (4.101)

are:

$$\frac{dP_0}{dt} = 0, \tag{4.103a}$$

$$\frac{d\tilde{Q}_0}{dt} = \hat{\rho}\,(1 - 2I_0)\,P_0, \tag{4.103b}$$

$$\frac{dC_0}{dt} = -\sigma I_0 C_0, \tag{4.103c}$$

$$\frac{dI_0}{dt} = -I_0 C_0. \tag{4.103d}$$

As stated in the analysis of the Model FCR-M-HP section, this yields

$$P_0 = 1, \tag{4.104}$$

$$I_0 = \frac{\phi\,(1 - \sigma\phi)\,e^{-(1-\sigma\phi)t}}{1 - \sigma\phi e^{-(1-\sigma\phi)t}}, \tag{4.105}$$

and,

$$C_0 = \frac{\sigma\phi\,(1 - \sigma\phi)\,e^{-(1-\sigma\phi)t}}{1 - \sigma\phi e^{-(1-\sigma\phi)t}} + (1 - \sigma\phi)\,. \tag{4.106}$$

Substituting (4.104) and (4.105) into (4.103b) leads to the separable ordinary differential equation,

$$\frac{d\tilde{Q}_0}{dt} = \hat{\rho}\left[1 - \frac{2\phi\,(1 - \sigma\phi)\,e^{-(1-\sigma\phi)t}}{1 - \sigma\phi e^{-(1-\sigma\phi)t}}\right], \tag{4.107}$$

with solution,

$$\tilde{Q}_0 = \hat{\rho}t - \frac{2\hat{\rho}}{\sigma}\ln\left(1 - \sigma\phi e^{-(1-\sigma\phi)t}\right) + \frac{2\hat{\rho}}{\sigma}\ln\left(1 - \sigma\phi\right). \tag{4.108}$$

We observe that as $t \to \infty$,

$$\left(P_0(t), \tilde{Q}_0(t), C_0(t), I_0(t)\right) \to \left(1, \hat{\rho}t, \left(1-\sigma\phi\right), 0\right).$$

It follows that the approximation solutions at Region I are:

$$P(t) = 1 + O(\epsilon), \tag{4.109a}$$

$$Q(t) = \epsilon\left[\hat{\rho}t - \frac{2\hat{\rho}}{\sigma}\ln\left(1-\sigma\phi e^{-(1-\sigma\phi)t}\right) + \frac{2\hat{\rho}}{\sigma}\ln\left(1-\sigma\phi\right)\right] + O(\epsilon^2), \tag{4.109b}$$

$$C(t) = \frac{\sigma\phi\left(1-\sigma\phi\right)e^{-(1-\sigma\phi)t}}{1-\sigma\phi e^{-(1-\sigma\phi)t}} + \left(1-\sigma\phi\right) + O(\epsilon), \tag{4.109c}$$

$$I(t) = \frac{\phi\left(1-\sigma\phi\right)e^{-(1-\sigma\phi)t}}{1-\sigma\phi e^{-(1-\sigma\phi)t}} + O(\epsilon). \tag{4.109d}$$

Region II: Induction Period

The second region can be represented as where the dependent variables Q, C, P are order 1, I is order ϵ and the independent variable $t = O(\epsilon^{-1})$, i.e., we re-scale $I = \epsilon\tilde{I}$ and $t = \epsilon^{-1}\tau$. The leading order for the asymptotic expansion of the Model FCR-H-HP (4.101) takes the form,

$$\frac{dP_0}{d\tau} = 0, \tag{4.110a}$$

$$\frac{dQ_0}{d\tau} = \hat{\rho}\left(1-Q_0\right)P_0 - \gamma\sigma\left(1-Q_0\right)Q_0 - \beta\hat{\rho}Q_0P_0, \tag{4.110b}$$

$$\frac{dC_0}{d\tau} = -\sigma\tilde{I}_0C_0, \tag{4.110c}$$

$$0 = \gamma\sigma\left(1-Q_0\right)Q_0 - \tilde{I}_0C_0. \tag{4.110d}$$

Note that the C_0 equation (i.e., (4.110c)) is balanced. We can solve the equation (4.110a) directly by matching to Region I, obtaining the solution

$$P_0 = 1, \tag{4.111}$$

and substituting (4.111) into (4.110b) yields

$$\frac{dQ_0}{d\tau} = \hat{\rho}\,(1 - Q_0) - \gamma\sigma\,(1 - Q_0)\,Q_0 - \beta\hat{\rho}Q_0, \tag{4.112}$$

which can be written as

$$\frac{dQ_0}{d\tau} = Q_0\,(\gamma\sigma Q_0 - a) + \hat{\rho}, \tag{4.113}$$

where,

$$a = \hat{\rho}\,(1 + \beta) + \gamma\sigma. \tag{4.114}$$

Solving (4.113) through integration, we find the following,

$$\frac{2}{\sqrt{4\gamma\sigma\hat{\rho} - a^2}} \arctan\left[\frac{2\gamma\sigma Q_0 - a}{\sqrt{4\gamma\sigma\hat{\rho} - a^2}}\right] = \tau + c_1, \tag{4.115}$$

where c_1 is the constant of integration, and the expression under the square root is negative since $a^2 - 4\gamma\sigma\hat{\rho}$ is positive because

$$\begin{aligned} a^2 - 4\gamma\sigma\hat{\rho} &= \hat{\rho}^2 (1+\beta)^2 + \sigma^2\gamma^2 + 2\gamma\sigma\hat{\rho}(\beta - 1) \\ &= \hat{\rho}^2 (1+\beta)^2 + \sigma^2\gamma^2 + 2\gamma\sigma\hat{\rho}(\beta - 1) + \hat{\rho}^2 (\beta-1)^2 - \hat{\rho}^2 (\beta-1)^2 \\ &= (\hat{\rho}(\beta - 1) + \gamma\sigma)^2 + 4\beta\hat{\rho}^2 \\ &> 0. \end{aligned} \tag{4.116}$$

Equation (4.115) can be expressed as

$$\frac{1}{ib} \arctan\left[\frac{1}{ib}\left(\gamma\sigma Q_0 - \frac{a}{2}\right)\right] = \tau + c_1. \tag{4.117}$$

The constant b is real-valued given by

$$b = \frac{\sqrt{a^2 - 4\gamma\sigma\hat{\rho}}}{2}. \tag{4.118}$$

Therefore, the solution for Q_0 is

$$Q_0 = \frac{ib}{\gamma\sigma} \tan\left[ib(\tau + c_1)\right] + \frac{a}{2\gamma\sigma}. \tag{4.119}$$

Using the relations between trigonometric and hyperbolic functions, $\tan(iz) = i\tanh(z)$, yields

$$Q_0 = \frac{-b}{\gamma\sigma} \tanh\left[b(\tau + c_1)\right] + \frac{a}{2\gamma\sigma}. \tag{4.120}$$

The constant c_1 of the integration can be determined by matching the conditions to Region I (as $t \to \infty$, $Q_0(t) \to 0$); therefore,

$$c_1 = \frac{1}{b} \operatorname{arctanh}\left(\frac{a}{2b}\right). \tag{4.121}$$

We express the solution (4.120) using the sum of angles properties, which is defined as,

$$\tanh(\theta_1 + \theta_2) = \frac{\tanh(\theta_1) + \tanh(\theta_2)}{1 + \tanh(\theta_1)\tanh(\theta_2)}, \tag{4.122}$$

by applying (4.122) into (4.120) leads to

$$Q_0 = \frac{-b}{\gamma\sigma}\left[\frac{\tanh(b\tau) + \tanh(bc_1)}{1 + \tanh(b\tau)\tanh(bc_1)}\right] + \frac{a}{2\gamma\sigma}. \tag{4.123}$$

Note that c_1 is given by (4.121), and, hence,

$$\tanh(bc_1) = \tanh\left(\frac{b \operatorname{arctanh}\left(\frac{-a}{2b}\right)}{b}\right), \tag{4.124}$$

or equivalently,

$$\tanh(bc_1) = \frac{a}{2b}. \tag{4.125}$$

Hence,

$$Q_0 = \frac{-b}{\gamma\sigma}\left[\frac{\tanh(b\tau) + \frac{a}{2b}}{1 + \frac{a}{2b}\tanh(b\tau)}\right] + \frac{a}{2\gamma\sigma}. \tag{4.126}$$

From equation (4.110d), we have

$$\tilde{I}_0 C_0 = \gamma\sigma(1 - Q_0)Q_0, \tag{4.127}$$

where Q_0 has the solution (4.126). Substituting (4.127) into (4.110c) leads to

$$\frac{dC_0}{d\tau} = \left\{\sigma b\left[\frac{2b\tanh(b\tau)+a}{2b+a\tanh(b\tau)}\right]-\frac{\sigma a}{2}\right\}\left\{1+\frac{b}{\gamma\sigma}\left[\frac{2b\tanh(b\tau)+a}{2b+a\tanh(b\tau)}\right]-\frac{a}{2\gamma\sigma}\right\}. \quad (4.128)$$

Solving the equation above through integration, we find

$$C_0 = w_1 \ln\left|\cosh(b\tau)+\frac{a}{2b}\sinh(b\tau)\right| + w_2\left[\frac{2b}{2b+a\tanh(b\tau)}\right] + w_3\tau + w_4, \quad (4.129)$$

where w_4 is the constant of integration and can be found by matching to Region I (as $t \to \infty$, $C_0(t) \to (1-\sigma\phi)$), and

$$w_1 = \frac{-\hat{\rho}(1+\beta)}{\gamma}, \quad (4.130)$$

$$w_2 = \frac{-2\sigma\hat{\rho}}{a}, \quad (4.131)$$

$$w_3 = \frac{\hat{\rho}\left[a(1+\beta)-2\gamma\sigma\right]}{2\gamma}, \quad (4.132)$$

$$w_4 = (1-\sigma\phi) - w_2, \quad (4.133)$$

(we remark that $w_1, w_2 < 0$ and $w_3, w_4 > 0$). Substituting (4.126) and (4.129) into (4.127) and rearranging for $\bar{I}_0$ completes the leading order solutions in Region II. As this expression is quite long, the solution is given below in terms of Q_0 and C_0.

The leading order solutions in Region II are therefore,

$$P_0(\tau) = 1, \tag{4.134a}$$

$$Q_0(\tau) = \frac{-b}{\gamma\sigma}\left[\frac{2b\tanh(b\tau)+a}{2b+a\tanh(b\tau)}\right] + \frac{a}{2\gamma\sigma}, \tag{4.134b}$$

$$C_0(\tau) = w_1 \ln\left|\cosh(b\tau) + \frac{a}{2b}\sinh(b\tau)\right| - w_2\left[\frac{a\tanh(b\tau)}{2b+a\tanh(b\tau)}\right] + w_3\tau + (1-\sigma\phi), \tag{4.134c}$$

$$\tilde{I}_0(\tau) = \frac{\gamma\sigma(1-Q_0(\tau))Q_0(\tau)}{C_0(\tau)}. \tag{4.134d}$$

Studying the clock reaction model's details means carefully looking at what factors affect the switchover time formula, helping us understand when the reaction changes state.

Switchover Time:

The switchover time occurs when the concentration of iodine (I) increases, indicating that the vitamin C concentration is low (that is, $C \approx 0$), and the solution changes color to dark blue, indicating the end of the induction period. The switchover time can again be approximated by solving $C_0(\tau_{sw}) \approx 0$, yielding

$$0 \approx w_1 \ln\left|\cosh(b\tau_{sw}) + \frac{a}{2b}\sinh(b\tau_{sw})\right| - w_2\left[\frac{a\tanh(b\tau_{sw})}{2b+a\tanh(b\tau_{sw})}\right] + w_3\tau_{sw} + (1-\sigma\phi), \tag{4.135}$$

which can be simplified using the following hyperbolic function properties:

$$\sinh\left(b\tau_{sw}\right) = \frac{1}{2}\left(e^{b\tau_{sw}} - e^{-b\tau_{sw}}\right), \tag{4.136}$$

$$\cosh\left(b\tau_{sw}\right) = \frac{1}{2}\left(e^{b\tau_{sw}} + e^{-b\tau_{sw}}\right), \tag{4.137}$$

$$\tanh\left(b\tau_{sw}\right) = \frac{e^{b\tau_{sw}} - e^{-b\tau_{sw}}}{e^{b\tau_{sw}} + e^{-b\tau_{sw}}}, \tag{4.138}$$

leading to

$$\begin{aligned} 0 \approx\ & w_1 \ln\left[e^{b\tau_{sw}}\left(\frac{1}{2} + \frac{a}{4b}\right) + e^{-b\tau_{sw}}\left(\frac{1}{2} - \frac{a}{4b}\right)\right] \\ & - w_2\left[\frac{a\left(e^{b\tau_{sw}} - e^{-b\tau_{sw}}\right)}{2b\left(e^{b\tau_{sw}} + e^{-b\tau_{sw}}\right) + a\left(e^{b\tau_{sw}} - e^{-b\tau_{sw}}\right)}\right] \\ & + w_3\tau + 1 - \sigma\phi. \end{aligned} \tag{4.139}$$

For even moderately sized values of $b\tau_{sw}$, the value of $e^{-b\tau_{sw}}$ is negligible due to exponential decay (i.e., $e^{-b\tau_{sw}} \to 0$ as $\tau_{sw} \to \infty$). Therefore, the solution for $C_0(\tau_{sw})$ can be written as

$$0 \approx C_0(\tau_{sw}) = w_1 \ln\left[e^{b\tau_{sw}}\left(\frac{1}{2} + \frac{a}{4b}\right)\right] - w_2\left(\frac{a}{2b+a}\right) + w_3\tau_{sw} + 1 - \sigma\phi. \tag{4.140}$$

Applying the logarithm properties for $\ln(xy) = \ln(x) + \ln(y)$ and rearranging (4.140) leads to

$$0 \approx \left(bw_1 + w_3\right)\tau_{sw} + w_1 \ln\left(\frac{1}{2} + \frac{a}{4b}\right) - \frac{aw_2}{(2b+a)} + 1 - \sigma\phi. \tag{4.141}$$

Accordingly, this yields

$$\tau_{sw} \approx \frac{-w_1 \ln\left(\frac{1}{2}+\frac{a}{4b}\right)+\frac{aw_2}{(2b+a)}-1+\sigma\phi}{(bw_1+w_3)}. \tag{4.142}$$

We simplify the expression in (4.142) in terms of the dimensionless parameters. Focusing on the numerator of (4.142), this can be written as,

$$\left[\frac{\hat{\rho}\,(1+\beta)}{\gamma}\ln\left(\frac{1}{2}+\frac{a}{2\sqrt{a^2-4\gamma\sigma\hat{\rho}}}\right)-\frac{2\sigma\hat{\rho}}{\sqrt{a^2-4\gamma\sigma\hat{\rho}}+a}\right]-1+\sigma\phi. \tag{4.143}$$

Using the logarithmic and binomial expansion formula of rational exponents where $4\sigma\gamma\hat{\rho}/a^2 < 1$ since $a^2 > 4\sigma\gamma\hat{\rho}$ (as mentioned above), the equation (4.143) leads to

$$\frac{\hat{\rho}\,(1+\beta)}{\gamma}\left(\frac{\gamma\sigma\hat{\rho}}{a^2}+...\right)-\frac{\sigma\hat{\rho}}{a}\,(1+...)-1+\sigma\phi, \tag{4.144}$$

and the leading order terms of the expansion is

$$\frac{\hat{\rho}\sigma}{a^2}\left[\hat{\rho}\,(1+\beta)-a\right]-1+\sigma\phi. \tag{4.145}$$

Substituting (4.114) into (4.145) renders this to

$$\frac{-\hat{\rho}\gamma}{\left(\frac{\hat{\rho}(1+\beta)}{\sigma}+\gamma\right)^2}-1+\sigma\phi. \tag{4.146}$$

Note that its maximum value occurs when $\gamma = \hat{\rho}\,(1+\beta)\,/\sigma$, in which case the term takes the value

$$\frac{-\sigma}{4\,(1+\beta)}-1+\sigma\phi. \tag{4.147}$$

We can neglect the first term in (4.147) since σ is small in comparison with $4\,(1+\beta)$, which means

$$\frac{-\sigma}{4\,(1+\beta)} \approx 0, \tag{4.148}$$

and hence, the numerator of (4.142) can be approximated by:

$$-1+\sigma\phi. \tag{4.149}$$

In dimensional variables, this assumption used above corresponds to $n_0/c_0 \ll 4\,(1+k_4/k_2)$, which holds if the initial vitamin C concentration is high enough.

Moving onto the denominator of (4.142) we have

$$\frac{-\hat{\rho}}{2\gamma}\left[(1+\beta)\left(a+\sqrt{a^2-4\gamma\sigma\hat{\rho}}\right)-2\gamma\sigma\right]. \tag{4.150}$$

The dimensionless expression of the switchover time formula can therefore be simplified to,

$$\tau_{sw} \approx \frac{2\gamma\,(-1+\sigma\phi)}{-\hat{\rho}\left[(1+\beta)\left(\sqrt{a^2-4\gamma\sigma\hat{\rho}}-a\right)+2\gamma\sigma\right]}, \tag{4.151}$$

or in dimensional variables (i.e., recall (4.7) and (4.9)),

$$t_{sw} \approx \frac{1}{\epsilon k_2 c_0}\frac{\left(1-\frac{n_0}{c_0}\phi\right)}{\left(\frac{\epsilon p_0}{c_0}\right)\left(\frac{n_0}{c_0}\right)\left[\frac{(1+\beta)(A-B)+2\gamma}{2\gamma}\right]}, \tag{4.152}$$

where,

$$A = \sqrt{\frac{\epsilon^2 p_0^2}{n_0^2}(1+\beta)^2 - 2\gamma\frac{\epsilon p_0}{n_0} + 2\gamma\beta\frac{\epsilon p_0}{n_0} + \gamma^2}, \tag{4.153}$$

$$\tag{4.154}$$

$$B = \left(\frac{\epsilon p_0}{n_0} + \gamma + \beta\frac{\epsilon p_0}{n_0}\right). \tag{4.155}$$

Therefore, the switchover time formula can be written as

$$t_{sw} \approx \frac{c_0 - \phi n_0}{n_0^2\left\{\epsilon k_2\left(\frac{\epsilon p_0}{n_0}\right)\left[\frac{(1+\beta)(A-B)+2\gamma}{2\gamma}\right]\right\}}. \tag{4.156}$$

We now compare this result with that derived by Kerr et al [27] with high hydrogen peroxide in the clock reaction, but with less detail used to capture the slow reaction. There, the switchover time formula was characterized by,

$$t_{sw}^{\text{Kerr}} \approx \frac{c_0 - \phi n_0}{k_0 n_0^2}, \tag{4.157}$$

(with dependence on initial concentrations c_0 and n_0, and the rate k_0 of the slow reaction). Hence, there is an agreement between our switchover time formula in (4.156) and the formula by Kerr et al [27] in (4.157). Both numerators of (4.156) and (4.157) are identical, and k_0 in the denominator of (4.157) can be described by the expression within the braces in (4.156). The switchover time in a clock reaction is the moment when a visible change (dark-blue color) occurs. Increasing the molecular iodine concentration (n_0) speeds up the switchover time in equations (4.156) and (4.157), which will shorten the duration of the induction period

because more molecular iodine (n_0) will be available to react with vitamin C (c_0), allowing the reaction to reach the visible color more quickly (i.e., as n_0 increases, t_{sw} decreases because the denominator grows quadratically). Decreasing the vitamin C concentration (c_0) reduces the amount of molecular iodine (n_0) needed to be consumed, thereby shortening the induction period. We can control the switchover time and the length of the induction period by adjusting the concentrations of iodine and vitamin C. This result highlights that an expression of the slow reaction rate (k_0, as stated in the article [27]) can be composed to

$$k_0 = \frac{\epsilon^2 k_2 \left(\frac{p_0}{n_0}\right) \left[(1+\beta)(A-B) + 2\gamma\right]}{2\gamma}. \tag{4.158}$$

The parameter k_0 depends on the initial concentrations p_0 and n_0 only through their ratio, expressed as

$$k_0 = \frac{\epsilon^2 k_2}{2\gamma}\left(\frac{p_0}{n_0}\right)\left\{(1+\beta)\left[\sqrt{\frac{\epsilon^2 p_0^2}{n_0^2}(1+\beta)^2 - 2\gamma\frac{\epsilon p_0}{n_0} + 2\gamma\beta\frac{\epsilon p_0}{n_0} + \gamma^2}\right.\right.$$
$$\left.\left. - \left(\frac{\epsilon p_0}{n_0} + \gamma + \beta\frac{\epsilon p_0}{n_0}\right)\right] + 2\gamma\right\}. \tag{4.159}$$

To keep our approximation as simple as possible and to minimise the number of parameters, we will assume that k_0 can be expressed as

$$k_0 \approx \epsilon^2 k_2 \left(\frac{p_0}{n_0}\right), \tag{4.160}$$

(we will see in Chapter 5 that this simplification works well). Therefore, the

switchover time formula in (4.156) can be simplified as :

$$t_{sw} = \frac{c_0 - \phi n_0}{k_3 n_0 p_0}, \tag{4.161}$$

(depending on initial concentrations c_0, p_0 and n_0, and the rate limiting k_3 of the slow reaction where $\epsilon^2 k_2 = k_3$). This result, the simplified switchover time formula in (4.161), is consistent with the switchover time formula obtained by Kerr et al [27] in (4.157) for the clock reaction model with high hydrogen peroxide.

Approximation solution at Steady-state in R-II:

To consider the approximate scaling to move to R-III, we consider the behaviour as $\tau \to \infty$:

$$P_0 = 1, \tag{4.162a}$$

$$Q_0 = Q_0^{ss}, \tag{4.162b}$$

$$C_0 = -\gamma\sigma^2 \left(1 - Q_0^{ss}\right) Q_0^{ss} \tau, \tag{4.162c}$$

$$\tilde{I}_0 = \frac{-1}{\sigma\tau}, \tag{4.162d}$$

with,

$$Q_0^{ss} = \frac{a \pm \sqrt{a^2 - 4\gamma\sigma\hat{\rho}}}{2\gamma\sigma} \quad \text{where} \quad a = \left(\hat{\rho} + \gamma\sigma + \beta\hat{\rho}\right). \tag{4.163}$$

Hence, for a more realistic (small) value for the reactant Q, the quasi-steady- state for Q_0^{ss} will be chosen as

$$Q_0^{ss} = \frac{\left(\hat{\rho} + \gamma\sigma + \beta\hat{\rho}\right) - \sqrt{\left(\hat{\rho} + \gamma\sigma + \beta\hat{\rho}\right)^2 - 4\gamma\sigma\hat{\rho}}}{2\gamma\sigma}. \tag{4.164}$$

That enables us to find the most structured balance for the corner region.

Region III: Corner

Scaling the variables $C = I = O(\epsilon^{1/2})$ and introducing the shifted time coordinate $\bar{\tau} = \epsilon^{-1/2}(\epsilon t - \tau_{sw})$. The leading order for the asymptotic expansion of the Model FCR-H-HP (4.101), of the re-scaled system, is then,

$$\frac{dP_0}{d\bar{\tau}} = 0, \tag{4.165a}$$
$$\frac{dQ_0}{d\bar{\tau}} = 0, \tag{4.165b}$$
$$\frac{d\bar{C}_0}{d\bar{\tau}} = -\sigma \bar{I}_0 \bar{C}_0, \tag{4.165c}$$
$$\frac{d\bar{I}_0}{d\bar{\tau}} = \gamma\sigma\,(1 - Q_0)\,Q_0 - \bar{I}_0\bar{C}_0. \tag{4.165d}$$

We can gain the solutions for the variables P_0 and Q_0, directly by matching to the steady-state solution in R-II (4.162), leading to

$$P_0 = 1, \tag{4.166}$$

and,

$$Q_0 = Q_0^{ss}, \tag{4.167}$$

which is given in (4.164). Hence, the system (4.165) can be reduced to

$$\frac{d\bar{C}_0}{d\bar{\tau}} = -\sigma \bar{I}_0 \bar{C}_0, \tag{4.168a}$$
$$\frac{d\bar{C}_0}{d\bar{\tau}} = \mu - \bar{I}_0\bar{C}_0, \tag{4.168b}$$

where,

$$\mu = \gamma\sigma\,(1 - Q_0^{ss})\,Q_0^{ss}; \tag{4.169}$$

note that μ is a constant. The system (4.168) can be rearranged to yield the Riccati equation:

$$\frac{d\bar{C}_0}{d\bar{\tau}} = -\left(\sigma\mu\bar{\tau} + \bar{c}_3 + \bar{C}_0\right)\bar{C}_0. \tag{4.170}$$

A similar analysis to Region III with a low hydrogen peroxide model can be done, therefore, the approximate solutions in Region III are

$$P(t) = 1, \tag{4.171a}$$

$$Q(t) = \frac{(\hat{\rho} + \gamma\sigma + \beta\hat{\rho}) - \sqrt{(\hat{\rho} + \gamma\sigma + \beta\hat{\rho})^2 - 4\gamma\sigma\hat{\rho}}}{2\gamma\sigma}, \tag{4.171b}$$

$$C(t) = \frac{\epsilon^{1/2}\sqrt{\sigma\mu}\exp\left\{-\sigma\mu/2\left[\left(\epsilon^{-1/2}\left(\epsilon t - \tau_{swt}\right)\right)\right]^2\right\}}{\sqrt{\pi/2}\left\{\mathrm{ref}\left[\sqrt{\sigma\mu/2}\left(\epsilon^{-1/2}\left(\epsilon t - \tau_{swt}\right)\right)\right] + 1\right\}}, \tag{4.171c}$$

$$I(t) = \frac{\epsilon^{1/2}\sqrt{\sigma\mu}\exp\left\{-\sigma\mu/2\left[\left(\epsilon^{-1/2}\left(\epsilon t - \tau_{swt}\right)\right)\right]^2\right\}}{\sigma\sqrt{\pi/2}\left\{\mathrm{ref}\left[\sqrt{\sigma\mu/2}\left(\epsilon^{-1/2}\left(\epsilon t - \tau_{swt}\right)\right)\right] + 1\right\}} + \mu\left(\epsilon t - \tau_{swt}\right). \tag{4.171d}$$

Region IV: Long-term state

The variables are now $P = Q = I = O(1)$, $C = O(\epsilon)$ and $t = O(\epsilon^{-1})$. Denoting $C = \epsilon\tilde{C}$ and the shifted time coordinate $t = \epsilon^{-1}\left(\tilde{\tau} - \tau_{sw}\right)$, the system (4.101) at

leading order of asymptotic expansion takes the form,

$$\frac{dP_0}{d\tilde{\tau}} = 0, \tag{4.172a}$$

$$\frac{dQ_0}{d\tilde{\tau}} = \hat{\rho}\left(1 - Q_0 - 2I_0\right)P_0 - \gamma\sigma\left(1 - Q_0 - 2I_0\right)Q_0 - \beta\hat{\rho}Q_0P_0, \tag{4.172b}$$

$$0 = -\sigma I_0\tilde{C}_0, \tag{4.172c}$$

$$\frac{dI_0}{d\tilde{\tau}} = \gamma\sigma\left(1 - Q_0 - 2I_0\right)Q_0 - I_0\tilde{C}_0. \tag{4.172d}$$

Hence,

$$P_0 = 1, \tag{4.173}$$

and,

$$\tilde{C}_0 = 0, \quad \text{at all} \quad O(\epsilon^n). \tag{4.174}$$

To obtain a more accurate matching for the variable P, we find the second-order term of the asymptotic expansion. Thus,

$$\frac{dP_1}{d\tilde{\tau}} = -\sigma\left(1 - Q_0 - 2I_0\right)P_0 - \beta\sigma Q_0P_0, \tag{4.175}$$

where $P_0 = 1$, and P_1 can be solved numerically to have the solution of the form

$$P(\bar{\tau}) = P_0(\bar{\tau}) + \epsilon P_1(\bar{\tau}). \tag{4.176}$$

We then obtain

$$\frac{dQ_0}{d\tilde{\tau}} = \hat{\rho}\left(1 - Q_0 - 2I_0\right) - \gamma\sigma\left(1 - Q_0 - 2I_0\right)Q_0 - \beta\hat{\rho}Q_0, \tag{4.177a}$$

$$\frac{dI_0}{d\tilde{\tau}} = \gamma\sigma\left(1 - Q_0 - 2I_0\right)Q_0. \tag{4.177b}$$

The pair of equations above (4.177) has two approaches for solving. One approach can be solving the pair of equations (4.177) numerically. The second approach can be solving the pair of equations (4.177) close to the equilibrium point. To find the equilibrium point, we set the pair of equations to zero and solve for Q_0 and I_0 which leads to

$$0 = \hat{\rho}\,(1 - Q_0 - 2I_0) - \gamma\sigma\,(1 - Q_0 - 2I_0)\,Q_0 - \beta\hat{\rho}Q_0, \tag{4.178a}$$

$$0 = \gamma\sigma\,(1 - Q_0 - 2I_0)\,Q_0. \tag{4.178b}$$

It is clear that the system (4.178) has a single equilibrium point $(0, 1/2)$, i.e. all iodide and hypoiodous acid has been converted to iodine. The Jacobian matrix of the system evaluated at the equilibrium point is given by

$$\begin{pmatrix} -\hat{\rho}\,(1+\beta) & -2\hat{\rho} \\ 0 & 0 \end{pmatrix}, \tag{4.179}$$

and the eigenvalues are 0 and $-\hat{\rho}\,(1+\beta)$. Note that the zero eigenvalue corresponds to the slow manifold, and the negative real eigenvalue indicates a stable manifold. The dynamics close to the equilibrium point can be deduced approximately by considering a quasi-state balance of substituting (4.178b) into (4.178a), yielding

$$0 \approx \hat{\rho}\,(1 - Q_0 - 2I_0) - \beta\hat{\rho}Q_0. \tag{4.180}$$

Rearranging provides the following approximate relationship between I_0 and Q_0,

$$I_0 \approx \frac{1}{2} - \frac{(1+\beta)\,Q_0}{2}, \tag{4.181}$$

from which we infer that,

$$\frac{dI_0}{d\bar{\tau}} \approx \frac{-(1+\beta)}{2}\frac{dQ_0}{d\bar{\tau}}. \tag{4.182}$$

Substituting equations (4.180) and (4.182) into equation (4.177b) gives

$$\frac{-(1+\beta)}{2}\frac{dQ_0}{d\bar{\tau}} \approx \gamma\sigma\beta Q_0^2, \tag{4.183}$$

leading to an approximation of the long-term dynamics of Q_0:

$$\frac{dQ_0}{d\bar{\tau}} \approx \frac{-2\beta\gamma\sigma}{(1+\beta)}Q_0^2. \tag{4.184}$$

The equation (4.184) has the following solution,

$$Q_0 \approx \frac{(1+\beta)}{2\beta\gamma\sigma\bar{\tau} + c_8}, \tag{4.185}$$

where c_8 is a constant of integration. Substituting equation (4.184) into (4.181) provides an approximation of the long-term dynamics of I_0:

$$I_0 \approx \frac{1}{2}\left[1 - \frac{(1+\beta)^2}{2\beta\gamma\sigma\bar{\tau} + c_8}\right]. \tag{4.186}$$

The constant c_8 can be determined by matching the solution for I_0 to the Region II solution (i.e., $I_0(\tau_{sw}) \approx 0$), giving the value $c_8 = (1+\beta)^2 - 2\beta\gamma\sigma\tau_{sw}$. Therefore, the approximate solutions in Region IV, expected to be increasingly accurate close

to the equilibrium point are:

$$P_0(\bar{\tau}) = 1, \tag{4.187a}$$

$$Q_0(\bar{\tau}) = \frac{(1+\beta)}{2\beta\gamma\sigma\left(\bar{\tau} - \tau_{sw}\right) + (1+\beta)^2}, \tag{4.187b}$$

$$C_0(\bar{\tau}) = 0, \tag{4.187c}$$

$$I_0(\bar{\tau}) = \frac{1}{2}\left[\frac{2\beta\gamma\sigma\left(\bar{\tau} - \tau_{sw}\right)}{2\beta\gamma\sigma\left(\bar{\tau} - \tau_{sw}\right) + (1+\beta)^2}\right]. \tag{4.187d}$$

Both approaches provide similar solutions in terms of validity in this region.

Comparison Of Asymptotic And Numerical Approximations Of Model FCR-H-HP

Figure 4.6 illustrates a comparison of the asymptotic and numerical solution of the model (4.101) with initial conditions $P(0) = 1$, $Q(0) = 0$, $C(0) = 1$ and $I(0) = \phi$, and the dimensionless parameter values are $\gamma = 0.7$, $\beta = 0.6$, $\hat{\rho} = 0.9$, $\sigma = 0.7$, $\phi = 0.2$ and $\epsilon = 0.001$, these values are chosen arbitrarily. The approximate solution of Region I closely follows the numerical solution up to $t = 100$. The approximate solution of Region II follows the numerical solution up to around $t \approx 10,000$, and the switchover time point ends the induction period. The approximate solution of Region III closely follows the numerical solution around the dimensionless changeover time $t = 10,354$, up to around $t = 11,500$ (Figure 4.6c is zoomed in to capture the transition between the induction period and the long-term steady state). The approximate solution of Region IV has an excellent match to the numerical solution, with the shifted time coordinate $t = \epsilon^{-1}\left(\epsilon^{1/2}\bar{\tau} + \tau_{sw}\right)$. The agreement between the asymptotic and numerical solutions improves for smaller

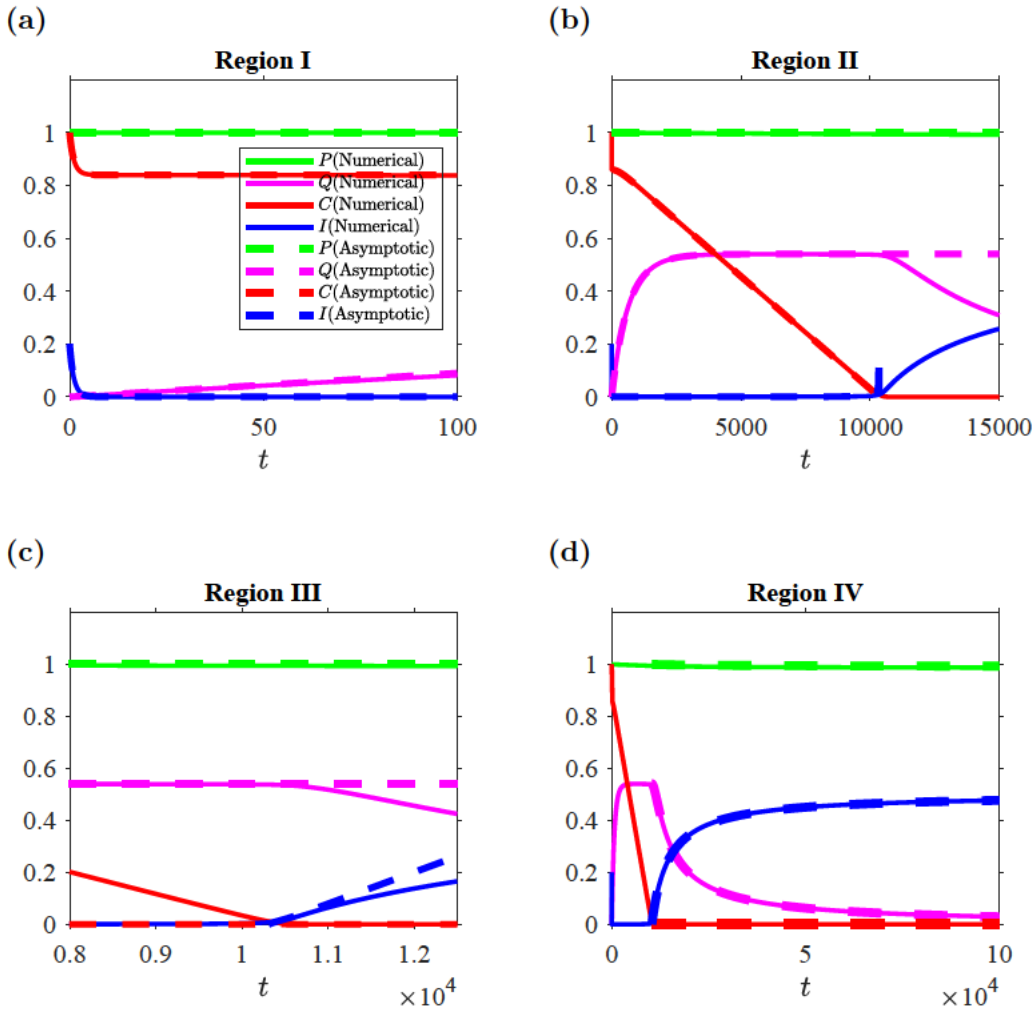

Figure 4.6: Comparison between numerical and asymptotic solutions of the model (4.101) with initial conditions $P(0) = 1$, $Q(0) = 0$, $C(0) = 1$ and $I(0) = \phi$, and the dimensionless parameter values are $\gamma = 0.7$, $\beta = 0.6$, $\hat{\rho} = 0.9$, $\sigma = 0.7$, $\phi = 0.2$ and $\epsilon = 0.001$. (a) Region I, (b) Region II, (c) Region III, (d) Region IV, where the variables $P(t)$, $Q(t)$ and $I(t)$ are numerically solved using the asymptotic expansion terms namely, equations (4.177) and (4.176).

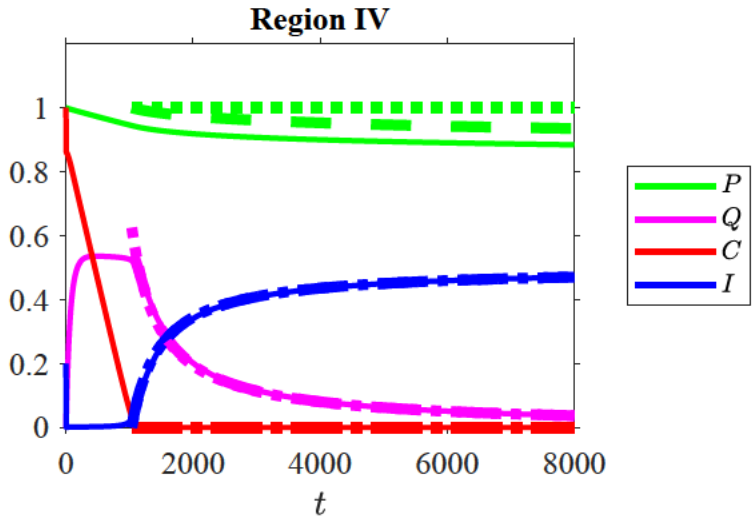

Figure 4.7: Solutions in Region IV illustrate the agreement between the two approaches of approximate solutions, with numerical solutions shown with solid lines, leading order asymptotic solutions shown with dashed lines, the analytical approximate solutions shown with dotted lines. The initial conditions $P(0) = 1$, $Q(0) = 0$, $C(0) = 1$ and $I(0) = \phi$, and dimensionless parameter values are $\gamma = 0.7$, $\beta = 0.6$, $\hat{\rho} = 0.9$, $\sigma = 0.8$, $\phi = 0.2$ and $\epsilon = 0.01$.

values of ϵ (examples not shown for brevity).

Figure 4.7 compares approximate solutions in Region IV in accordance with the two approaches stated in the previous section, namely, equations (4.177) and (4.176) solved numerically in the first approach, and the second approach is the constant approximate solution close to the equilibrium point in (4.187). The solutions are quite close in their region of validity. As time progresses, a significant drift develops between the numerically computed values of P in the first approach (where $\bar{\tau} = \epsilon^{1/2}t - \epsilon^{-1/2}\tau_{sw}$) and the constant approximation close to the equilibrium point in the second approach; the discrepancy appears to be on the order of $\epsilon^{1/2}$.

Figure 4.8 indicates the intersecting point of the numerical solutions for c and

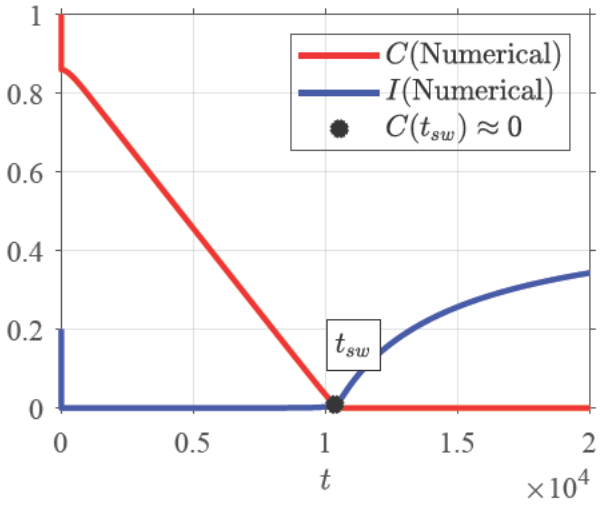

Figure 4.8: Numerical solutions $C(t)$ and $I(t)$ of the model (4.101) shown alongside the value of the switchover time (intersecting point) calculated by the approximate formula (4.142), with initial conditions $P(0) = 1$, $Q(0) = 0$, $C(0) = 1$ and $I(0) = \phi$, and dimensionless parameter values are $\gamma = 0.7$, $\beta = 0.6$, $\hat{\rho} = 0.9$, $\sigma = 0.7$, $\phi = 0.2$ and $\epsilon = 0.001$.

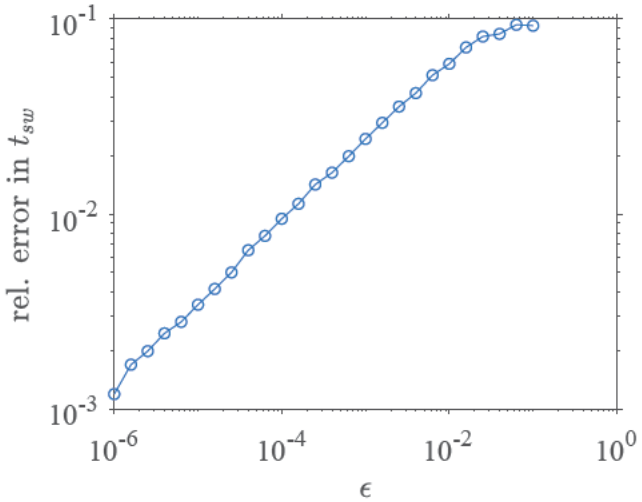

Figure 4.9: Relative error between the asymptotic approximation for the switchover time formula (4.142) of the model (4.101) and the point at which the numerical solution falls below a threshold value of ϵ, as a function of the small parameter ϵ. The dimensionless parameter values are $\gamma = 0.7$, $\beta = 0.6$, $\hat{\rho} = 0.9$, $\sigma = 0.7$ and $\phi = 0.2$.

I from the model (4.101) and the evaluated switchover time (t_{sw}); again there is good agreement. Figure 4.6b and Figure 4.8 show that $t_{sw} \approx 10,000$, when $\epsilon = 0.001$, is the point at which the concentration of the iodine (I) chemical reaction of the clock increases after the concentration of vitamin (C) has been used. Figure 4.9 plots the relative error between the asymptotic approximation of the switchover time formula (4.142) and the switchover time point computed from the numerical solution of the model (4.101), as a function of ϵ. As ϵ decreases, errors decrease. The convergence of the error as $\epsilon \to 0$ is approximately sublinear and the gradient on a log-log scale approaches approximately 0.45 (determined using MATLAB based on the last two points of smaller ϵ values from the log-log plot). These results provide evidence that the asymptotic expansion has sublinear accuracy in this region, and therefore a correction with a fractional power of ϵ may be needed. We will not pursue this analysis as it appears likely to involve significant additional complications for limited additional insight.

It is worth noting that the outcomes of the asymptotic analysis for all regions align precisely with the numerical solution of both models (Model FCR-M-HP and Model FCR-H-HP). A combined plot of all regions of the asymptotic solutions is given in Figure 4.10, showing the concentrations of the reactants against a logarithmic time axis. This result matches the previous one of the numerical solutions in Figure 4.2. Moreover, Figure 4.11 illustrates the merged results of Figure 4.2 and Figure 4.10, demonstrating a close correlation between the asymptotic and numerical solutions within the relevant time range, and the dash-dotted lines indicate the boundaries of each region.

(a)

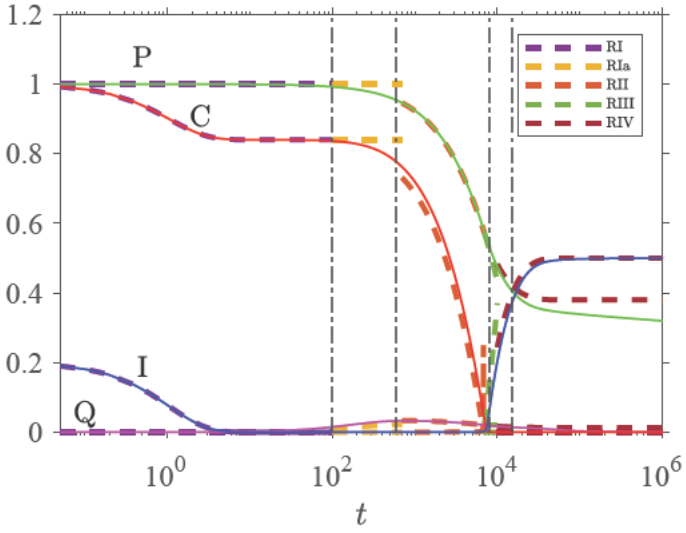

(b)

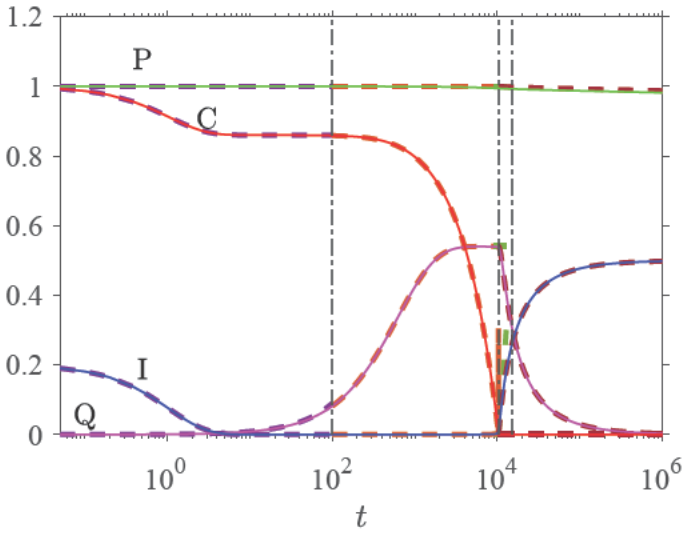

Figure 4.10: Asymptotic solutions of the concentrations of the reactants as a function of time (logarithmic scale) for all regions of the model (4.101) to match Figure 4.2, where the dash-dotted lines indicate the ends of each region. The dimensionless parameters are chosen as in Figure 4.2. (4.10a) The Model FCR-M-HP (4.12). (4.10b) The Model FCR-H-HP (4.101).

(a)

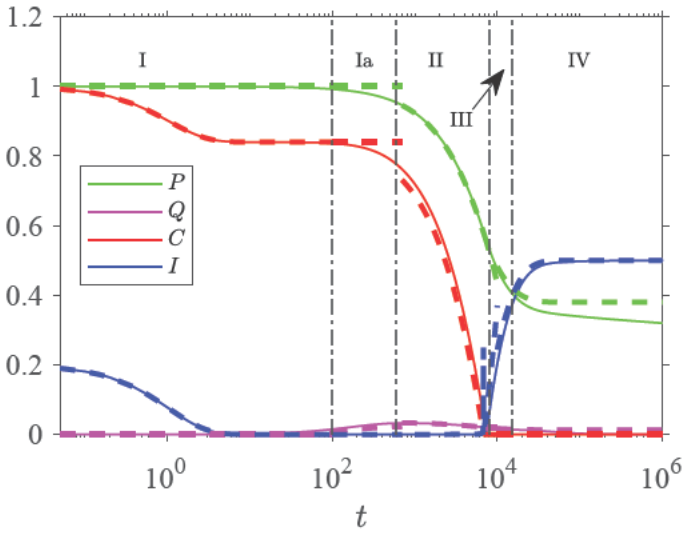

(b)

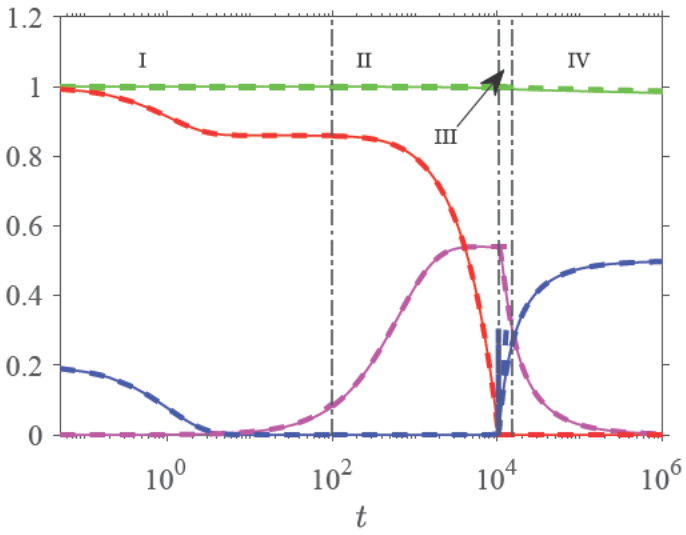

Figure 4.11: Asymptotic solutions of the concentrations of the reactants as a function of time (logarithmic scale) for all regions of the model (4.101) to match Figure 4.2. The solid lines represent the numerical solutions, the dashed lines represent the approximate asymptotic solutions, and the dash-dotted lines indicate the ends of each region. The dimensionless parameters are chosen as in Figure 4.2. (4.11a) Model FCR-M-HP (4.12). (4.11b) Model FCR-H-HP (4.101).

4.4 Conclusion

This chapter incorporates the detailed slow reaction with the fast reaction associated with vitamin C. Asymptotic analysis on the full model of chemical clock reaction (slow and fast) was explored in each case, of moderate and high hydrogen peroxide concentration regimes. Through the development of a new non-linear differential equation model, this study explores the kinetics of the reaction, particularly focusing on the role of hydrogen peroxide concentration.

By employing an asymptotic analysis, the study provides a better understanding of the clock reaction, supported by approximation solutions for each model. Asymptotic approximations are found to agree closely with numerical solutions in the appropriate time regions. This enables us to obtain an approximate formula for the switchover time of each model, depending on initial concentrations and the rate of the slow reaction. The quantitative analysis illustrates the relative errors between the asymptotic approximation switchover time formula and the switchover time point calculated from the numerical solution of both models, based on ϵ. A log-log plot shows decreasing errors as ϵ decreases.

An interesting result is that the switchover time formula of the model with moderate hydrogen peroxide provided here is identical to the simplified linear kinetic model illustrated earlier in Chapter 2. In addition, the switchover time formula of the high hydrogen peroxide model presented here is in line with the switchover formula derived by Kerr et al. [27] in their paper, which pertains to the clock reaction model with high concentrations of hydrogen peroxide.

In the next chapter, both switchover time formulas of moderate and high hydrogen peroxide models will be tested through running experiments, fitting the

parameters in these formulas to the data.

Chapter 5

Experiments And Validation Of Asymptotic Analysis Of Model FCR

5.1 Motivation

It is of interest to test the switchover time formula of Model FCR-M-HP and Model FCR-H-HP by running experimental data for parameter fitting. This chapter will present the results of several experimental series in the moderate and high-peroxide regimes, with starting quantities of each of iodine, vitamin C and hydrogen peroxide varied individually, and the switchover time measured through imaging the colour of the solution. Analysis of the data is conducted using least-squares fitting, with uncertainty quantified through log-likelihood ratios and bootstrapping. The models are tested by fitting to several of the experimental series simultaneously, then testing the fit against the remaining data; this process is carried out for

three different partitions of fitting and test data. It will be found that parameter estimates and confidence intervals agree closely for each choice of fitting data.

5.2 Experimental Testing

The switchover time formulas of Model III-M-HP and Model III-H-HP, namely (4.49) and (4.161) will be tested through tabletop experiments, using a combination of vitamin C powder, Lugol's iodine, hydrogen peroxide solution, and powdered laundry starch.

The procedure of the tabletop experiment is similar to that described in [27, 56], with the refinement of using a webcam sensor running under Matlab (R2020b) to detect the point at which the colour change occurred, different choices of vitamin C and iodine increments, and a greater range of hydrogen peroxide concentrations. The experiments employed by [56] used the tincture of iodine 2%, whereas we followed Kerr et al. in using 3% Lugol's iodine. The switchover time experimental results by [27] were performed with two repeats for varying vitamin C concentration and varying iodine concentration of the high hydrogen peroxide model. In our experiments, we looked at both moderate and high hydrogen peroxide concentrations and varied hydrogen peroxide across this range in 6 separate series. The setup for clock reaction experiments follows the structure outlined in the provided Figure 2.1, in Chapter 2. There are two solutions to this clock reaction. Solution A when iodine is converted to iodide in the presence of vitamin C, and uses up vitamin C in the process. The brownish yellow color of iodine disappears (fast reaction). Solution B when iodide is converted to iodine in the presence of hydrogen peroxide. Pouring Solution A to Solution B, the dark blue color appears (slow

reaction). First, preparing Vitamin C stock solution (diluted) is by dissolving a 1000 mg vitamin C tablet with 30–120 ml water. The beaker of Solution A is prepared from 60 ml of warm water at $40°C$, 5 ml of vitamin C stock solution, and 3-10 ml of 3% Lugol's iodine. The beaker of Solution B is prepared from 60 ml of warm water at $40°C$, 1-20 ml of 3% hydrogen peroxide and 1 teaspoon of powdered laundry starch. Starch is not directly involved in the chemical reaction but used as an indicator that signals when all the vitamin C has been consumed and results in an abrupt change of color from clear to dark blue in the presence of iodine. Also, more precisely, starch directly reveals the presence of iodine, not whether or not the vitamin C has been used up. The beaker of Solution A is poured into the beaker of Solution B, at which point a webcam starts filming via Matlab code, then the mixture is stirred well for 5 seconds. The filming is completed after the colour change from clear to blue occurs.

The practical experiment for the clock reaction was primarily based on the work by Kerr et al. [27], we used different quantities of the chemical reactants which included various levels derived from multiple experiments conducted over 6 months of work. The presented results in this thesis represent the best outcomes obtained during this period, enabling us to run the clock reaction over a timescale that was practical for the subsequent image analysis. We conducted our experiments using natural light from the office window without specific lighting controls. To minimize the influence of variations in ambient light, we designed a 'corner detection' strategy rather than relying on absolute intensity values, ensuring that the result is not sensitive to changes in natural light. More details on corner detection are provided in the next section.

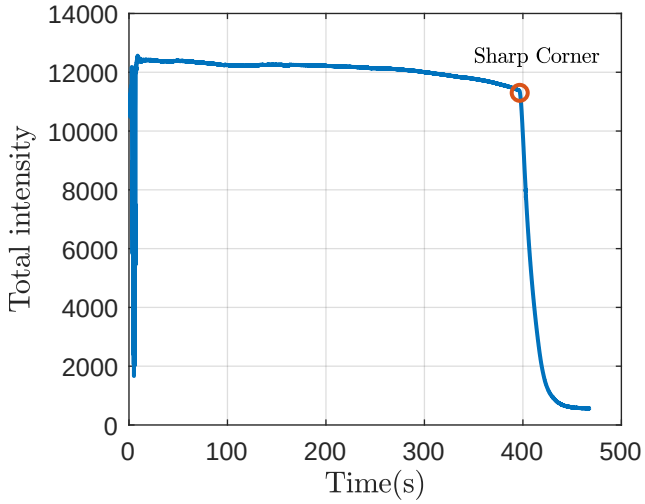

Figure 5.1: Identifying the switchover time point (sharp corner) where the intensity signal undergoes notable change. The total red channel intensity as a function of time, the sharp corner at $t_{sw} = 396.76$ (red circle) is located by MATLAB code at the highest difference between forward and backward averages.

5.2.1 Imaging

The switchover time point (t_{sw}) was measured by imaging the solution from above the beaker under natural lighting conditions using a RGB USB camera running in Matlab with Image Processing Toolbox (Mathworks, Natick) 2020b, recording images at 15 frames per second. The region of interest was set at 80 x 100 pixels in the center of the beaker.

The digital images are formed of pixels containing three colour channels (RGB) which are red, green, and blue. The intensity of each channel expresses the amount of colour in the pixel. The red channel was sufficient for a clear measurement because it displays the brightness of each pixel, ranging from 0 (black) to 255 (white). Briefly, the signal values were processed by adding the intensity across all pixels in the red channel of an image. To account for fluctuations in the data we utilized

forward and backward moving averages with 10 frame windows. The point of the largest difference of the forward and backward moving averages then revealed the point of the sharpest change in the signal, as shown in Figure 5.1 (as one example of the data set has been collected). It demonstrates a sample of the imaging process using MATLAB code to locate the 'sharp corner' (indicating the greatest decrease in intensity between the forward and backward averages) as the switchover time point (t_{sw} = 396.76 s) in which a significant change has occurred, for one of the experimental trials has done with high hydrogen peroxide concentration (5 ml as 0.032666595 mol/l), 5 ml iodine concentration (as 0.007380894 mol/l) and 5 ml of 30 ml of vitamin C diluted as 0.007009652 mol/l. The key concept behind using the corner feature is that the outcome becomes less affected to changes in lighting levels. More details of the experimental trials will be discussed in the next sections.

5.2.2 Fitting Series

Four experimental series will be carried out for fitting of the parameters ϕ and k_3, referred to as N_M and C_M (moderate hydrogen peroxide regime), and N_H and C_H (high hydrogen peroxide regime).

Moderate Hydrogen Peroxide Trials (N_M&C_M):

The amount of hydrogen peroxide is fixed as 1 ml of 3% hydrogen peroxide in these trials. Results for both trials, (N_M) varying iodine with fixed vitamin C, and (C_M) varying vitamin C with fixed iodine, are shown in Table 5.1. The molar mass of hydrogen peroxide, H_2O_2, is 34.01368 grams per mole. The concentrations of 1 ml of 3% hydrogen peroxide are 0.00656–0.00678 mol/l (varied due to total volume

Table 5.1: Switchover time experimental results for Moderate Hydrogen Peroxide Trials.

Trial (N_M) Variable iodine concentration.							
VitC Diluted (ml)	Lugol's (ml)	Hydrogen Peroxide (ml)	c_0 (mol/l)	n_0 (mol/l)	p_0 (mol/l)	t_{sw} (s)	p_0/n_0
90	4	1	0.002426418	0.00613182	0.006784601	714.92	1.11
90	4.5	1	0.002417121	0.006871867	0.006758606	503.75	0.98
90	5	1	0.002407896	0.007606265	0.00673281	432.67	0.89
90	5.5	1	0.00239874	0.008335078	0.00670721	332.83	0.80
90	6	1	0.002389654	0.00905837	0.006681804	237.2	0.74
90	6.5	1	0.002380636	0.009776203	0.006656589	204.26	0.68
90	7	1	0.002371687	0.010488639	0.006631564	185.21	0.63
90	7.5	1	0.002362804	0.011195738	0.006606727	122.68	0.59
90	8	1	0.002353988	0.01189756	0.006582075	101.26	0.55
90	8.5	1	0.002345237	0.012594165	0.006557606	60.22	0.52
Trial (C_M) Variable vitamin C concentration.							
VitC Diluted (ml)	Lugol's (ml)	Hydrogen Peroxide (ml)	c_0 (mol/l)	n_0 (mol/l)	p_0 (mol/l)	t_{sw} (s)	p_0/n_0
70	5	1	0.003095866	0.007606265	0.00673281	707.98	0.89
75	5	1	0.002889475	0.007606265	0.00673281	604.37	0.89
80	5	1	0.002708883	0.007606265	0.00673281	538.51	0.89
85	5	1	0.002549537	0.007606265	0.00673281	426.54	0.89
90	5	1	0.002407896	0.007606265	0.00673281	372.71	0.89
100	5	1	0.002167106	0.007606265	0.00673281	315.48	0.89
110	5	1	0.001970096	0.007606265	0.00673281	225.23	0.89
120	5	1	0.001805922	0.007606265	0.00673281	185.21	0.89

Table 5.2: Switchover time experimental results for High Hydrogen Peroxide Trials.

Trial (N_H) Variable iodine concentration.							
Vitamin C Diluted (ml)	Lugol's (ml)	Hydrogen Peroxide (ml)	c_0 (mol/l)	n_0 (mol/l)	p_0 (mol/l)	t_{sw} (s)	p_0/n_0
30	3	20	0.006393939	0.004039543	0.119188928	191.42	29.51
30	3.5	20	0.006372411	0.004696932	0.118787618	138.49	25.29
30	4	20	0.006351027	0.00534991	0.118389002	135.28	22.13
30	4.5	20	0.006329786	0.005998519	0.117993052	121.86	19.67
30	5	20	0.006308687	0.006642804	0.117599742	107.89	17.70
30	5.5	20	0.006287727	0.007282809	0.117209045	87.74	16.08
30	6	20	0.006266907	0.007918575	0.116820936	79.43	14.75
30	6.5	20	0.006246224	0.008550144	0.116435388	72.8	13.62
30	7.5	20	0.006205265	0.009800859	0.115671878	53.45	11.80
30	10	20	0.006105181	0.012857041	0.113806202	37.63	8.85
Trial (C_H) Variable vitamin C concentration.							
Vitamin C Diluted (ml)	Lugol's (ml)	Hydrogen Peroxide (ml)	c_0 (mol/l)	n_0 (mol/l)	p_0 (mol/l)	t_{sw} (s)	p_0/n_0
30	5	20	0.006308687	0.006642804	0.117599742	91.34	17.70
40	5	20	0.004731515	0.006642804	0.117599742	64.62	17.70
50	5	20	0.003785212	0.006642804	0.117599742	49.22	17.70
60	5	20	0.003154343	0.006642804	0.117599742	42.08	17.70
70	5	20	0.002703723	0.006642804	0.117599742	36.87	17.70
80	5	20	0.002365757	0.006642804	0.117599742	26.05	17.70
90	5	20	0.002102896	0.006642804	0.117599742	23.46	17.70

effect). The molar mass of vitamin C, or ascorbic acid, $C_6H_8O_6$, is 176.124 grams per mole. The concentrations of 5 ml of vitamin c stock solution (1000 mg tablet diluted in 70–120 ml water) are 0.00181–0.00310 mol/l.

The formula of Lugol's iodine is a 1 : 2 mixture of iodine (I_2) and potassium iodide (KI). The molar mass of iodine is 126.9 grams per mole and the molar mass of potassium iodide is 166 g/mol, and hence, the molar mass of 3% Lugol's iodine is 25.28916 g/mol. The concentrations of 4-8.5 ml of 3% Lugol's iodine are 0.00613–0.01259 mol/l.

High Hydrogen Peroxide Trials (N_H&C_H):

The amount of hydrogen peroxide is fixed as 20 ml of 3% hydrogen peroxide in these trials. Results for both trials, (N_H) varying iodine with fixed vitamin C, and (C_H) varying vitamin C with fixed iodine, are shown in Table 5.2. The concentrations of 20 ml of 3% hydrogen peroxide are 0.11381–0.11919 mol/l (varied due to total volume effect). The concentrations of 5 ml of vitamin C stock solution (1000 mg tablet diluted in 30-90 ml water) are 0.00210–0.00639 mol/l. The concentrations of 3-10 ml of 3% Lugol's iodine are 0.00404–0.01286 mol/l.

Figure 5.2 illustrates the experimental data results of Moderate and High Hydrogen Peroxide Trials from Table 5.1 and Table 5.2.

5.2.3 Testing Series

The switchover time models and the fitted parameters, $\hat{\phi}$ and $\hat{k}_3$, will be then tested by comparing against two independent data series, referred to as P_H and P_M.

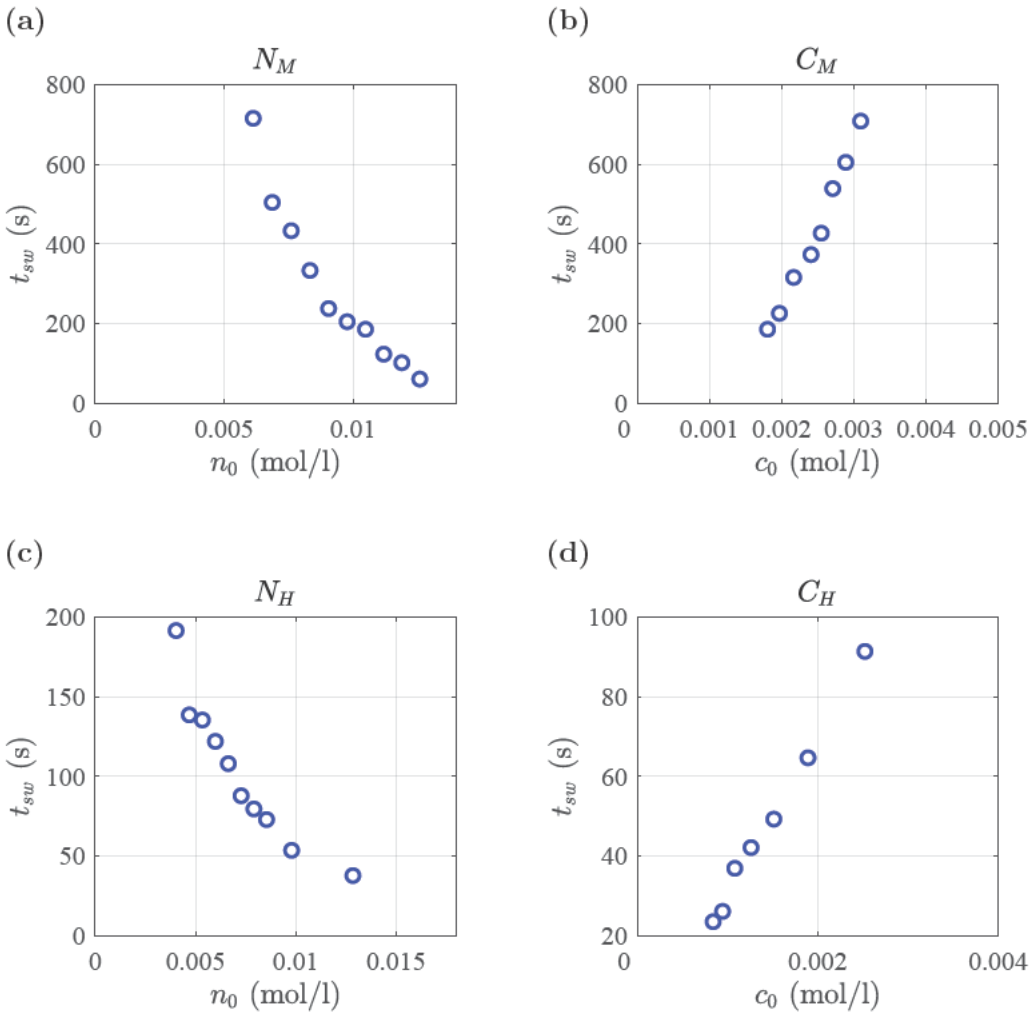

Figure 5.2: Experimental data results of Moderate and High Hydrogen Peroxide Trials from Table 5.1 and Table 5.2. (a) Varying iodine concentration with moderate hydrogen peroxide. (b) Varying vitamin C concentration with moderate hydrogen peroxide. (c) Varying iodine concentration with high hydrogen peroxide. (d) Varying vitamin C concentration with high hydrogen peroxide

Table 5.3: Switchover time experimental results for Varying Hydrogen Peroxide Trials.

Trial (P_H) Variable high hydrogen peroxide concentration.						
Vitamin C Diluted (ml)	Lugol's (ml)	Hydrogen Peroxide (ml)	c_0 (mol/l)	n_0 (mol/l)	p_0 (mol/l)	t_{sw} (s)
30	5	5	0.007009652	0.007380894	0.032666595	396.76
30	5	7.5	0.006882204	0.007246696	0.048108985	263.09
30	5	10	0.006759307	0.007117291	0.062999862	180.06
30	5	12.5	0.006640723	0.006992426	0.077368251	155.12
30	5	15	0.006526227	0.006871867	0.091241179	122.42
30	5	17.5	0.006415613	0.006755394	0.104643838	109.27
30	5	20	0.006308687	0.006642804	0.117599742	100.69
30	5	22.5	0.006205265	0.006533906	0.130558924	93.07
30	5	25	0.006105181	0.00642852	0.142257753	78.85
30	5	30	0.005914394	0.006227629	0.165374637	70.11
Trial (P_M) Variable moderate hydrogen peroxide concentration.						
Vitamin C Diluted (ml)	Lugol's (ml)	Hydrogen Peroxide (ml)	c_0 (mol/l)	n_0 (mol/l)	p_0 (mol/l)	t_{sw} (s)
90	5	5.5	0.002327929	0.007353658	0.03580066	67.35
90	5	5	0.002336551	0.007380894	0.032666595	59.91
90	5	4.5	0.002345237	0.007408332	0.029509229	84.14
90	5	4	0.002353988	0.007435975	0.0263283	91.91
90	5	3.5	0.002362804	0.007463825	0.023123545	107.06
90	5	3	0.002371687	0.007491885	0.019894693	136.06
90	5	2.5	0.002380636	0.007520156	0.016641473	155.99
90	5	2	0.002389654	0.007548641	0.013363607	202.02
90	5	1.5	0.00239874	0.007577344	0.010060814	312.84
90	5	1	0.002407896	0.007606265	0.00673281	446.06

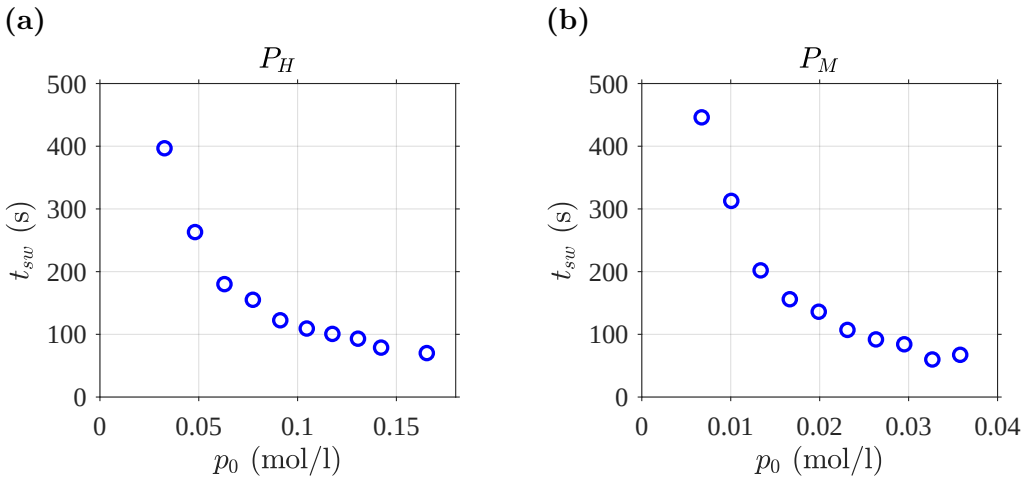

Figure 5.3: Experimental data results of Varying Hydrogen Peroxide Trials from Table 5.3. (a) Varying High hydrogen peroxide. (b) Varying Moderate hydrogen peroxide.

Varying Hydrogen Peroxide Trials (P_H&P_M):

The amount of iodine is fixed as 5 ml of 3% Lugol's iodine in these trials. Results for both trials, (P_H) varying high hydrogen peroxide concentration ($5 - 30$ ml) with fixed vitamin C (5 ml of 30 ml of vitc solution), and (P_M) varying moderate hydrogen peroxide concentration ($1 - 5.5$ ml) with fixed vitamin C (5 ml of 90 ml of vitc solution), are shown in Table 5.3. The concentrations of 5 ml of 3% Lugol's iodine are 0.00623–0.00764 mol/l (varied due to total volume effect). The concentrations of 5 ml of vitamin C stock solution (1000 mg tablet diluted in 30 and 90 ml water) are 0.00233–0.00701 mol/l. The concentrations of 1–30 ml of 3% hydrogen peroxide are 0.00673–0.16537 mol/l.

Figure 5.3 displays the experimental data results of Varying Hydrogen Peroxide Trials from Table 5.3.

5.3 Parameter Estimation Methods

Parameter estimation involves determining the values of the two parameters ϕ and k_3 in the switchover time formula of Model FCR-M-HP and Model FCR-H-HP, namely (4.49) and (4.161), that best fit to experimental data in Table 5.1 and Table 5.2. Henceforth, for simplicity, we shall denote the switchover time formula (4.49) of the Model FCR-M-HP as follows:

$$t_{sw}^{M} = \frac{1}{k_3 n_0} \ln\left(\frac{p_0}{p_0 + \phi n_0 - c_0}\right), \tag{5.1}$$

and denote the switchover time formula (4.161) of the Model FCR-H-HP as follows:

$$t_{sw}^{H} = \frac{c_0 - \phi n_0}{k_3 n_0 p_0}. \tag{5.2}$$

Both formulas above, (5.1) and (5.2), can be combined in one formula and written as follows:

$$t_{sw} = \begin{cases} \frac{1}{k_3 n_0} \ln\left(\frac{p_0}{p_0+\phi n_0 - c_0}\right) & \text{for} \quad (p_0 < 1.5 n_0)\,, \\ \left(\frac{c_0 - \phi n_0}{k_3 n_0 p_0}\right) & \text{for} \quad (p_0 \geq 1.5 n_0)\,, \end{cases} \tag{5.3}$$

where the threshold value of 1.5 being chosen arbitrarily. Our data, presented in Table 5.1 and Table 5.2, revealed a significant distinguishing feature: The condition $(p_0/n_0 < 1.5)$ is satisfied when $\rho = O(1)$; hydrogen peroxide is moderate while the condition $(p_0/n_0 \geq 1.5)$ is satisfied when $\rho = O(\epsilon^{-1})$; hydrogen peroxide is high. To ensure clarity and consistency, the three switchover time formulas above are in dimensional quantities and the units stated earlier in Chapter 4.

This chapter examines the three switchover time formulas mentioned earlier, namely (5.1), (5.2) and (5.3), in relation to our data in Tables (Table 5.1, Table

5.2 and Table 5.3), employing parameter techniques such as least-squares, likelihood ratio, and bootstrapping. The approach will entail introducing each method individually initially, followed by a subsequent discussion of the results.

5.3.1 Least-squares Fitting

The method of least-squares is applied to approximate the parameters ϕ and k_3 by minimising the total sum of the squares of the differences between the experimental data (experimental data; $t_{sw,data}$) and the switchover time formula of the model (the model values; $t_{sw,model}$) [33]. It aims to find the parameter values of ϕ and k_3 that optimize the model's fit to the data. Hence, the least-squares standard objective function to minimise is

$$S(\phi, k_3) = \sum^{N} \left(t_{sw,model} - t_{sw,data}\right)^2, \tag{5.4}$$

where N is the number of experimental data.

In Matlab, *fminsearch* is an optimisation function [37], used for nonlinear optimization to find the minimum values of a sum squared errors with initial guesses $\phi = 0.2$ and $k_3 = 0.6$ chosen arbitrarily.

5.3.2 The 95% Confidence Intervals For Parameters

The 95% confidence interval is a statistical range that provides an estimated range of values which is likely to include the true value of unknown parameters ϕ and k_3 in the switchover time formula of Model FCR-M-HP and Model FCR-H-HP, namely (5.1) and (5.2). The log-likelihood ratio test and bootstrap sampling are two different methods used to obtain the 95% confidence intervals for parameters.

Each method has its strengths and methodologies. Throughout this section, we will describe each method and its implementation individually, and then discuss the results of applying them to our models.

The Log-Likelihood Ratio (Wilk's Theorem)

Wilk's Theorem provides an asymptotic distribution of the log-likelihood ratio, which can be used to produce the 95% confidence intervals [50, 54]. The log-likelihood ratio is a statistical measure used in hypothesis testing, particularly in the context of maximum likelihood estimation. The test involves the log-likelihood ratio, which is the logarithm of the ratio of the maximum likelihoods for two competing models.

$$2\log\left(\frac{L(\hat{\phi},\hat{k}_3)}{L(\phi,k_3)}\right) < \chi^2_{2,0.95}, \tag{5.5}$$

where $(\hat{\phi},\hat{k}_3)$ is the estimated values and $\chi^2_{2,0.95}$ is the critical value corresponding to Chi-squared distribution with 2 degree of freedom [50, 54] (the number of unknown parameters), at confidence level of 0.95. Hypothesis testing requires both null (H_0) and alternative (H_1) hypotheses to be defined:

$$H_0 :(\phi,k_3) = (\hat{\phi},\hat{k}_3), \tag{5.6}$$

$$H_1 :(\phi,k_3) \neq (\hat{\phi},\hat{k}_3); \tag{5.7}$$

we reject the null hypothesis (H_0) if the likelihood ratio $>$ critical value and we fail to reject if it is $<$ critical value.

When the errors are assumed to be normally distributed, the likelihood function

is given as follows

$$L(\phi, k_3) = \prod^{N} \frac{1}{\sigma_e \sqrt{2\pi}} \exp\left\{ \frac{-1}{\sigma_e} \left(t_{sw,model} - t_{sw,data}\right)^2 \right\}, \tag{5.8}$$

where σ_e is the standard deviation of errors, which can be found by taking the partial derivative of the log-likelihood, and hence,

$$\sigma_e = \frac{1}{N} \sum^{N} \left(t_{sw,model}(\hat{\phi}, \hat{k}_3) - t_{sw,data} \right)^2. \tag{5.9}$$

The log-likelihood function, $l(\phi, k_3) = \log(L(\phi, k_3))$ yields

$$l(\phi, k_3) \propto \frac{-1}{\sigma_e} \sum^{N} \left(t_{sw,model} - t_{sw,data}\right)^2. \tag{5.10}$$

Obviously, maximizing l in (5.10) is equivalent to minimizing S in (5.4) (i.e., the negative log-likelihood is equivalent to the sum squared errors). Therefore,

$$\begin{aligned} 2\log\left(\frac{L(\hat{\phi}, \hat{k}_3)}{L(\phi, k_3)}\right) &= -2\left[l(\hat{\phi}, \hat{k}_3) - l(\phi, k_3)\right], \\ &= -2\Bigg[\sum^{N} \frac{\left(t_{sw,model}(\hat{\phi}, \hat{k}_3) - t_{sw,data} \right)^2}{\sigma_e} \\ &\qquad - \sum^{N} \frac{\left(t_{sw,model}(\phi, k_3) - t_{sw,data}\right)^2}{\sigma_e}\Bigg], \\ &= -2N\left[1 - \frac{\sum^{N} \left(t_{sw,model}(\phi, k_3) - t_{sw,data}\right)^2}{\sum^{N} \left(t_{sw,model}(\hat{\phi}, \hat{k}_3) - t_{sw,data} \right)^2}\right]. \end{aligned} \tag{5.11}$$

Hence, the log-likelihood ratio test in (5.5) can be written as

$$-2N\left[1-\frac{\sum^{N}\left(t_{sw,model}(\phi,k_3)-t_{sw,data}\right)^2}{\sum^{N}\left(t_{sw,model}(\hat{\phi},\hat{k}_3)-t_{sw,data}\right)^2}\right]<\chi^2_{2,0.95}. \tag{5.12}$$

In Matlab, we start by generating a parameter grid using *meshgrid* of 100 values of the parameters (ϕ, k_3) and calculate the objective function in (5.4) (such as the sum of the squared errors between a model and data) for each combination of (ϕ, k_3). Finally, we need to determine the 95% confidence intervals by calculating the log-likelihood ratio test in (5.12) and the critical value, $\chi^2_{2,0.95}$, can be found using *Chi2inv(0.95,2)* $= 5.9914$.

Bootstrap Sampling

Bootstrap sampling is a resampling method used to quantify the accuracy of parameter estimates. The technique introduced by Efron in 1979, is a statistical resampling technique that involves repeatedly sampling from data with replacement [19]. Bootstrapping will be used below to estimate 95% confidence intervals for the two parameters ϕ and k_3 of the switchover time formulae, namely (5.1), (5.2) and (5.3).

Bootstrap sampling was implemented using built-in functions in Matlab. The function *bootstrp* was used to create $10,000$ resampled results through randomly sampling with replacement from the experimental data in Table 5.1 and Table 5.2. The seed for reproducibility was set to be $rng(42)$ (random number generator, ensuring that each time we run the code, we get the same sequence of bootstrap samples). The parameter estimation was then carried out on each bootstrap sample. The 95% confidence interval was then constructed from the percentiles of the

bootstrap resampling of the data. As an alternative method, the *bootci* function in Matlab was also used, which implements the bias corrected and accelerated percentile method [20].

5.4 Parameter Estimation Results

In this section, we demonstrate the results of parameter estimation techniques including least-squares, likelihood ratio test, and bootstrapping of the three switchover time formulas, namely (5.1), (5.2) and (5.3), with our experimental data (Table 5.1, Table 5.2 and Table 5.3). The results will be presented as follows:

- the outcome of fitting to the series experiments N_M and C_M using the least-squares equation (5.1) of the Model FCR-M-HP for the two parameters ϕ and k_3, and the testing against series P_M and P_H using these estimated values;
- the outcome of fitting to the series experiments N_H and C_H using the least-squares equation (5.2) of the Model FCR-H-HP for the two parameters ϕ and k_3, and the testing against series P_M and P_H using these estimated values;
- the outcome of fitting to all series experiments N_M, C_M, N_H and C_H using the least-squares equation (5.3) for both models FCR-M-HP and FCR-H-HP for the two parameters ϕ and k_3, and the testing against series P_M and P_H using these estimated values;
- (observing the other way around) the outcome of fitting the series experiments P_M and P_H using the least-squares equation (5.3) for both models FCR-M-HP and FCR-H-HP for the two parameters ϕ and k_3, and the testing against series N_M, C_M, N_H and C_H using these estimated values.

The discussion of the experimental validation will be analysed further in the following sections.

5.4.1 Model FCR-M-HP

The results for different increments of Moderate Hydrogen Peroxide Trials, (N_M) varying iodine with vitamin C and moderate hydrogen peroxide fixed, and (C_M) varying vitamin C with iodine and moderate hydrogen peroxide fixed, are shown in Table 5.1. The outcome of least-squares fitting equation (5.1) for the two parameters ϕ and k_3 to both experimental data simultaneously, involves fitting a moderate HP model to multiple sets of data points at once (Trails N_M and C_M), and aiming to find the best-fitting parameters that minimize the overall sum of squared differences across all dataset ($\sum^{N_M} (t_{sw,model} - t_{sw,data})^2 + \sum^{C_M} (t_{sw,model} - t_{sw,data})^2$). These are shown in Figure 5.4 (note that the curve is plotted for the full range of the independent variable). Therefore, the estimated values of the switchover time (5.1) of Model FCR-M-HP is $\left(\hat{\phi}^M, \hat{k}_3^M\right) = (0.1676, 0.0586)$.

Figure 5.5 illustrates an independent test (i.e. against data not used during the fitting process) across a full range of varying hydrogen peroxide data from Table 5.3 and least-squares fitting of the switchover time formula of Model FCR-M-HP (5.1). This result ties well with moderate hydrogen peroxide trials more than the high hydrogen peroxide trials as we predicted.

In Figure 5.6, the contour plot provides a visual representation of the logarithm of the objective function (5.4), evaluated at each combination of the two parameters, in two dimensions. Each contour line corresponds to a specific level of the objective function. It identifies the estimated values $\left(\hat{\phi}^M, \hat{k}_3^M\right) = (0.1676, 0.0586)$

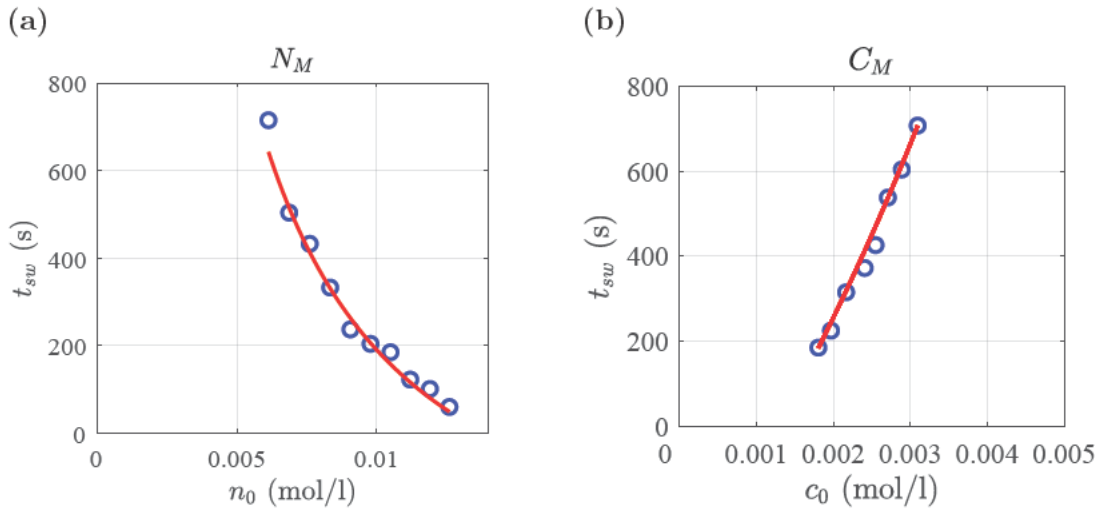

Figure 5.4: Experimental data results of Moderate Hydrogen Peroxide Trials (blue circles) from Table 5.1 and least-squares fitting equation (5.1) to both experimental data, namely N_M and C_M, simultaneously with $\left(\hat{\phi}^M, \hat{k}_3^M\right) = (0.1676, 0.0586)$ (red lines). (a) Varying iodine concentration. (b) Varying vitamin C concentration.

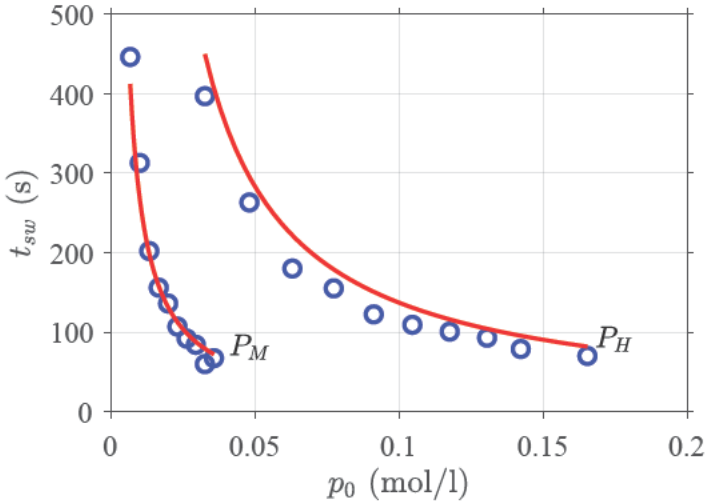

Figure 5.5: An independent test (i.e. against data not used during the fitting process) across full range of Varying Hydrogen Peroxide Trials (blue circles) from Table 5.3 and least-squares fitting of the switchover time formula of Model FCR-M-HP (5.1) to both experimental data, namely N_M and C_M, simultaneously with $\left(\hat{\phi}^M, \hat{k}_3^M\right) = (0.1676, 0.0586)$ (red lines).

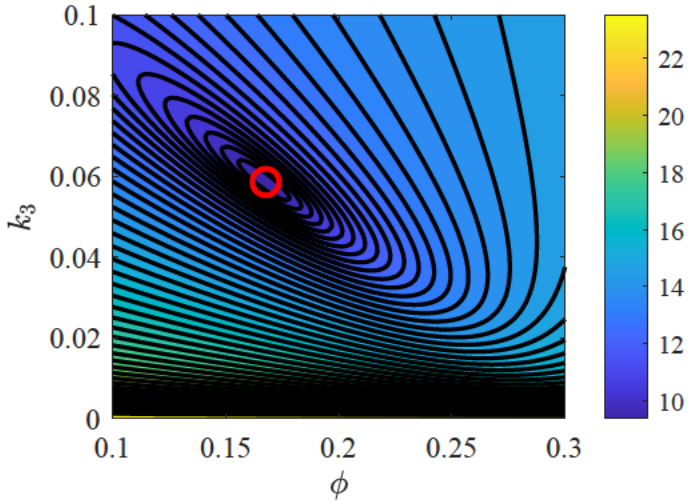

Figure 5.6: A contour plot of the logarithm of the objective function with the estimated value $\left(\hat{\phi}^M, \hat{k}_3^M\right) = (0.1676, 0.0586)$ (red circle mark) of the switchover time formula (5.1) of the Model FCR-M-HP.

located in the centre, of the inner ellipse, of the minimum level in the contour plot, which means that they have the minimum errors. Significantly, the estimated values using the least-squares fitting have the best model fit to the data. These results demonstrate the consistency with what has been found previously.

Figure 5.7 displays the pcolor plot of the satisfying condition; the log-likelihood ratio $<$ critical value. It indicates two colour regions, where the yellow region typically represents true (i.e., the condition is satisfied), while the blue region represents false (i.e., the condition is not satisfied). As a result, the 95% confidence interval using the log-likelihood ratio test (Wilk's Theorem) for the two parameters ϕ and k_3 of the switchover time formula (5.1) of Model FCR-M-HP, of all moderate

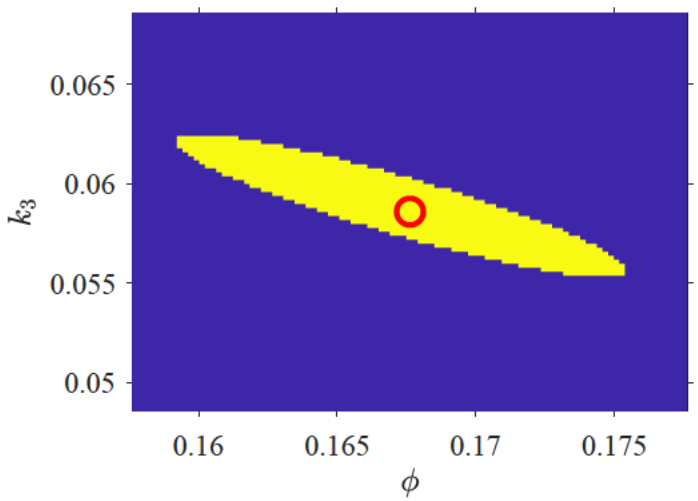

Figure 5.7: A pcolor plot of the satisfying condition; log-likelihood ratio < critical value with the bar plot of the numeric values (the yellow region for true, and the blue region for false), and the estimated value $\left(\hat{\phi}^M, \hat{k}_3^M\right) = (0.1676, 0.0586)$ (red circle mark) of the switchover time formula (5.1) of the Model FCR-M-HP.

hydrogen peroxide trials (N_M, C_M) is as follows:

$$CI^M_{\phi,95\%} = [0.1592,\ 0.1752], \tag{5.13a}$$

$$CI^M_{k_3,95\%} = [0.0554,\ 0.0622]. \tag{5.13b}$$

Figure 5.8 shows the 95% confidence region of the objective function at the specific level v, which is calculated by re-arranging the expression of the log-likelihood ratio test in (5.12) as:

$$\begin{aligned}\sum^N \left(t_{sw,model}(\phi, k_3) - t_{sw,data}\right)^2 &= \left[1 + \left(\frac{\chi^2_{2,0.95}}{2N}\right)\right] \sum^N \left(t_{sw,model}(\hat{\phi}, \hat{k}_3) - t_{sw,data}\right)^2 \\ &= v. \end{aligned} \tag{5.14}$$

We now analyse the histogram derived from bootstrap samples to gain a better

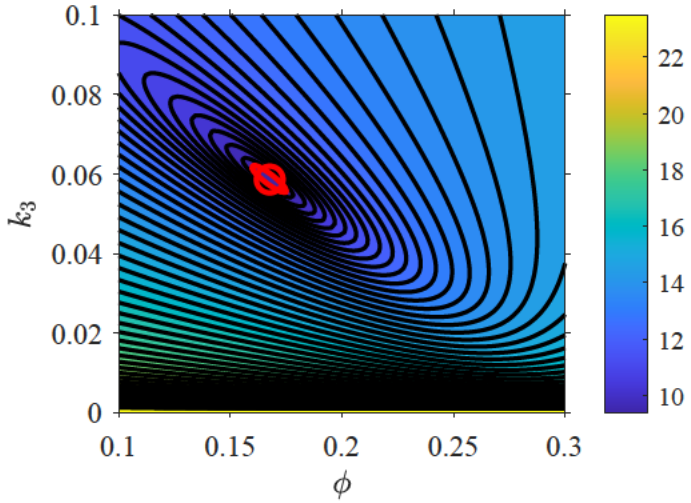

Figure 5.8: A contour plot of the logarithm of the objective function at level v (satisfied the 95% confidence region) with the estimated value $\left(\hat{\phi}^M, \hat{k}_3^M\right) = (0.1676, 0.0586)$ (red circle mark) of the switchover time formula (5.1) of the Model FCR-M-HP.

understanding of parameter behaviour under different re-sampling scenarios. Figure 5.9 indicates the histogram plots and frequency of the two parameters (ϕ and k_3) with the lower and upper bounds of the 95% confidence interval of the parameters as dashed vertical lines, using the bootstrap sampling of the switchover time formula of Model FCR-M-HP (5.1). Figure 5.10 illustrates a scatter plot of the two parameters ϕ and k_3 of each bootstrap sample with the lower and upper bounds of the parameter ϕ with the 95% confidence interval as dashed vertical lines, and the lower and upper bounds of the parameter k_3 with the 95% confidence interval as dashed horizontal lines.

Figure 5.11 indicates the lower and upper quantiles of the 95% confidence interval using the bootstrapping method. By carrying out bootstrapping on our moderate HP data, Table 5.1, we calculate the minimum sum of squared errors

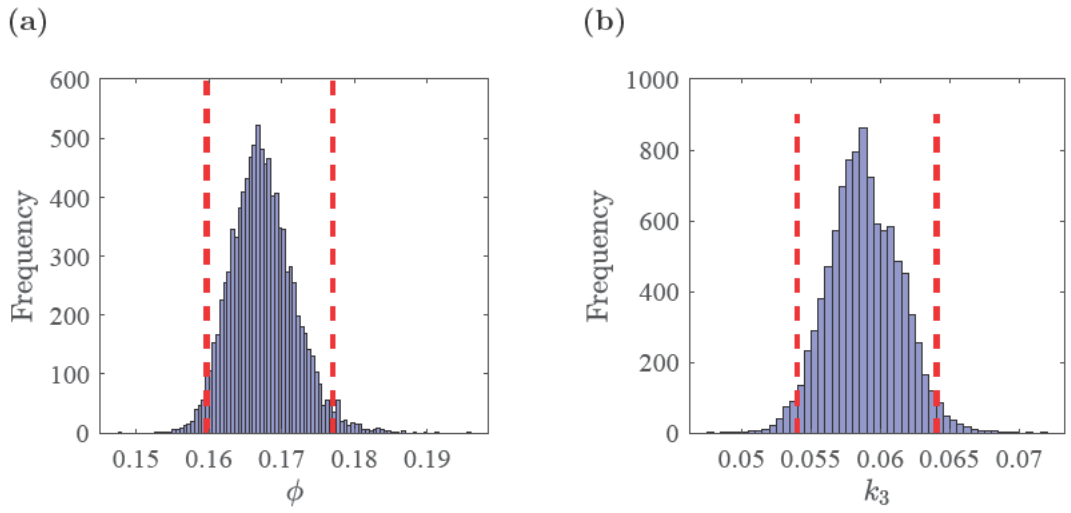

Figure 5.9: Histogram of the bootstrapping re-sampling for estimating the two parameters ϕ and k_3 of the switchover time formula (5.1) of the Model FCR-M-HP with 95% confidence intervals as red dashed lines. (a) For the parameter ϕ. (b) For the parameter k_3.

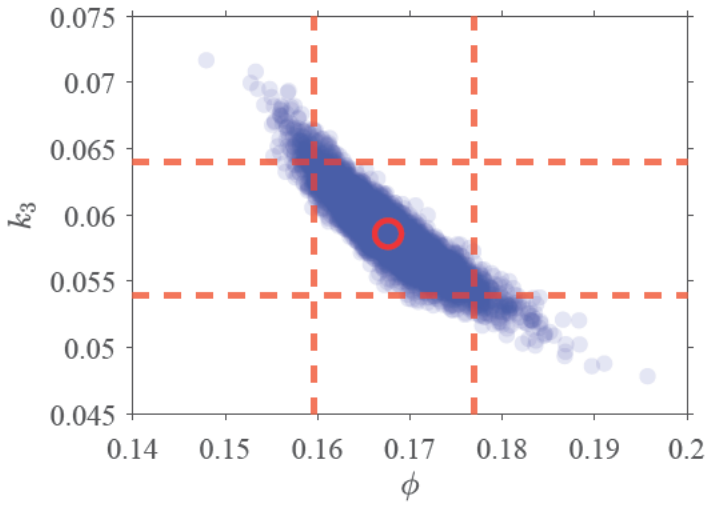

Figure 5.10: A scatter plot of the two parameters ϕ and k_3 of each bootstrap sample with the lower and upper bounds of the parameters with the 95% confidence intervals as dashed lines (red), and the estimated value $\left(\hat{\phi}^M, \hat{k}_3^M\right) = (0.1676, 0.0586)$ (red circle mark).

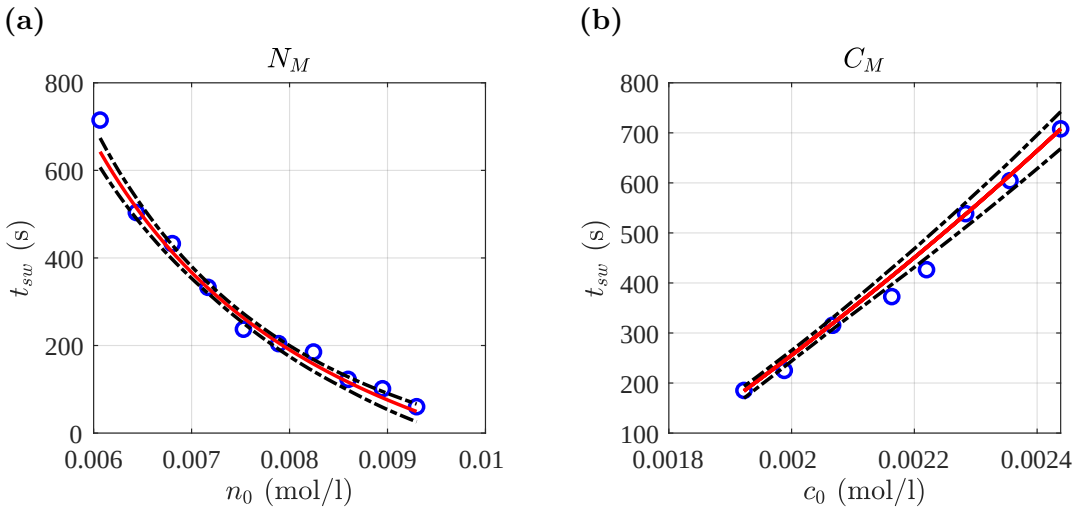

Figure 5.11: The lower and upper quantiles of the bootstrapping method (black dash-dotted lines) for the experimental data results of Moderate Hydrogen Peroxide Trials (blue circles) from Table 5.1 and least-squares fitting equation (5.1) to both experimental data, namely N_M and C_M, simultaneously with $\left(\hat{\phi}^M, \hat{k}_3^M\right) = (0.1676, 0.0586)$ (red lines). (a) Varying iodine concentration. (b) Varying vitamin C concentration.

to estimate the parameters (ϕ and k_3) for each bootstrap sample, and then find the 2.5th and 97.5th precentiles of the bootstrap distribution to construct 95% confidence intervals.

Our findings on the 95% confidence interval using bootstrapping resampling for the two parameter ϕ and k_3 of the switchover time formula (5.1) of Model FCR-M-HP, of all moderate hydrogen peroxide trials (N_M, C_M) is as follows:

$$CI^{M}_{\phi,95\%} = [0.1597,\ 0.1770], \tag{5.15a}$$

$$CI^{M}_{k_3,95\%} = [0.0540,\ 0.0640]. \tag{5.15b}$$

The 95% confidence intervals for the two parameter ϕ and k_3 of the switchover time formula (5.1) of Model FCR-M-HP obtained through both the likelihood ratio test (Wilk's Theorem) and bootstrapping methods, namely in (5.13) and (5.15), show agreement. We have verified that using the function $ci = bootci$ produces similar results which computes a 95% bootstrap confidence interval precisely given by

$$CI^{M}_{\phi,95\%,ci} = [0.1598,\ 0.1773], \tag{5.16a}$$

$$CI^{M}_{k_3,95\%,ci} = [0.0538,\ 0.0639]. \tag{5.16b}$$

5.4.2 Model FCR-H-HP

Similarly, results for different increments of High Hydrogen Peroxide Trials, (N_H) varying iodine with vitamin C and low hydrogen peroxide fixed, and (C_H) varying vitamin C with iodine and low hydrogen peroxide fixed, are shown in Table 5.2. The outcome of least-squares fitting equation (5.2) for the parameters ϕ and k_3 to both experimental data simultaneously is shown in Figure 5.12 (note that the

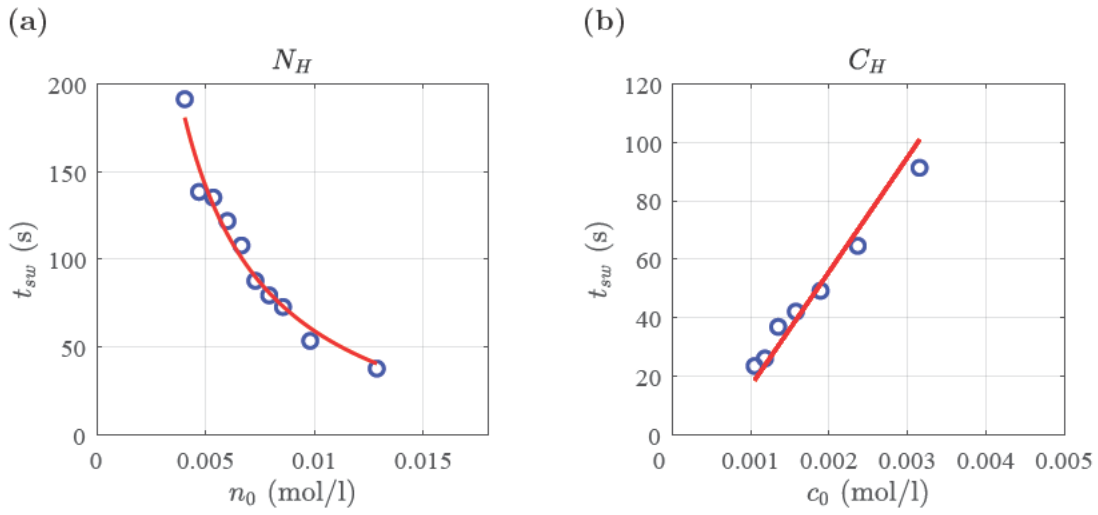

Figure 5.12: Experimental data results of High Hydrogen Peroxide Trials (blue circles) from Table 5.2 and least-squares fitting equation (5.2) to both experimental data, namely N_H and C_H, simultaneously with $\left(\hat{\phi}^H, \hat{k}_3^H\right) = (0.1734, 0.0654)$ (red lines). (a) Varying iodine concentration. (b) Varying vitamin C concentration.

curve is plotted for the full range of the independent variable). The estimated value of Model FCR-H-HP is $\left(\hat{\phi}^H, \hat{k}_3^H\right) = (0.1734, 0.0654)$.

Figure 5.13 illustrates an independent test across a full range of varying hydrogen peroxide data from Table 3 and least-squares fitting of the switchover time formula of Model FCR-H-HP (5.2). This outcome ties agreeably with high hydrogen peroxide trials more than the moderate hydrogen peroxide trials as we expected.

In Figure 5.14, the contour plot provides a visual representation of the logarithm of the objective function (5.4), with the estimated values $\left(\hat{\phi}^H, \hat{k}_3^H\right) = (0.1734, 0.0654)$ located in the centre, of the inner ellipse, of the minimum level in the contour plot.

Figure 5.15 displays the pcolor plot of the satisfying condition; the log-likelihood

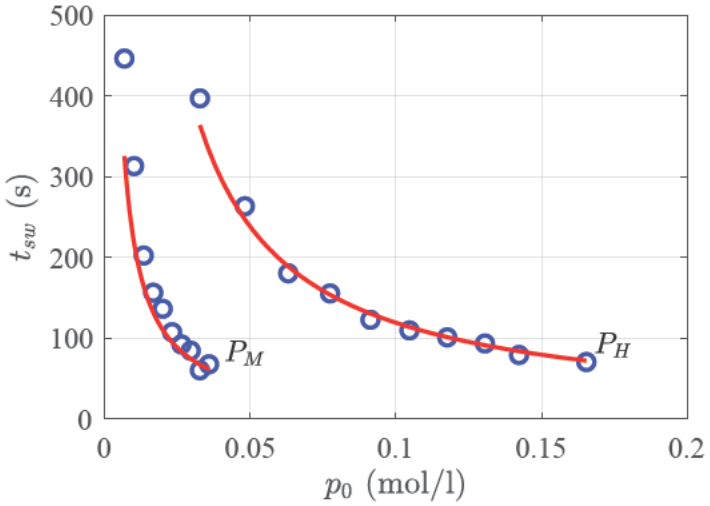

Figure 5.13: An independent test across full range of Varying Hydrogen Peroxide Trials (blue circles) from Table 5.3 and least-squares fitting of the switchover time formula of Model FCR-H-HP (5.2) to both experimental data, namely N_H and C_H, simultaneously with $\left(\hat{\phi}^H, \hat{k}_3^H\right) = (0.1734, 0.0654)$ (red lines).

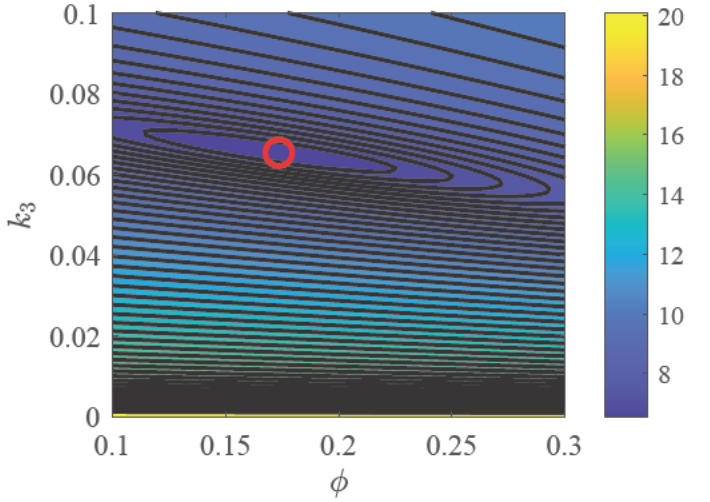

Figure 5.14: A contour plot of the logarithm of the objective function with the estimated value $\left(\hat{\phi}^H, \hat{k}_3^H\right) = (0.1734, 0.0654)$ (red circle mark) of the switchover time formula (5.2) of the Model FCR-H-HP.

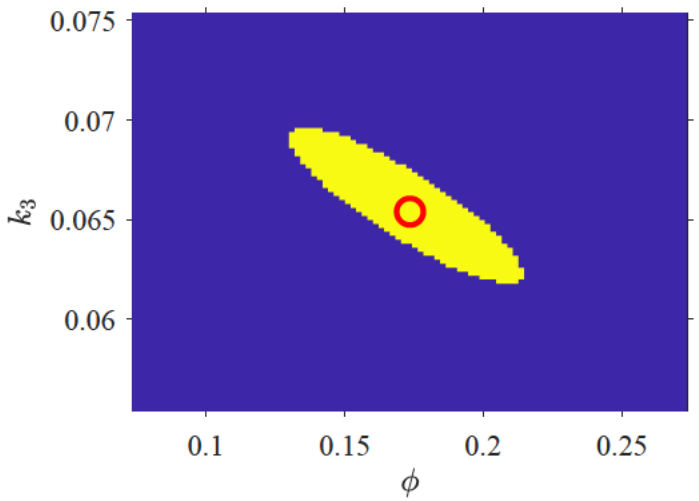

Figure 5.15: A pcolor plot of the satisfying condition; log-likelihood ratio < critical value with the bar plot of the numeric values (the yellow region for true, and the blue region for false), and the estimated value $\left(\hat{\phi}^H, \hat{k}_3^H\right) = (0.1734, 0.0654)$ (red circle mark) of the switchover time formula (5.2) of the Model FCR-H-HP.

ratio < critical value. The 95% confidence interval using the log-likelihood ratio test (Wilk's Theorem) for the two parameters ϕ and k_3 of the switchover time formula (5.2) of Model FCR-H-HP, of all high hydrogen peroxide trials (N_H, C_H) as follows:

$$CI^H_{\phi,95\%} = [0.1300,\ 0.2128], \tag{5.17a}$$

$$CI^H_{k_3,95\%} = [0.0618,\ 0.0694]. \tag{5.17b}$$

Figure 5.16 shows the 95% confidence region of the objective function at the specific level v as given in (5.14).

Figure 5.17 indicates the histogram plots and frequency of the two parameters (ϕ and k_3). Figure 5.18 illustrates a scatter plot of the two parameters ϕ and k_3 of each bootstrap sample with the 95% confidence interval of the parameter ϕ and

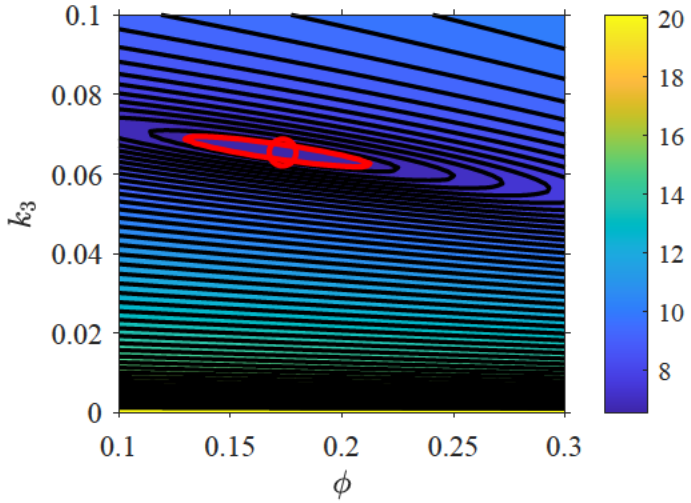

Figure 5.16: A contour plot of the logarithm of the objective function at level v (satisfied the 95% confidence region) with the estimated value $\left(\hat{\phi}^H, \hat{k}_3^H\right) = (0.1734, 0.0654)$ (red circle mark) of the switchover time formula (5.2) of the Model FCR-H-HP.

k_3.

A bootstrapping method is used to calculate the lower and upper quantiles of the 95% confidence interval shown in figure 5.19.

Our results on the 95% confidence interval using bootstrapping resampling for the two parameters ϕ and k_3 of the switchover time formula (5.2) of Model FCR-H-HP, of all high hydrogen peroxide trials (N_H, C_H) are as follows:

$$CI^H_{\phi,95\%} = [0.1190,\ 0.2188], \tag{5.18a}$$

$$CI^H_{k_3,95\%} = [0.0608,\ 0.0733]. \tag{5.18b}$$

In Model FCR-H-HP, the 95% confidence intervals for the parameters ϕ and k_3 of the switchover time formula (5.2) have shown agreement using both the likelihood ratio test (Wilk's Theorem) and bootstrapping methods, namely (5.17) and (5.18).

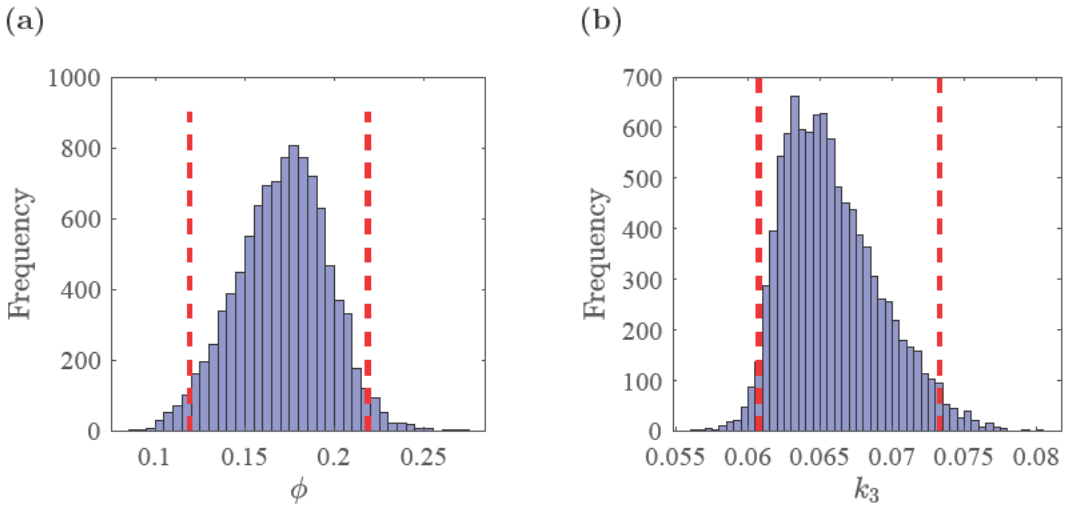

Figure 5.17: Histogram of the bootstrapping re-sampling for estimating the two parameters ϕ and k_3 of the switchover time formula (5.2) of the Model FCR-H-HP. (a) For the parameter ϕ. (b) For the parameter k_3.

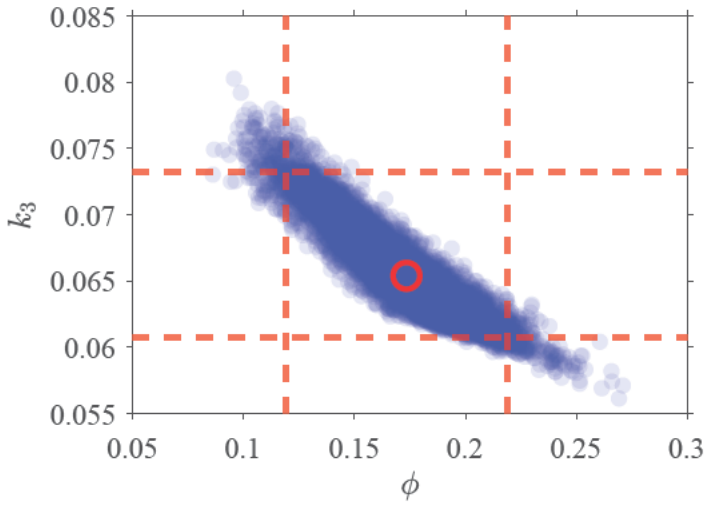

Figure 5.18: A scatter plot of the two parameters ϕ and k_3 of each bootstrap sample with the 95% confidence interval as dashed horizontal vertical lines (red), and the estimated value $\left(\hat{\phi}^H, \hat{k}_3^H\right) = (0.1734, 0.0653)$ (red circle mark).

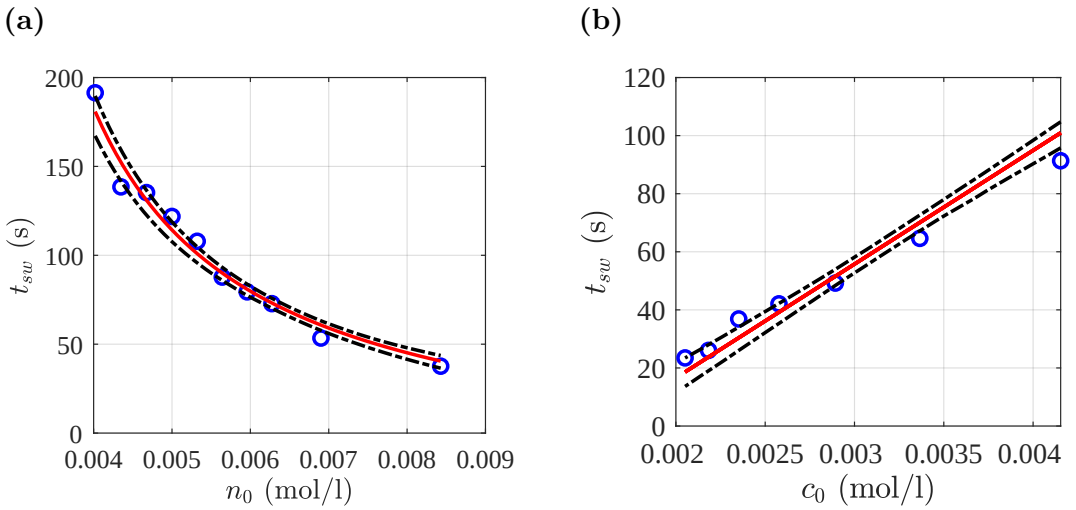

Figure 5.19: The lower and upper quantiles of the bootstrapping method (black dash-dotted lines) for the experimental data results of High Hydrogen Peroxide Trials (blue circles) from Table 5.2 and least-squares fitting equation (5.2) to both experimental data, namely N_H and C_H, simultaneously with $\left(\hat{\phi}^H, \hat{k}_3^H\right) = (0.1734, 0.0653)$ (red lines). (a) Varying iodine concentration. (b) Varying vitamin C concentration.

We have ascertained that using the function $ci = bootci$ produces similar results which computes a 95% bootstrap confidence interval precisely given by

$$CI^{H}_{\phi,95\%,ci} = [0.1196,\ 0.2196], \tag{5.19a}$$

$$CI^{H}_{k_3,95\%,ci} = [0.0607,\ 0.0733]. \tag{5.19b}$$

It should be pointed out that the confidence intervals of the two parameters ϕ and k_3 are consistent between the two models above, Model FCR-M-HP and Model FCR-H-HP, and their experimental data because they represent the same reactants regardless of the level of hydrogen peroxide (moderate or high). We anticipate similarities in parameter estimates from the two models and driven data, although we acknowledge that data noise prevents them from being identical. The 95% confidence intervals of the Model FCR-M-HP, in (5.13) and (5.15) are overlapping with the confidence intervals of the Model FCR-H-HP, in (5.17) and (5.18).

5.4.3 Both Models FCR-M-HP and FCR-H-HP

We now determine the values of the two parameters ϕ and k_3 in the switchover time formula for both models, Model FCR-M-HP and Model FCR-H-HP, when given in one formula (5.3). In this study, we apply the least squares method to find the estimated values of the two parameters ϕ and k_3 in the switchover time formula (5.3) that best fit all the experimental data in Table 5.1 and Table 5.2. Hence, the least-squares fitting with relative errors is useful to account for the wide range of measured switchover times, especially when dealing with data of different

scales. We now seek to minimise

$$S(\phi, k_3) = \sum^{N} \frac{\left(t_{sw,model} - t_{sw,data}\right)^2}{t^2_{sw,data}}, \tag{5.20}$$

where N is the number of experimental data. This approach ensures that the resulting model provides the closest approximation to the observed data.

Figure 5.20 shows the outcome of fitting to the series experiments N_M, C_M, N_H and C_H, and least-squares fitting of the switchover time formula of both models (5.3) with $\hat{\phi} = 0.15835$ and $\hat{k}_3 = 0.066302$. The results provide an excellent fit to the experimental data for moderate and high hydrogen peroxide, as shown in Figure 5.21.

In Figure 5.22, the contour plot provides a visual representation of the logarithm of the objective function (5.20).

Figure 5.23 shows the pcolor plot of the satisfying condition with the log-likelihood ratio. The 95% confidence interval using the log-likelihood ratio test (Wilk's Theorem) for the two parameters ϕ and k_3 of the switchover time formula (5.3) of all moderate and high hydrogen peroxide trials (N_M, C_M, N_H, C_H) is as follows:

$$CI_{\phi,95\%} = [0.1553,\ 0.1610], \tag{5.21a}$$

$$CI_{k_3,95\%} = [0.0644,\ 0.0683]. \tag{5.21b}$$

Figure 5.24 shows the 95% confidence regions for the two parameters ϕ and k_3, using the log-likelihood ratio test given in (5.21), of the objective function with relative errors of the switchover time formula (5.3).

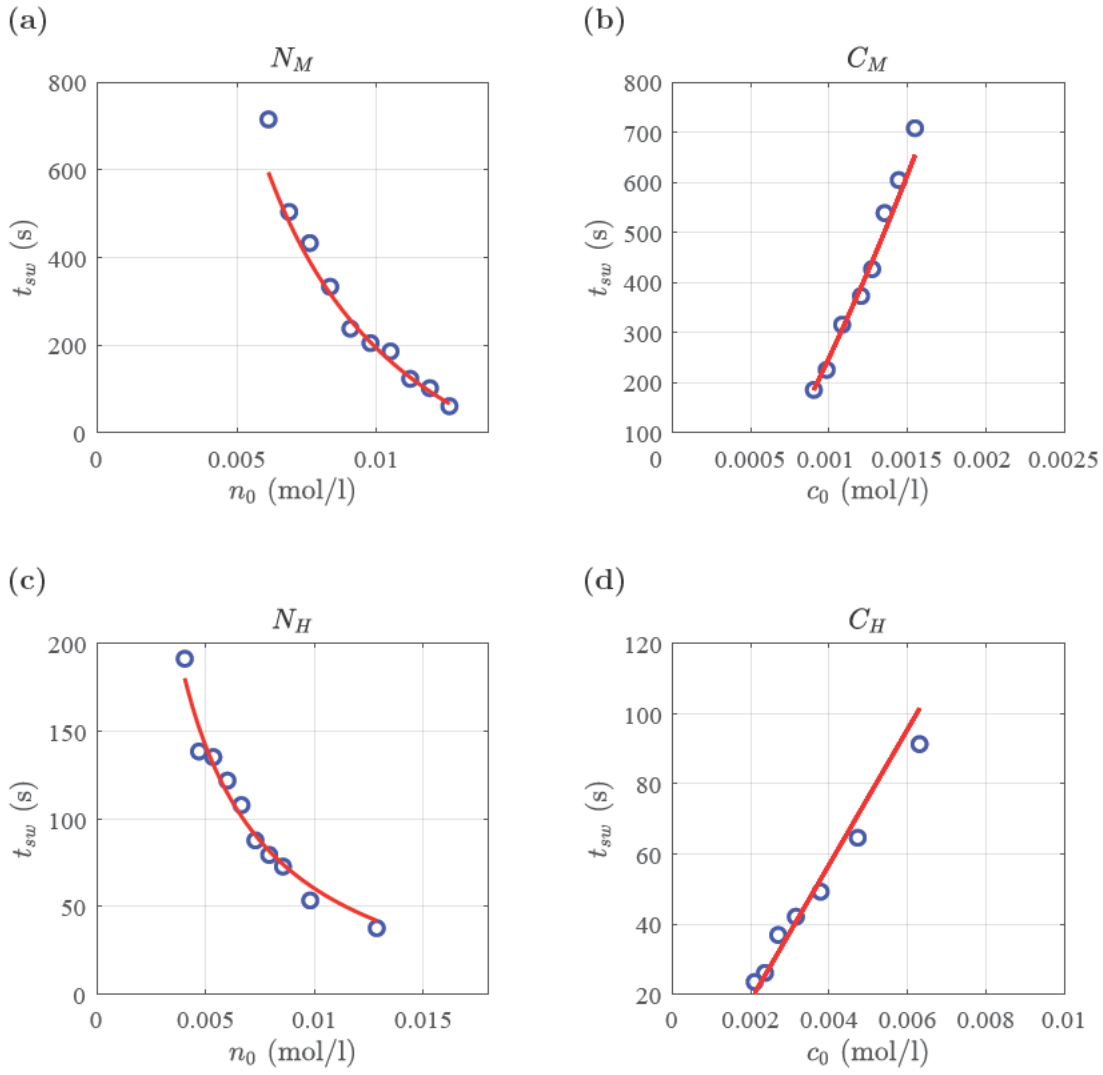

Figure 5.20: Outcome of simultaneous fitting to data series N_M, C_M, N_H and C_H. The experimental (blue circles) and fitted switchover time equation (5.3) with sum square relative error best fit of $\left(\hat{\phi}, \hat{k}_3\right) = (0.15835, 0.066302)$ (red lines).

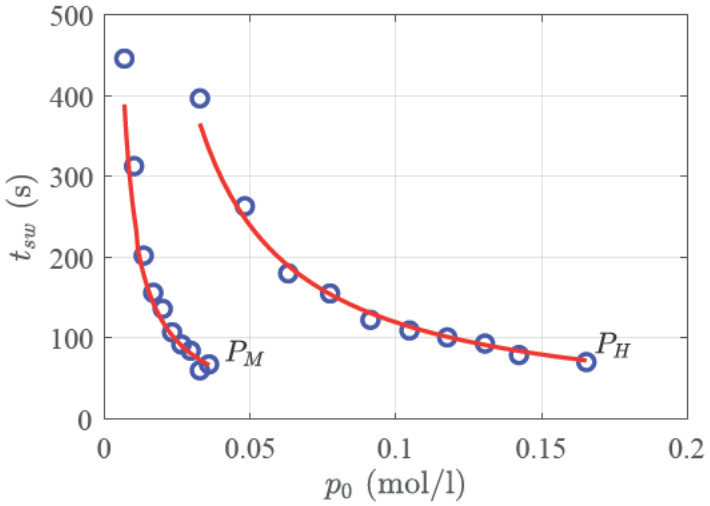

Figure 5.21: Test of the parameter fits (from Figure 5.20) with $\left(\hat{\phi}, \hat{k}_3\right) = (0.15835, 0.066302)$, against independent experimental series P_M and P_H in which initial hydrogen peroxide mass is varied.

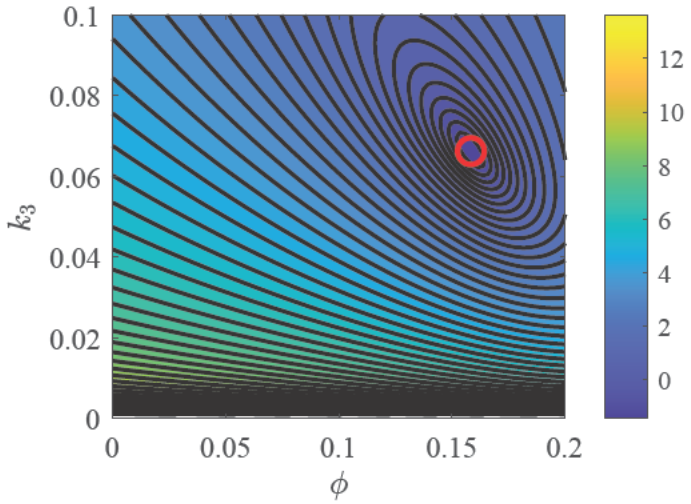

Figure 5.22: A contour plot of the logarithm of the objective function (5.20) with the estimated value $\left(\hat{\phi}, \hat{k}_3\right) = (0.15835, 0.066302)$ (red circle mark) of the switchover time formula (5.3).

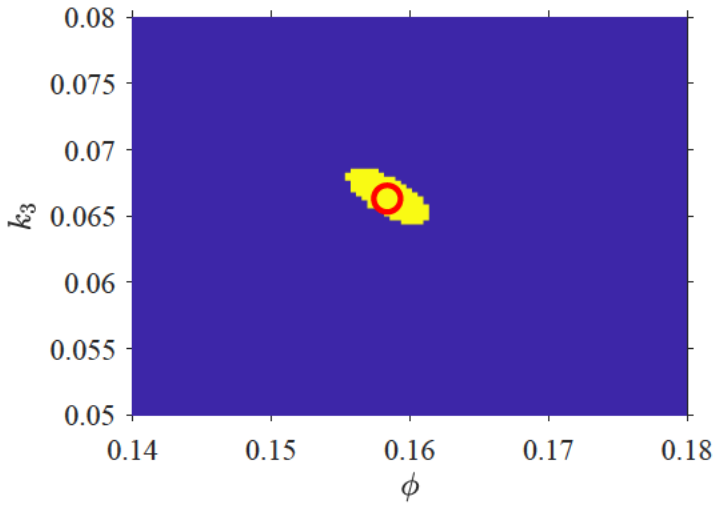

Figure 5.23: A pcolor plot of the satisfying condition; log-likelihood ratio < critical value (yellow region for true, and blue region for false), and the estimated value $\left(\hat{\phi}, \hat{k}_3\right) = (0.15835, 0.066302)$ (red circle mark) of the switchover time formula (5.3).

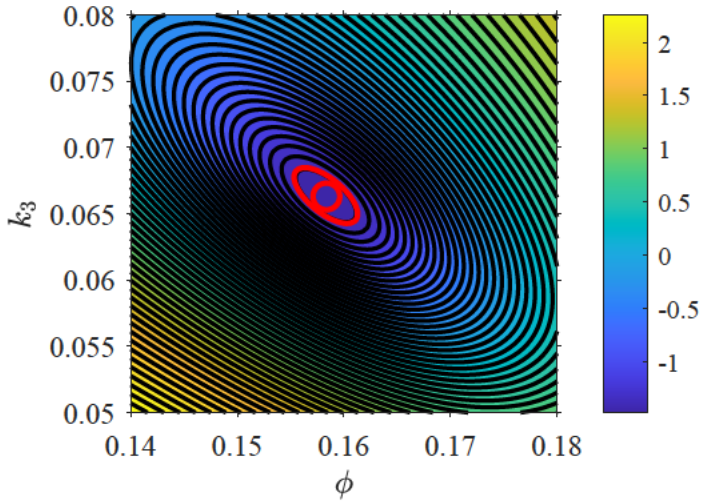

Figure 5.24: A contour plot of the logarithm of the objective function at level v (satisfied the 95% confidence region) with the estimated value $\left(\hat{\phi}, \hat{k}_3\right) = (0.15835, 0.066302)$ (red circle mark) of the switchover time formula (5.3).

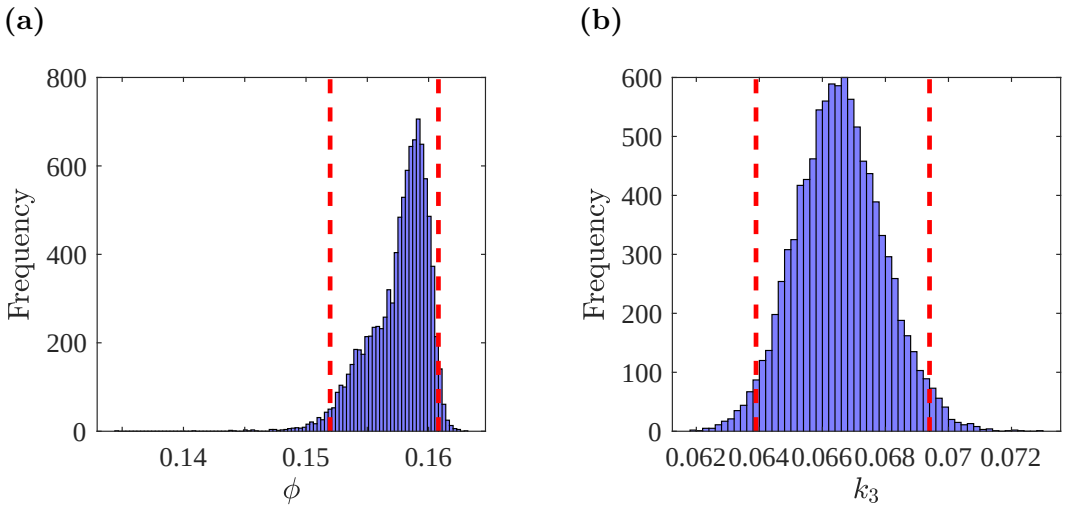

Figure 5.25: Histogram of the bootstrapping re-sampling for estimating the two parameters ϕ and k_3 of the switchover time formula (5.3) of both models, Model FCR-M-HP and Model FCR-H-HP, with the lower and upper bounds of the parameters confidence interval as dashed vertical lines (red). (a) For the parameter ϕ. (b) For the parameter k_3.

Figure 5.25 displays the histogram plots and frequency of the two parameters (ϕ and k_3) using the bootstrap sampling of the switchover time formula for both models (5.3). Figure 5.26 demonstrates a scatter plot of the two parameters ϕ and k_3 with the 95% confidence intervals.

A bootstrapping method is used to calculate the lower and upper quantiles of the 95% confidence interval across full range of hydrogen peroxide concentrations, shown in Figure 5.27. Our findings on the 95% confidence interval using the bootstrapping of the switchover time formula (5.3) of the two models, Model FCR-M-HP and Model FCR-H-HP, of all moderate and high trials (N_M, C_M, N_H, C_H)

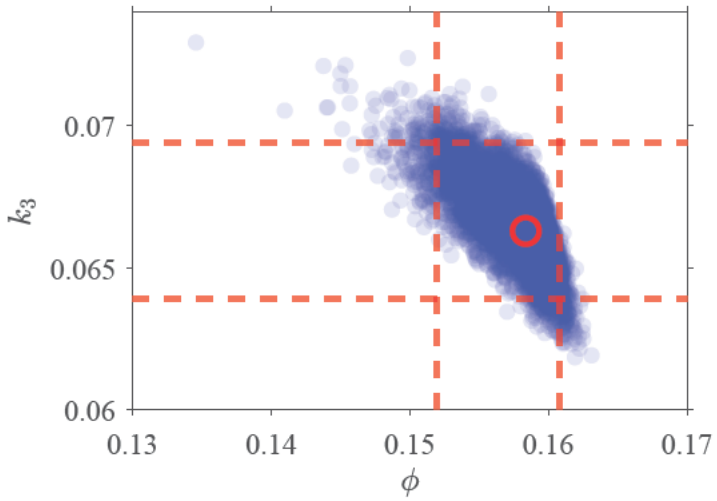

Figure 5.26: A scatter plot of the two parameters ϕ and k_3 of each bootstrap sample with 95% confidence intervals (red dashed lines) with the estimated value $\left(\hat{\phi}, \hat{k}_3\right) = (0.15835, 0.066302)$ (red circle mark).

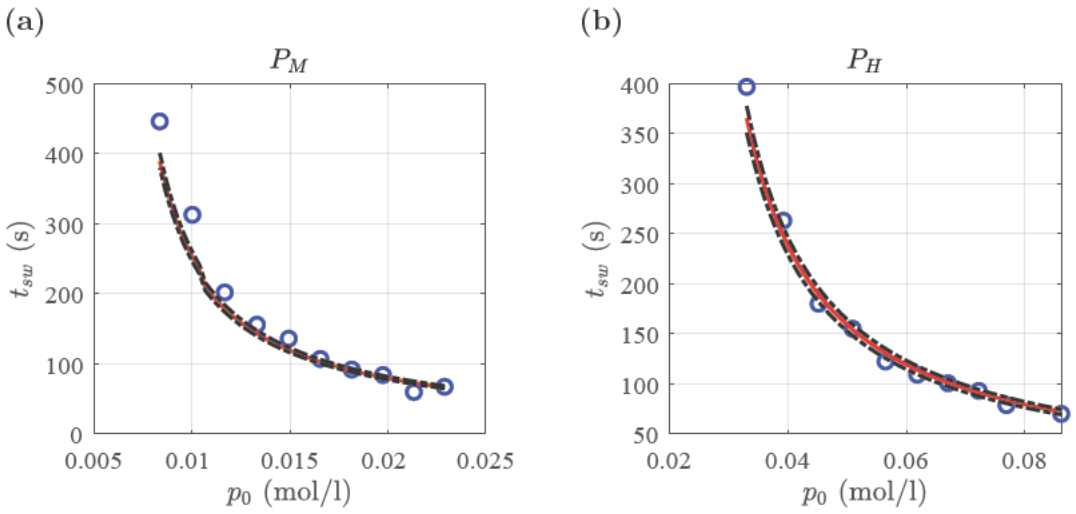

Figure 5.27: The lower and upper quantiles of the bootstrapping method (black dash-dotted lines) for the experimental data results of Varying Hydrogen Peroxide Trials (blue circles) from Table 5.3 and least-squares fitting equation (5.3) to all experimental data, namely N_M, C_M, N_H and C_H, with $\left(\hat{\phi}, \hat{k}_3\right) = (0.15835, 0.066302)$ (red lines).

is as follows:

$$CI_{\phi,95\%} = [0.15197,\ 0.16080], \tag{5.22a}$$

$$CI_{k_3,95\%} = [0.06389,\ 0.06940]. \tag{5.22b}$$

The bootstrap confidence interval is computed using the function $ci = bootci$ which produces equivalent results:

$$CI_{\phi,95\%,ci} = [0.1519,\ 0.1608], \tag{5.23a}$$

$$CI_{k_3,95\%,ci} = [0.0640,\ 0.0693]. \tag{5.23b}$$

The confidence intervals of the combined formula (5.3) of both moderate and high model, in (5.21) and (5.22) are consistent with the confidence intervals we have found earlier of the moderate model (Model FCR-M-HP), in (5.13) and (5.15), and the confidence intervals of the high model (Model FCR-H-HP), in (5.17) and (5.18). We would expect that parameters estimated from different models and datasets will be similar, but not exactly the same due to data noise. There is agreement between all the confidence intervals of the two parameters ϕ and k_3 between the results of the three models. Table 5.4 summarizes our results for each parameter estimation technique and model.

By switching this final approach around (fitting to the series P_M and P_H, and then testing against series C_M, N_M, C_H, and N_H) was also performed and is presented in Appendix A.

Models	The switchover time formula	Least-squares method	Log-likelihood method	Bootstrapping method
Model FCR-M-HP	$\mathrm{t}_{sw}^{M} = \frac{1}{k_3 n_0} \ln\left(\frac{p_0}{p_0+\phi n_0-c_0}\right).$	$\left(\hat{\phi}^{M}, \hat{k}_3^{M}\right) =$ $(0.1676, 0.0586)$	$CI_{\phi,95\%}^{M}=$ $[0.1592, 0.1752]$ $CI_{k_3,95\%}^{M}=$ $[0.0554, 0.0622]$	$CI_{\phi,95\%}^{M}=$ $[0.1597, 0.1770]$ $CI_{k_3,95\%}^{M}=$ $[0.0540, 0.0640]$
Model FCR-H-HP	$\mathrm{t}_{sw}^{H} = \frac{c_0-\phi n_0}{k_3 n_0 p_0}.$	$\left(\hat{\phi}^{H}, \hat{k}_3^{H}\right) =$ $(0.1734, 0.0654)$	$CI_{\phi,95\%}^{H}=$ $[0.1300, 0.2128]$ $CI_{k_3,95\%}^{H}=$ $[0.0618, 0.0694]$	$CI_{\phi,95\%}^{H}=$ $[0.1190, 0.2188]$ $CI_{k_3,95\%}^{H}=$ $[0.0608, 0.0733]$
Both Models	$\mathrm{t}_{sw} = \begin{cases} \frac{1}{k_3 n_0} \log\left(\frac{p_0}{p_0+\phi n_0-c_0}\right) & \text{for} \quad (p_0 < 1.5n_0)\,, \\ \left(\frac{c_0-\phi n_0}{k_3 n_0 p_0}\right) & \text{for} \quad (p_0 \geq 1.5n_0)\,. \end{cases}$	$\left(\hat{\phi}, \hat{k}_3\right) =$ $(0.1584, 0.06630)$	$CI_{\phi,95\%}=$ $[0.1553, 0.1610]$ $CI_{k_3,95\%}=$ $[0.0644, 0.0683]$	$CI_{\phi,95\%}=$ $[0.15197, 0.16080]$ $CI_{k_3,95\%}=$ $[0.06389, 0.06940]$

Table 5.4: Summary diagram of our results in comparison with parameter estimation methods.

5.5 Conclusion

This chapter presented the results of six experimental series designed to test the model of chapter 4 through both moderate and high hydrogen peroxide regimes. Model parameters were fitted through relative error least squares fitting to account for the large range of switchover times measured, with uncertainties quantified through the likelihood ratio test and bootstrapping. The switchover time formulas have been proven highly accurate when tested with different concentrations of hydrogen peroxide, iodine, and vitamin C, with excellent consistency across different combinations of fitting and testing datasets. In certain conditions (not presented here) the clock reaction failed to occur; this can be the subject of future work.

Chapter 6

Conclusions And Future Work

The study of chemical kinetics, particularly the interesting phenomenon of clock reactions, has a rich history spanning over a century. This research contributes to this field by employing mathematical modeling and analysis to gain deeper insights into clock reactions involving vitamin C and hydrogen peroxide. Through the development of new nonlinear differential equation models, this study explores the kinetics of the reaction, particularly focusing on the role of hydrogen peroxide concentration. Through our analysis, we have resolved the discrepancy between the choice of kinetics in the slow reaction, demonstrating mathematically that linear kinetics are appropriate when hydrogen peroxide is present in moderate levels, and quadratic kinetics are appropriate when hydrogen peroxide concentration exceeds that of the other chemicals. Using asymptotic analysis, the study provides a better understanding of the clock reaction, supported by both approximation solutions and experimental validation. Furthermore, this research explores the applicability of parameter estimation, such as least-squares and bootstrapping in analyzing experimental data.

6.1 Contributions of the Thesis

We can conclude the thesis by providing a summary of each chapter separately. Chapter 1 revealed the main aim of this thesis which is to use mathematical modelling to understand a specific chemical reaction. We reviewed some of the basic chemical reaction preliminaries needed for the thesis. An outline of the thesis is also included. In Chapter 2, we discussed and analysed the simple clock reaction model (fast and slow) by extending the work of Kerr et al. [27] to include hydrogen peroxide and assuming that the rate of the slow reaction is linear in both iodine and hydrogen peroxide concentrations as predicted by the experimental data of Copper and Koubek [16]. Here, we assumed hydrogen peroxide was present in comparable concentrations to the other reactants – i.e. the moderate case – (unlike in the experiments performed in Kerr et al. [27]). Our asymptotic solutions closely matched the numerical results over appropriate time intervals. Additionally, we formulated a useful switchover time formula to identify the significant occurrence of when the clock reaction occurs and the solution appears dark blue. Crucially, our derived switchover time formula closely correlates with the outcome presented by Parra Cordova and Peña [40], lending weight to its validity.

Chapter 3 investigated whether the chemical slow reaction converting iodide to iodine should be quadratic or linear and the role of hydrogen peroxide concentration. To understand how hydrogen peroxide concentration affects the kinetics of the chemical clock reaction, the slow reaction was analyzed in isolation by including the hypoiodous acid reactant and reverse reaction. The analysis demonstrates that the kinetics of the clock reaction can exhibit either linear or quadratic behaviour depending on the ratio of hydrogen peroxide to iodide. Thus we were able

to demonstrate why the linear assumption worked in the study of Copper and Koubek [16] (where moderate levels of hydrogen peroxide were used), while the quadratic assumption was valid in Kerr et al. [27] (where high hydrogen peroxide levels were used).

In Chapter 4, we explored the incorporation of the more detailed slow reaction with the fast reaction associated with vitamin C. Asymptotic analysis on this unified full model of the chemical clock reaction (slow and fast) was explored in each case of moderate and high hydrogen peroxide concentration regimes. In this chapter a nonlinear differential equation model was developed to examine the kinetics of the reaction, with a focus on hydrogen peroxide concentration again. In appropriate time regions, asymptotic approximations agree closely with numerical solutions. Using this approach, we could estimate the switchover time for either hydrogen peroxide regime as a function of initial concentrations and the slow reaction rates. Essentially, we found that the switchover time formula of the model with moderate hydrogen peroxide provided is identical to the simplified linear kinetic model illustrated earlier in Chapter 2. In addition, the simplified switchover time formula of the high hydrogen peroxide model presented is in line with the switchover formula derived by Kerr et al. [27].

It has been shown in Chapter 5 that the switchover time formulae for both cases, moderate and high hydrogen peroxide, are highly accurate when tested through experiments with various concentrations of hydrogen peroxide, iodine, and vitamin C. The effectiveness of the parameter estimation methods least-squares, log-likelihood ratio, and bootstrapping were considered in analyzing the data. There was good agreement between the parameter estimates using each approach presented, with significant overlap on the confidence intervals for the two

parameters ϕ and k_3.

Overall, this research advances our understanding of the clock reaction and its kinetics. The insights gained from this research advance our deep mathematical analysis and offer practical implications for experimental design. The approach we have taken enables an experimentalist to be able to conduct the clock reaction and determine the induction duration of the experiment needed to capture the switchover point depending on how much of each chemical ingredient they are using initially. We have further developed the theory and experimental framework for clock chemical reactions based on kinetics principles, performing numerical and asymptotic analyses, conducting experiments to test the model, using statistical techniques to optimize the parameters, and documenting the results. This research paves the way for future research endeavours in the study of the clock reaction.

6.2 Future Work

The work in this thesis can be extended in several directions, such as exploring the effect of temperature on the reaction kinetics, both through how this might affect the ODE structure, but also by running the experiments at different temperatures to see how this might change our parameter estimates. We could also investigate the iodate variation via three-step reaction, involving the iodate ion (IO_3^-), iodide (I^-), and iodine (I_2) (see Figure 3.1) to bring additional detail and complexity into the model. We could also explore further optimization against additional experimental data to enhance the sensitivity of the model outcomes to initial conditions of the reactants. Finally, there are many other chemical clock reactions that could similarly be investigated through asymptotic analysis.

In respect of experimental technique, another area for development would be the use of ultraviolet light spectrophotometry [52] to measure the time evolution of iodine levels (via blue iodine-starch complex) rather than simply the switchover time, so that model curves could be fitted directly, providing a more complete test of the accuracy of the solutions in each asymptotic region. Explicit mathematical modelling of the formation of starch-iodine complex may in turn be required to interpret spectrophotometry data.

These potential avenues for further examining the chemical clock reactions, however, should not detract from the valuable findings of this work: we have used asymptotic analyses to resolve the discrepancy in the literature regarding the form of the reaction kinetics involved, developed a unified model capable of capturing the effect of either moderate or high hydrogen peroxide levels, derived analytical formulae for the switchover time, and demonstrated the validity of these formulae against novel experimental data.

Bibliography

[1] JM Anderson. Computer simulation in chemical kinetics. *Journal of Chemical Education*, 53(9):561, 1976.

[2] P Asrani, MS Eapen, C Chia, G Haug, HC Weber, MdI Hassan, and SS Sohal. Diagnostic approaches in COVID-19: clinical updates. *Expert review of respiratory medicine*, pages 1–16, 2020.

[3] A Bermúdez and LM García-García. Mathematical modeling in chemistry. Application to water quality problems. *Applied numerical mathematics*, 62(4):305–327, 2012.

[4] Y Bichsel and U Von Gunten. Oxidation of iodide and hypoiodous acid in the disinfection of natural waters. *Environmental science & technology*, 33(22):4040–4045, 1999.

[5] Y Bichsel and U Von Gunten. Formation of iodo-trihalomethanes during disinfection and oxidation of iodide-containing waters. *Environmental Science & Technology*, 34(13):2784–2791, 2000.

[6] J Billingham and PV Coveney. Simple chemical clock reactions: application to cement hydration. *Journal of the Chemical Society, Faraday Transactions*, 89(16):3021–3028, 1993.

[7] J Billingham and PV Coveney. Kinetics of self-replicating micelles. *Journal of the Chemical Society, Faraday Transactions*, 90(13):1953–1959, 1994.

[8] J Billingham and DJ Needham. Mathematical modelling of chemical clock reactions. I. induction, inhibition and the iodate-arsenous-acid reaction. *Philosophical Transactions of the Royal Society of London. Series A: Physical and Engineering Sciences*, 340(1659):569–591, 1992.

[9] J Billingham and DJ Needham. Mathematical modelling of chemical clock reactions. *Journal of Engineering Mathematics*, 27(2):113–145, 1993.

[10] Science Bob. Rapid color changing chemistry. `https://sciencebob.com/rapid-color-changing-chemistry`. [Online; accessed 19-December-2020].

[11] AE Burgess and JC Davidson. Kinetics of the rapid reaction between iodine and ascorbic acid in aqueous solution using UV–visible absorbance and titration by an iodine clock. *Journal of Chemical Education*, 91(2):300–304, 2014.

[12] GM Burnett and HW Melville. Determination of the velocity coefficients for polymerization processes. I. The direct photopolymerization of vinyl acetate. *Proceedings of the Royal Society of London. Series A. Mathematical and Physical Sciences*, 189(1019):456–480, 1947.

[13] J-Y Chien. Kinetic analysis of irreversible consecutive reactions. *Journal of the American Chemical Society*, 70(6):2256–2261, 1948.

[14] KA Connors. *Chemical kinetics: the study of reaction rates in solution*. Wiley-VCH Verlag GmbH, 1990.

[15] W J Conway. A modified lecture experiment. *Journal of Chemical Education*, 17(8):398, 1940.

[16] CL Copper and E Koubek. A kinetics experiment to demonstrate the role of a catalyst in a chemical reaction: a versatile exercise for general or physical chemistry students. *Journal of chemical education*, 75(1):87, 1998.

[17] AJ Demello. Control and detection of chemical reactions in microfluidic systems. *Nature*, 442(7101):394–402, 2006.

[18] ET Denisov, E Denisov, O Sarkisov, and GI Likhtenshtein. *Chemical kinetics: fundamentals and recent developments*. Elsevier, 2003.

[19] B Efron. *The jackknife, the bootstrap and other resampling plans*. SIAM, 1982.

[20] B Efron. Better bootstrap confidence intervals. *Journal of the American statistical Association*, 82(397):171–185, 1987.

[21] P Eykhoff. *System identification*, volume 14. Wiley New York, 1974.

[22] T M Farris, J P Humes, and M A Nussbaum. Mix-bricks and flip-lids: 3d printed devices for simple, simultaneous mixing of reactant solutions. *Analytical chemistry*, 92(5):3522–3527, 2020.

[23] M Galajda, G Lente, and I Fábián. Photochemically induced autocatalysis in the chlorate ion- iodine system. *Journal of the American Chemical Society*, 129(25):7738–7739, 2007.

[24] A Hanna, A Saul, and K Showalter. Detailed studies of propagating fronts in the iodate oxidation of arsenous acid. *Journal of the American Chemical Society*, 104(14):3838–3844, 1982.

[25] A K Horváth and I Nagypál. Classification of clock reactions. *ChemPhysChem*, 16(3):588–594, 2015.

[26] E Jones, CG Munkley, ED Phillips, and G Stedman. Kinetics and equilibria in the nitric acid–nitrous acid–sodium thiocyanate system. *Journal of the Chemical Society, Dalton Transactions*, (9):1915–1920, 1996.

[27] R Kerr, WM Thomson, and DJ Smith. Mathematical modelling of the vitamin C clock reaction. *Royal Society Open Science*, 6(4):181367, 2019.

[28] H Landolt. Ueber die zeitdauer der reaction zwischen jodsáure und schwefliger sáure. *Berichte der deutschen chemischen Gesellschaft*, 19(1):1317–1365, 1886.

[29] G Lente, G Bazsa, and I Fábián. What is and what isn't a clock reaction? *New Journal of Chemistry*, 31(10):1707–1707, 2007.

[30] J Li, J Jiang, Y Zhou, S-Y Pang, Y Gao, C Jiang, J Ma, Y Jin, Y Yang, G Liu, et al. Kinetics of oxidation of iodide (I–) and hypoiodous acid (HOI) by peroxymonosulfate (PMS) and formation of iodinated products in the

PMS/I–/NOM system. *Environmental Science & Technology Letters*, 4(2):76–82, 2017.

[31] HA Liebhafsky and A Mohammad. The kinetics of the reduction, in acid solution, of hydrogen peroxide by iodide ion. *Journal of the American Chemical Society*, 55(10):3977–3986, 1933.

[32] A Molla and J H Youk. Chemical clock reactions with organic dyes: Perspective, progress, and applications. *Dyes and Pigments*, 202:110237, 2022.

[33] Douglas C Montgomery, Elizabeth A Peck, and G Geoffrey Vining. *Introduction to linear regression analysis*. John Wiley & Sons, 2021.

[34] J C Nagy, K Kumar, and D W Margerum. Nonmetal redox kinetics: oxidation of iodide by hypochlorous acid and by nitrogen trichloride measured by the pulsed-accelerated-flow method. *Inorganic Chemistry*, 27(16):2773–2780, 1988.

[35] I Nagypál and IR Epstein. Fluctuations and stirring rate effects in the chlorite-thiosulfate reaction. *The Journal of Physical Chemistry*, 90(23):6285–6292, 1986.

[36] I Nagypál and IR Epstein. Stochastic behavior and stirring rate effects in the chlorite-iodide reaction. *The Journal of chemical physics*, 89(11):6925–6928, 1988.

[37] J A Nelder and R Mead. A simplex method for function minimization. *The computer journal*, 7(4):308–313, 1965.

[38] AP Oliveira and RB Faria. The chlorate- iodine clock reaction. *Journal of the American Chemical Society*, 127(51):18022–18023, 2005.

[39] M C Pagnacco, J P Maksimović, N T Nikolić, D V Bajuk Bogdanović, M M Kragović, M D Stojmenović, S N Blagojević, and J V Senćanski. Indigo carmine in a food dye: Spectroscopic characterization and determining its micro-concentration through the clock reaction. *Molecules*, 27(15):4853, 2022.

[40] A Parra Cordova and O I Gonzalez Pena. Enhancing student engagement with a small-scale car that is motion-controlled through chemical kinetics and basic electronics. *Journal of Chemical Education*, 97(10):3707–3713, 2020.

[41] L Perko. *Differential equations and dynamical systems*, volume 7. Springer Science & Business Media, 2013.

[42] MJ Pilling and PW Seakins. *Reaction kinetics*. Oxford University Press, 1995.

[43] TV Porgo, SL Norris, G Salanti, LF Johnson, JA Simpson, N Low, M Egger, and CL Althaus. The use of mathematical modeling studies for evidence synthesis and guideline development: A glossary. *Research synthesis methods*, 10(1):125–133, 2019.

[44] PD Sattsangi. A microscale approach to chemical kinetics in the general chemistry laboratory: the potassium iodide hydrogen peroxide iodine-clock reaction. *Journal of Chemical Education*, 88(2):184–188, 2011.

[45] J Shin, Y Lee, and U von Gunten. Kinetics of the reaction between hydrogen peroxide and aqueous iodine: Implications for technical and natural aquatic systems. *Water research*, 179:115852, 2020.

[46] J Shin, U von Gunten, D A Reckhow, S Allard, and Y Lee. Reactions of ferrate (vi) with iodide and hypoiodous acid: Kinetics, pathways, and implications for the fate of iodine during water treatment. *Environmental science & technology*, 52(13):7458–7467, 2018.

[47] AP Silverman and ET Kool. Detecting RNA and DNA with templated chemical reactions. *Chemical reviews*, 106(9):3775–3789, 2006.

[48] Murray R Spiegel. *Schaum's Outline Series of Theory and Problems of Mathematical Handbook of Formulas and Tables*. McGraw-Hill Publishing Company, 1968.

[49] G Stedman, E Jones, and MS Garley. Travelling waves in autocatalytic oxidations by nitric acid. *Reaction Kinetics and Catalysis Letters*, 42(2):395–399, 1990.

[50] K Strimmer. Statistical methods: Likelihood, bayes and regression. likelihood-based confidence interval and likelihood ratio. `https://strimmerlab.github.io`, June 2023. [Online; accessed 12-October-2023].

[51] E Sucre-Rosales, R Fernández-Terán, D Carvajal, L Echevarría, and FE Hernández. Experience-based learning approach to chemical kinetics: Learning from the covid-19 pandemic. *Journal of Chemical Education*, 97(9):2598–2605, 2020.

[52] H Sulistyarti, Q Fardiyah, S Febriyanti, and Asdauna. A simple and safe spectrophotometric method for iodide determination. *Makara Journal of Science*, 19(2):1, 2015.

[53] CFH Tipper, SA Rice, CH Bamford, RG Compton, and NJB Green. *Comprehensive chemical kinetics. Section 8. Heterogeneous reactions.* Elsevier, 1969.

[54] SS Wilks. The large-sample distribution of the likelihood ratio for testing composite hypotheses. *The annals of mathematical statistics*, 9(1):60–62, 1938.

[55] SW Wright. Tick tock, a vitamin C clock. *Journal of Chemical Education*, 79(1):40A, 2002.

[56] SW Wright. The vitamin C clock reaction. *Journal of Chemical Education*, 79(1):41, 2002.

[57] X Zhao, E Salhi, H Liu, J Ma, and U Von Gunten. Kinetic and mechanistic aspects of the reactions of iodide and hypoiodous acid with permanganate: Oxidation and disproportionation. *Environmental science & technology*, 50(8):4358–4365, 2016.

Appendix A

A.1 Results of Setting The Fitting to Series P_M and P_H, and Then Testing against Series C_M, N_M, C_H and N_H

A.1.1 Fitting series

Two experimental series were carried out for fitting of the constants ϕ and k_3, referred to as P_M (moderate hydrogen peroxide regime), and P_H (high hydrogen peroxide regime. The results of different increments of varying Hydrogen Peroxide Trials, (P_M and P_H), with vitamin C and iodine fixed, are shown in Table 5.3.

Again, the values of ϕ and k_3 were estimated through relative error least squares fitting in order to account for the wide range of measured switchover time, carried out in Matlab with the optimisation function *fminsearch*. The 95% confidence limits were estimated through bootstrapping with the function *bootci*.

A.1.2 Testing Series

The switchover time equation (5.3), of both models III-M-HP and III-H-HP, and fitted parameters were then tested by comparing against the independent data series, referred to as C_M, N_M, C_H and N_H.

A.1.3 Results

Figure A.1 shows the outcome of fitting to the series experiments P_M and P_H, where the estimated parameter values are $\hat{\phi} = 0.1467$ and $\hat{k}_3 = 0.0683$. Figure A.2 illustrates the testing of the series against C_M, N_M, C_H and N_H, using the estimated parameters; we see a match between the experiment and the fitted model that is roughly the same as the fitted data. Figure A.3 demonstrates a scatter plot of the two parameters ϕ and k_3 of each bootstrap sample with the lower and upper bounds. Our results on the 95% confidence interval using the bootstrapping of the switchover time formula (5.3) of fitting series (P_M, P_H) are as follows:

$$CI_{\phi,95\%} = [0.1296,\ 0.1640], \tag{A.1a}$$

$$CI_{k_3,95\%} = [0.0654\ 0.0712]. \tag{A.1b}$$

Our results match well with all of the confidence intervals of the two parameters ϕ and k_3 reported in Chapter 5.

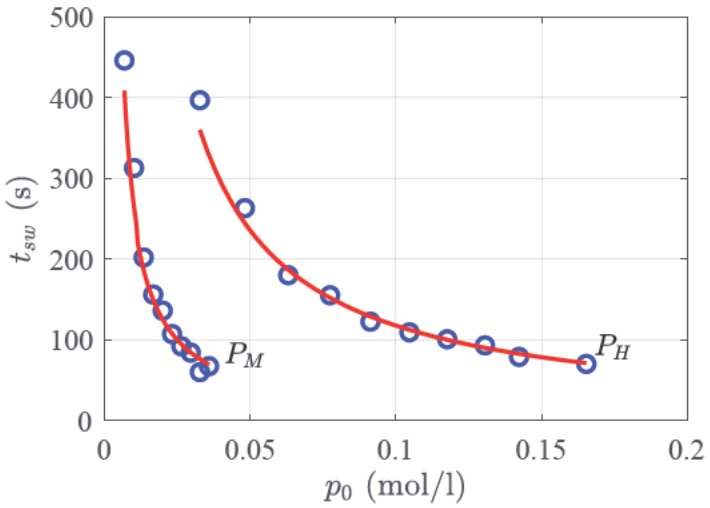

Figure A.1: Outcome of simultaneous fitting to data series P_M and P_H. The experimental data (blue circles) and fitted switchover time (red lines) with sum square relative error best fit of $\hat{\phi} = 0.1467$ and $\hat{k}_3 = 0.0683$.

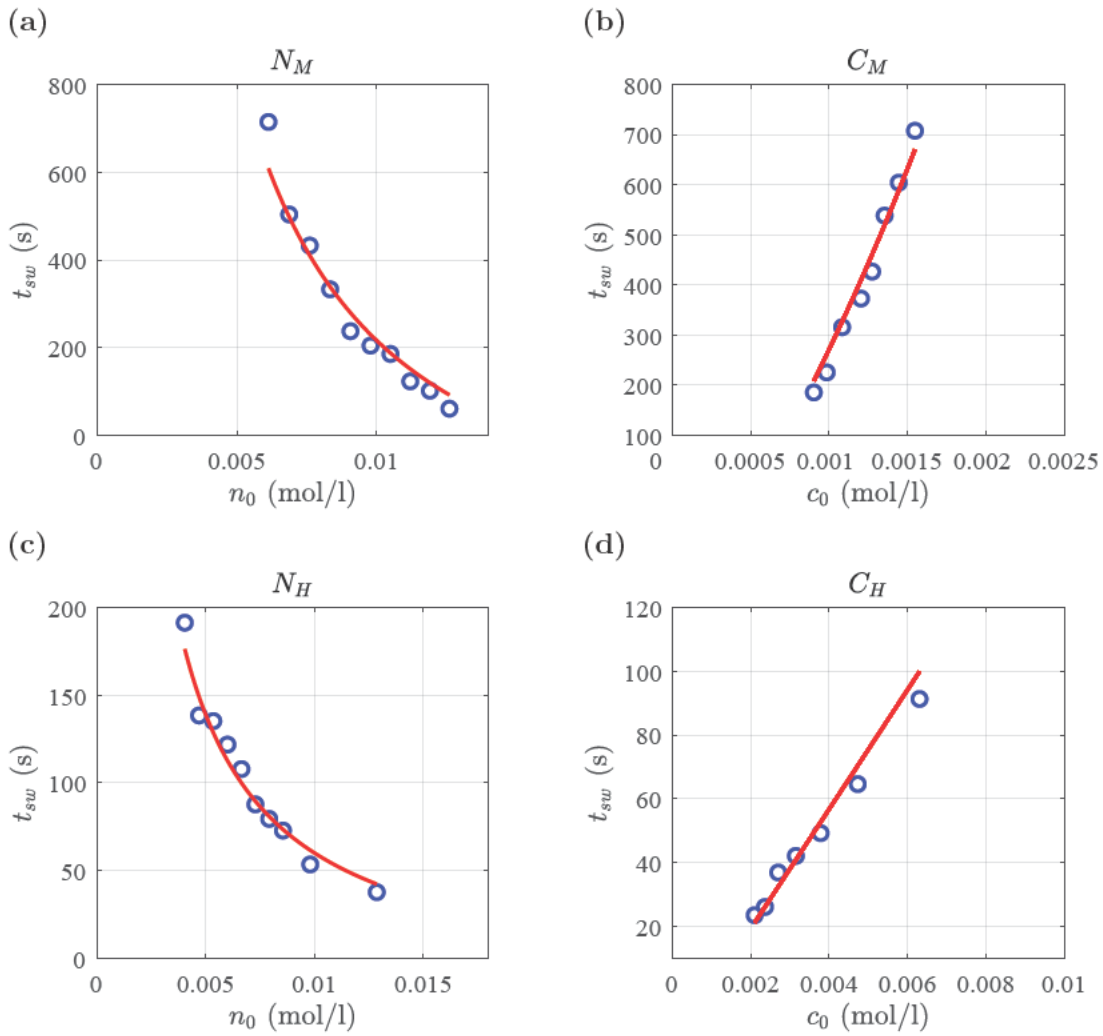

Figure A.2: Test of the parameter fits (Figure A.1) against independent experimental series C_M, N_M, C_H and N_H, in which initial vitamin C and iodine concentrations are varied.

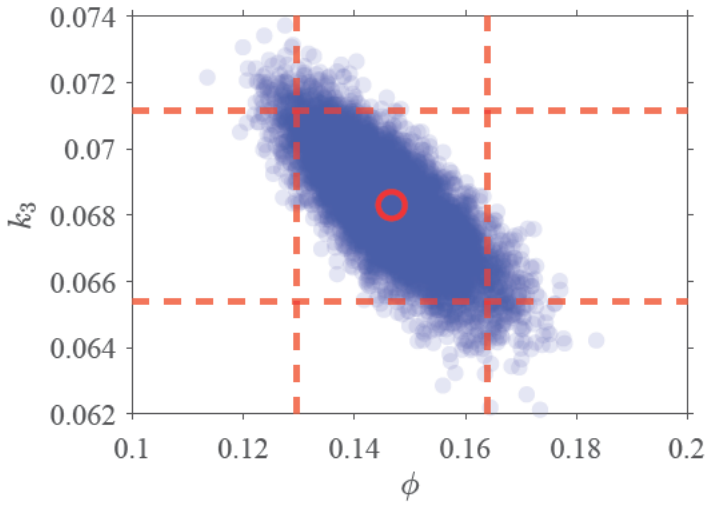

Figure A.3: Bootstrapping results with 10000 repeats (blue dots), best fit (red circle mark) and 95% confidence intervals for each parameter (dashed red lines).